



TECHNICAL UNIVERSITY OF LIBEREC

Faculty of Sciences, Humanities and Education

Ph. D. Thesis

POLING OF PZT CERAMICS

Liberec 2012

Tetyana Malysh

TECHNICAL UNIVERSITY OF LIBEREC

Faculty of Sciences, Humanities and Education

POLING OF PZT CERAMICS

Author: Tetyana Malysh
Study program: P 3901 – Applied sciences in engineering
(Aplikované vědy v inženýrství)
Specialization area: 3901V012 – Physical engineering (Fyzikální inženýrství)
Department: Department of Physics,
Faculty of sciences, humanities and education,
Studentská 2, 461 17 Liberec 1
Supervisor: Prof. Mgr. Jiří Erhart, Ph.D.

Work extent:

| | |
|-----------------------|------------|
| Number of pages: | 118 |
| Number of figures: | 100 |
| Number of tables: | 17 |
| Number of equations: | 08 |
| Number of appendixes: | 07 |

Abstract

Poling of PZT ceramics

The work deals with the investigation of poling conditions and their influence on soft and hard PZT ceramics samples with different geometry. The literature overview describes poling dynamics of ferroelectric crystals and ceramics. Experimental part of work is connected with detailed study of poling methods with different orientation of applied electric field and their further impact on electromechanical properties of PZT ceramics. Electric field applicability limits were measured by the resonant methods for D.C. and pulse electric field de-poled PZT ceramics. Temperature dependences of remnant polarization and coercive field were observed for PZT ceramics during hysteresis loop measurement. Polarization reversal in PZT ceramics was studied during observation of switching current. The temperature and electric field influence on switching current and coercive field values was investigated.

Keywords: PZT ceramics, poling, switching current, hysteresis loop.

Statement

I am aware that my Ph.D. work is fully covered by the Act No. 121/2000 Coll. Copyright, in particular §60 - the school thesis.

I note that the Technical University of Liberec (TUL) does not interfere with my copyrights by using of my Ph.D. thesis for internal use of TUL.

If Ph.D. thesis or the license to use will be provided, I am aware of the obligation to inform TUL about this fact; in this case TUL has the right to demand the overhead costs, which it has incurred in the creation of the work, until their actual amount.

Ph.D. thesis was created by me personally using referenced literature and consultations with supervisor.

Liberec

.....

Tetyana Malysh

Acknowledgements

I would like to extend sincere thanks to supervisor of my Ph.D. Thesis Prof. Mgr. J. Erhart, Ph.D. for his professional managing, advices and patience. I also thank to Mgr. S. Panoš, Ph.D. for his help and experimental software support. Finally I thank my family for their patience and understanding.

Tetyana Malysh

Abstrakt

Polarizace PZT keramiky

Práce pojednává o studiu polarizačních podmínek a jejich vlivů na měkkou a tvrdou PZT keramiku pro vzorky různé geometrie. V rešeršní části jsou popsány polarizační dynamiky feroelektrických krystalů a keramik. Experimentální část práce je spojena se studiem polarizačních metod, které mají různé orientace aplikovaných elektrických polí. Změna elektromechanických vlastností PZT keramiky je analyzovaná v závislosti na druhu aplikovaných polarizačních metod. Elektrické limity použití byly změřeny rezonanční metodou pro D.C. a pulzně depolarizovanou keramiku. Měření hysterezních smyček sloužilo ke zjištění teplotní závislosti remanentní polarizace a koercitivního pole u PZT keramiky. Průběh polarizačního procesu v PZT keramice byl studován za pomoci snímání přepolarizačního proudu. Z naměřených dat a jejich následného vyhodnocení tak lze určit vliv teploty a elektrického pole na přepolarizační proud a koercitivní pole.

Klíčová slova: PZT keramika, polarizace, přepolarizační proud, hysterezní smyčka.

Аннотация

Поляризация сегнетоэлектрической керамики

Работа посвящена исследованию условий поляризации и их влияния на образцы из мягких и твердых видов керамики с различной геометрией. Теоретический обзор литературы описывает динамику поляризации сегнетоэлектрических кристаллов и керамики. Экспериментальная часть работы связана с детальным изучением методов поляризации. Рассматриваются различные направления используемых электрических полей при поляризации и их дальнейшее влияние на электромеханические свойства сегнетоэлектрической керамики. Граничные величины применяемого электрического поля измерялись резонансными методами для постоянного и импульсного электрического поля переполаризованной керамики. Температурная зависимость остаточной поляризации и коэрцитивного поля наблюдались при измерении петли гистерезиса. Изучение изменения направления поляризации сегнетоэлектрической керамики проводилось с помощью переполаризовательного тока. Исследована температура и воздействие электрического поля на ток коммутации и коэрцитивного значения поля.

Ключевые слова: сегнетоэлектрическая керамика, поляризация, ток коммутации, петля гистерезиса.

List of equations

- 1 Maximum value of switching current
- 2 Sideways motion velocity of domain walls
- 3 Activation field dependence on crystal thickness
- 4 Parameter δ dependence on crystal thickness
- 5 Equation of motion
- 6 Maxwell's equation
- 7 Equation of state
- 8 Relative changes formula

List of tables

- 1.1.1. Symmetry relationships of piezoelectricity, pyroelectricity and ferroelectricity and some ferroelectric materials
- 3.1.1.1 Some typical electrical and mechanical limits
- 3.1.4.1 Some properties of grain-oriented PbNb_2O_6 made by FDC
- 4.1.1 Basic properties of PZT ceramics
- 4.4.1 Material properties of poled PZT ceramics before depoling
- 4.4.2 Electric field applicability limits for soft PZT ceramics
- 4.4.3 Relative changes (in %) of material coefficients for hard PZT ceramics
- 4.5.1 Material properties of poled PZT ceramics before re-poling
- 4.6.1 Cross-poling experiment structure
- 4.6.2 Material of control samples (LE and TE mode)
- 4.6.3 Material properties after cross-poling (LE and TE mode)
- 4.6.4 Material properties of control samples (TS mode)
- 4.6.5 Material properties after cross-poling (TS mode)
- 4.7.1 Spontaneous polarization calculated values for different PZT ceramics. Data from i_{max} pulse poling at RT
- 4.7.2 Electric field related to i_{max} for different PZT ceramics. Data from pulse poling.
- 4.8.1 Spontaneous polarization and coercive field for PZT ceramics at RT. Data from hysteresis loops (frequency 10Hz)
- 4.8.2 Spontaneous polarization of APC850 ceramics at RT. Data from hysteresis loops

Contents

| | |
|--|-----|
| 1. Introduction | 1 |
| 1.1 Introduction | 1 |
| 1.2 Different types of domain state reorientation | 3 |
| 1.3 Velocity of domain walls | 7 |
| 1.4 Goals of Ph.D. thesis | 8 |
| 2. Poling dynamics of ferroelectric crystals | 11 |
| 2.1 Barium titanate | 11 |
| 2.2 Lithium niobate | 12 |
| 2.3 Lithium tantalate | 17 |
| 2.4 Lead germanate | 18 |
| 2.5 Potassium niobate | 20 |
| 3. Poling of ferroelectric ceramics | 23 |
| 3.1 External fields and microstructure influence on the electromechanical properties of PZT ceramics | 23 |
| 3.2 Lead zirconate titanate (PZT ceramics) | 41 |
| 3.3 Lead lanthanum zirconate titanate (PLZT) ceramics | 48 |
| 4. Experimental procedure and results | 51 |
| 4.1 Samples material description | 51 |
| 4.2 Crystal orientation and material properties | 52 |
| 4.3 Resonance method | 53 |
| 4.4 De-poling method | 55 |
| 4.5 Re-poling method | 69 |
| 4.6 Cross-poling method | 75 |
| 4.7 Pulse poling method | 78 |
| 4.8 Hysteresis loops measurement | 88 |
| 4.9 Results discussion | 93 |
| 5. Conclusions | 95 |
| Literature | 97 |
| Appendix I - Parameters of impedance measurement | 105 |
| Appendix II - Length-extensional vibration of thin bar | 106 |
| Appendix III - Thickness-extensional vibration of thin plate | 107 |
| Appendix IV - Radial (planar) vibration of thin disc | 109 |
| Appendix V - Thickness-shear vibration of thin plate | 110 |
| Appendix VI - Other calculations | 111 |
| Appendix VII – Gauss fit method (OriginPro 8) | 113 |

| | |
|--------------------------------------|-----|
| Publications and presentations | 115 |
| Curriculum Vitae | 117 |

List of figures

- 1.2.1 Merz circuit to measure switching in a ferroelectric capacitor
- 1.2.2 Voltage trace (top), and current trace (bottom) showing the switching (solid line) and non-switching (dashed) components
- 1.2.3 Sawyer-Tower circuit for the polarization vs. electric field hysteresis measurement in ferroelectric materials
- 1.2.4 Typical hysteresis loop diagram
- 2.1.1 Dielectric spectra in BaTiO₃ crystal in [001] direction
- 2.1.2 Etching pattern of (001) surface of BaTiO₃ crystal: a) before poling, b) in step 3
- 2.2.1 Displacement current i and voltage U_k applied to LiNbO₃ crystal vs. time t
- 2.2.2 The spatial dynamics of a poling process 7,5 s after start
- 2.2.3 Schematic of the resultant inverted domain structures as a function of the empirical factor EF
- 2.2.4 SEM picture of surface domains revealed by HF/HNO₃ acid etching. The period of the domain inverted structure is 2.5 μm
- 2.2.5 A diagram of the calligraphic poling machine
- 2.2.6 Phase diagram of the LiO₂-Nb₂O₅ system
- 2.3.1 Optical micrographs of 180° domain walls in a) LiNbO₃ and b) LiTaO₃
- 2.4.1 Arising of domains at the primary domain wall during partial switching from the multidomain state. Delay from the front of switching voltage pulse: A-0; B- 40 ms. Scale bar – 100 μm
- 2.4.2 Microphotographs of domains arising during the switching process in the same PGO sample: A – hexagonal domains; B – irregular-shaped domains; C– trigonal domains; D – schematic of regular shape domains of PGO single crystal
- 2.5.1 Concepts of electric poling: (a) Polarization vector poling; (b) Differential vector poling concept
- 2.5.2 Schematic view of experimental setup
- 2.5.3 Optical microscope image of $(10\bar{1})_{pc}$ plane at generated domain boundary
- 3.1.1.1 Piezoelectric coefficient d_{31} as a function of static pressure perpendicular to the polar axis (samples – bars: APC 840, 841, 850, 856, 880)
- 3.1.1.2 d_{31} and d_{32} vs. lateral stress perpendicular to the polar axis
- 3.1.1.3 The dependence of d_{33} coefficient (sample – ring APC 850) from cyclic stress application along the polar axis
- 3.1.1.4 The dependence of d_{33} on the compressive stress T_3 while under the 5kV/cm DC bias electric field that is parallel to the original poling direction for PZT-5H
- 3.1.1.5 Variation of piezoelectric strain constants with hydrostatic pressure
- 3.1.1.6 Variation of permittivity with hydrostatic pressure
- 3.1.2.1 Schematic of the measurement system for determining the various piezoelectric coefficients

- 3.1.2.2 Piezoelectric d coefficients of two types of PZT as a function of an applied 100 Hz AC electric field
- 3.1.2.3 AC field dependence of d_{33} (a) and soft (b) PZT under negative DC bias fields
- 3.1.2.4 DC bias dependence of d_{33} for PZT at various frequencies
- 3.1.3.1 PZT coupling factor k_{31} and strain coefficient d_{33} versus temperature
- 3.1.3.2 Temperature dependences of the real and imaginary parts of (a) piezoelectric constant, (b) dielectric constant, and (c) elastic compliance
- 3.1.3.3 Temperature dependences of the (a) remanent polarization P_r , (b) electromechanical coupling factor, and (c) mechanical quality factor
- 3.1.4.1 SEM micrographs of template particles grown by molten salt or hydrothermal synthesis methods
- 3.1.4.2 Unipolar strain–electric field curves of PMN–32.5PT ceramics containing 5 vol% BaTiO₃ templates (PMN–32.5PT–5BT) displaying various degree of texture
- 3.1.4.3 Low-field (< 5 kV/cm) d_{33} coefficients measured from unipolar strain–electric field curves of ~90% textured PMN–32.5PT–5BT ceramics and a random PMN–32.5PT ceramics measured up to maximum unipolar fields between 1 and 50 kV/cm
- 3.1.5.1 Dielectric susceptibility of BaTiO₃ as a function of grain size
- 3.1.5.2 Permittivity of barium titanate ceramics obtained by different methods
- 3.1.5.3 P-E hysteresis curve of the PLZT ceramics with various grain sizes
- 3.1.5.4 Relationships between the remnant polarization and applied electric field at different grain sizes. The values are obtained by the P-E hysteresis measurement
- 3.1.6.1 Etched surface of BaTiO₃ ceramics herringbone and square net pattern
- 3.1.6.2 (a) Surface charge associated with spontaneous polarization; (b) formation of 180° domains to minimize electrostatic energy
- 3.1.6.3 Detwinning process observed during heating of the BaTiO₃ specimen. The heating direction is (a) parallel and (b) perpendicular to the band walls
- 3.2.1 Phase stabilities in the system Pb(Ti_{1-x}Zr_x)O₃
- 3.2.2 Change in the relative dielectric constant (measured from the slope of P-E curves as E field passed through 0 kV/mm) with increasing preload stress
- 3.2.3 Schematic sketch of a cut through the sample holder used for electromechanical poling
- 3.2.4 Remnant polarization P_r (a) and piezoelectric coefficient d_{33} vs. poling field for three poling protocols
- 3.2.5 Time dependence of polarization for the PZT, PZTN, and PZTF obtained from switching integration while applying and after removing a poling electric field
- 3.2.6 Bipolar pulse for the measurement P-E hysteresis in PZT ceramics and generation of space charge field by applying bipolar pulses
- 3.2.7 1) Comparison of ferroelectric properties in (a) soft and (b) hard PZT ceramics between pulse poling (○) and DC poling (●). 2) Bipolar pulse cycle dependence of k_p when the pulses were applied to (1) as-fired and (2) DC poled (a) soft and (b) hard PZT ceramics

- 3.2.8 Typical indentation cracks under an indent load of 49 N on polished side surfaces of (a) unpoled and (b) poled PZT samples
- 3.2.9 Poling directions
- 3.3.1 a) PLZT 8/65/35 and b) PLZT 12/40/60 P_r for different poling
- 4.1.1 Disc and bar samples used for depoling
- 4.1.2 Depoling – a) re-poling – b) cross-poling – c) methods
- 4.2.1 Piezoelectric constant d_{33} of tetragonal (a) and (b) rhombohedral PZT
- 4.3.1 Four terminal pair measurement principle
- 4.4.1 Poling experimental setup
- 4.4.2 Depoling voltage D.C. and pulse shapes
- 4.4.3 Scheme of resonant spectrum measurement
- 4.4.4 Piezoelectric charge constant d_{33} after depoling: a) by D.C. and b) after voltage pulses applied for bar samples
- 4.4.5 Piezoelectric charge constant d_{31} after depoling: a) by D.C. and b) after voltage pulses applied for bar samples
- 4.4.6 Electromechanical coupling factor k_{31} after depoling: a) by D.C. and b) after voltage pulses applied for bar samples. Data missing in curves for APC850 and APC856 are due to the non-resonant response of samples
- 4.4.7 Electromechanical coupling factor k_p after depoling: a) by D.C. and b) after voltage pulses applied for disc samples. Data missing in curves for APC850 and APC856 are due to the non-resonant response of samples
- 4.4.8 Electromechanical coupling factor k_t after depoling: a) by D.C. and b) after voltage pulses applied for bar samples
- 4.4.9 Elastic compliance s_{11}^E after depoling: a) by D.C. and b) after voltage pulses applied for bar samples
- 4.4.10 Poisson's ratio after depoling: a) by D.C. and b) after voltage pulses applied for disc samples. Data missing in curves for APC850 and APC856 are due to the non-resonant response of samples
- 4.4.11 Elastic modulus c_{33}^E after depoling: a) by D.C. and b) after voltage pulses applied for bar samples
- 4.4.12 Permittivity ε_{33}^T after depoling: a) by D.C. and b) after voltage pulses applied for disc samples
- 4.5.1 Samples used in re-poling experiment
- 4.5.2 Plate samples design for TS mode measurement
- 4.5.3 Electric field dependence of electromechanical coupling factor k_{15} (plate sample)
- 4.5.4 Electric field dependence of permittivity ε_{11}^T (plate sample)
- 4.5.5 Electric field dependence of elastic stiffness c_{55}^E (plate sample)
- 4.5.6 Electric field dependence of piezoelectric coefficient d_{15} (plate sample)
- 4.5.7 Electric field dependence of free permittivity ε_{33}^T (disc sample)
- 4.5.8 Electric field dependence of planar electromechanical coupling factor k_p (disc sample)
- 4.5.9 Electric field dependence of thickness electromechanical coupling factor k_t (disc sample)
- 4.5.10 Electric field dependence of Poisson's ratio σ (disc sample)

- 4.5.11 Electric field dependence of transversal electromechanical coupling factor k_{31} (disc sample)
- 4.5.12 Electric field dependence of elastic stiffness c_{33}^E (disc sample)
- 4.7.1 Scheme of pulse poling measurement
- 4.7.2 Current and applied electric field curves observed for APC856 at 50°C
- 4.7.3 Gaussian fitting of current spectrum for APC856 at RT. Applied pulse field amplitude was $\pm 4\text{kV/mm}$
- 4.7.4 Switching current curve of APC850 ceramics at 2kV/mm applied field and 100°C
- 4.7.5 Change in $\ln(i_{\max})$ vs. $1/E$ in PZT ceramics. Dashed curves are linear fit
- 4.7.6 Reciprocal switching time t_s vs. electric field for different PZT ceramics. Dashed curves are linear fit
- 4.7.7 Change in $\ln(i_{\max})$ vs. $1/E$ as a function of temperature - soft PZT, APC850. Dashed curves are linear fit
- 4.7.8 Change in $\ln(i_{\max})$ vs. $1/E$ as a function of temperature - soft PZT, APC856. Dashed curves are linear fit
- 4.7.9 Change in $\ln(i_{\max})$ vs. $1/E$ as a function of temperature - hard PZT, APC840. Dashed curves are linear fit
- 4.7.10 Change in $\ln(i_{\max})$ vs. $1/E$ as a function of temperature - hard PZT, APC841. Dashed curves are linear fit
- 4.7.11 Temperature dependence of P_s for APC856 ceramics measured from i_{\max} pulse poling
- 4.7.12 Temperature dependence of P_s for APC850 ceramics measured from i_{\max} pulse poling
- 4.7.13 Temperature dependence of P_s for APC841 ceramics measured from i_{\max} pulse poling
- 4.7.14 Temperature dependence of P_s for APC840 ceramics measured from i_{\max} pulse poling
- 4.7.15 Temperature dependence of activation field in PZT ceramics. Data from i_{\max} pulse poling
- 4.8.1 Experimental scheme of hysteresis loops measurement
- 4.8.2 Hysteresis loops of APC856 ceramics measured at different temperatures and 10Hz
- 4.8.3 Temperature dependence of spontaneous polarization P_s for PZT ceramics. Data from hysteresis loops
- 4.8.4 Temperature dependence of coercive field E_c for PZT ceramics. Data from hysteresis loops
- 4.8.5 Hysteresis loops of different PZT ceramics measured at RT and 10Hz
- 4.8.6 Hysteresis loops of APC850 ceramics measured at different frequencies and RT

Chapter 1. Introduction.

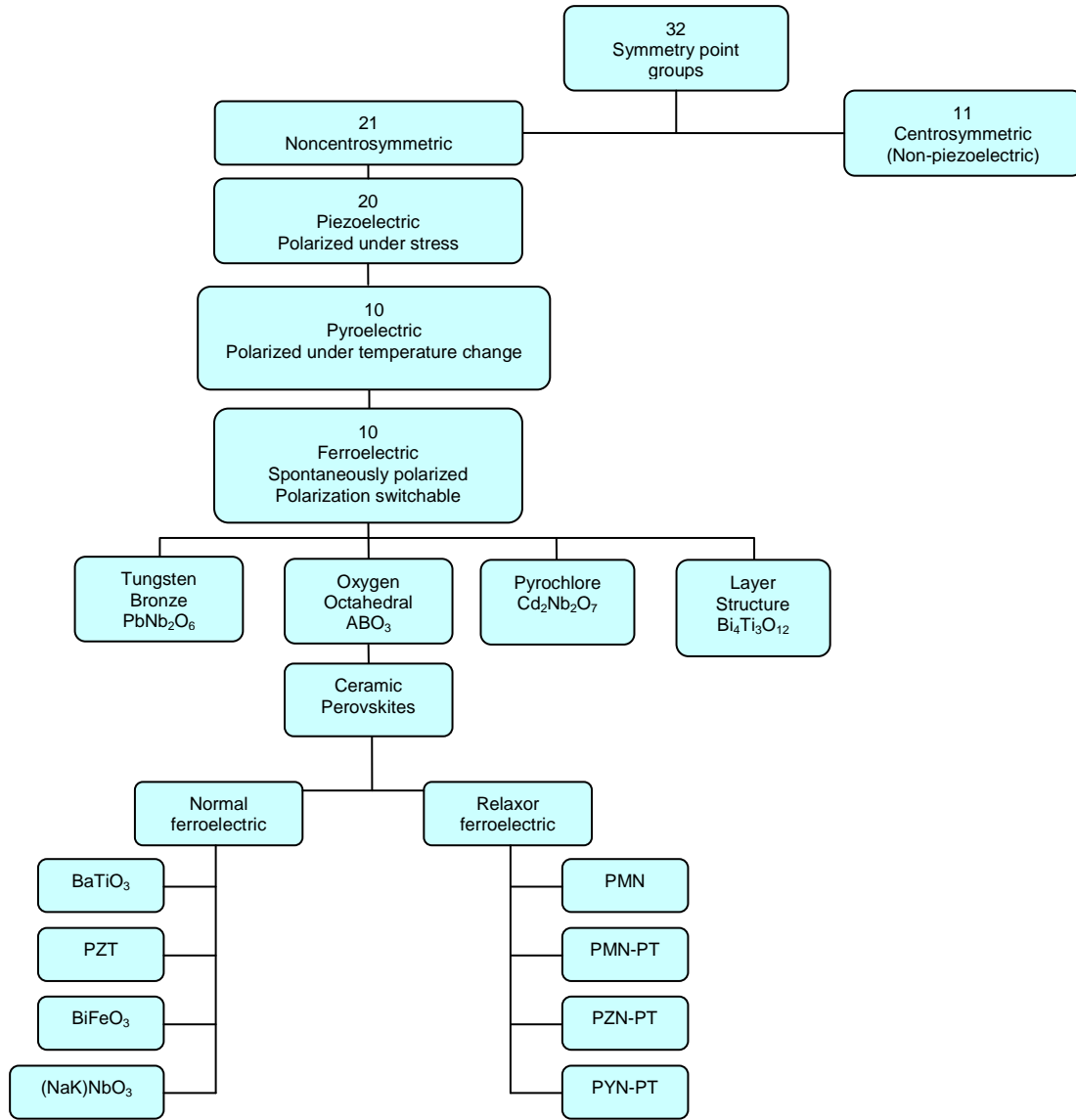
1.1. Introduction.

Ferroelectric materials are applied in a wide range of fields including, for example, industrial process control (high displacement actuators) [1], information systems (ferroelectric thin-film memories), medicine (diagnostic transducers, ultrasonic cleaners) [2], environment monitoring (piezoelectric sonar) and in communications (surface acoustic wave filters) [3]. Applied materials include single crystals, bulk ceramics, multi-layer ceramics, thin films, polymers and ceramic-polymer composites. All ferroelectric materials are pyroelectric and piezoelectric.

Since the ferroelectricity discovery in single crystal materials (Rochelle salt, 1921 [4]) the technical production of ferroelectric materials has began because of their unique properties such as high piezoelectric constants and electromechanical coupling, high pyroelectric coefficients and high optical transparency and electro-optic coefficients under certain conditions [5]. High dielectric permittivity was observed in BaTiO_3 .

Piezoelectric ceramics belong to the group of ferroelectric materials. Material is piezoelectric if external mechanical stress induces electrical polarization, i.e. electric charge on the surface. The electrical response on external mechanical influence is called the direct piezoelectric effect. The mechanical response to electric field is called the converse piezoelectric effect [6]. Ferroelectrics are a subgroup of pyroelectric (Tab.1.1.1) materials [7]. Ferroelectric materials possess spontaneous dipole moments which are reversible by an electric field of the magnitude less than the dielectric breakdown field of material. So, there are two conditions needed for material definition as ferroelectrics: spontaneous existence of polarization (P_s) and demonstrated reorientation of the polarization. Spontaneous polarization (vector) can be reoriented between several possible equivalent directions (determined by the crystallography of ferroelectric species) by appropriately oriented electric field. The required field must be below the breakdown electric field. Ferroic state may be considered as a result of structural phase transition from parent (higher symmetry, paraelectric) phase to ferroic (lower symmetry, ferroelectric phase) [8]. Ferroelectric species are defined by the symmetry of both parent and ferroic phase, e.g. $m\bar{3}m \rightarrow 4mm$ for ferroelectric tetragonal phase of BaTiO_3 .

Ferroelectric materials show hysteresis effects in the relation between electric displacement (D) and electric field (E). This behaviour is observed within certain temperature range limited by the Curie point. Crystals are not ferroelectric above Curie temperature (no dipoles are present) and they behave as non-polar dielectrics (transition to paraelectric phase). The phase transition occurs due to small displacement of some ions from their centre-symmetric position.



Tab.1.1.1. Symmetry relationships of piezoelectricity, pyroelectricity and ferroelectricity and some ferroelectric materials [7].

Continuous regions with the same P_s orientation in crystal are called ferroelectric domains. Domain boundaries are domain walls, which have typical thickness of 1-2 unit cells [9]. Criteria for derivation of permissible domain wall orientations in ferroelectric materials were described by Fousek and Janovec [10]. Oriented states with the same crystal structure, but different direction of the spontaneous polarization at zero applied electric field are called domain states. The crystal splitting into domain regions corresponds to minimization of electrostatic energy of the system. The direction of the spontaneous polarization is called the polar axis. If there are several equivalent directions of spontaneous polarization in ferroelectrics, spontaneous polarization will be oriented in the direction, which creates the least angle with the direction of the applied electric field strong enough to reorient polarization. The application of electric field to the sample and reorientation of domains inside grains in the direction of the field is called poling. Random orientations of P_s directions in single grains will be aligned in the direction of electric field in case of polycrystalline PZT ceramics. As a result, macroscopic

electrical dipole moment will occur. Maximum net polarization was calculated in [11] as a fraction of single-grain P_s polycrystalline ferroelectrics. Result integral for polarization determination was evaluated for non-polar and polar crystal classes.

Number of domain states is limited by ferroelectric species but actual domain structure in the sample is determined by the boundary conditions (electric and elastic), crystal size, defect structure, applied forces and the sample's history (how the sample was treated before observation). Typical dimensions of domains are between 0.1 and 100 μm in multi-domain samples, but might be up to 1-10 cm range in single crystals (LiNbO_3). Domain walls have the typical thickness of 1 to 10 lattice parameters. Aggregates of domains form domain structures which may be rather complicated. If sample exists in one of these domain states, it is in single-domain state. In finite sample of ferroelectric material, domain states can coexist in spatially defined regions and these are multidomain samples. Single-domain crystal may be produced by heating sample above the Curie temperature and subsequent cooling under the applied external electric field. Domains and domain walls behaviour is very important to ferroelectric materials due to impact on their macroscopic properties. For example, alignment of the polar directions of ferroelectric domains is essential for piezoelectric activity in poled ferroelectric ceramics. Periodically poled crystals are used in nonlinear optical materials (the width of the inverted domains controls the desired wavelength of operation). Domain walls and their dynamics contribute to the high permittivity of ferroelectrics which is used in capacitors. Dynamics of domain walls influence also the piezoelectric response of actuators and transducers.

From the crystallographic point of view the most important piezoelectric materials belong to so called perovskite crystalline structure [12]. In perovskites such as barium titanate or lead zirconate titanate, it is common to observe "herringbone" domain substructures [13], characteristic for hierarchical domain structure. Domain structure can be observed optically, by chemical etching, by local piezoelectric or pyroelectric response, specialized scanning probe microscopies, etc.

The main commercially used piezoceramics today – solid solution $\text{Pb}(\text{Zr,Ti})\text{O}_3$ - are synthesized from the oxides of lead, titanium and zirconium. Special doping of lead zirconate – lead titanate ceramics (PZT) with Fe, Na, Nb ions etc., gives the possibility to adjust individual piezoelectric and dielectric parameters according to customer needs. Acceptor doped (Fe, Na) PZT ceramics are called „hard“ PZT. Created internal field in hard PZT stabilizes the domain configuration and decreases the mobility of domain walls. Hard PZT ceramics piezoelectric constants are lower, coercive field and mechanical quality factor is higher. Donor doping (Nb, La) have the opposite influence on material properties of PZT ceramics („soft“ PZT). Piezoelectric constants and permittivity are higher, mechanical quality factor is reduced.

1.2. Different types of domain state reorientation.

Domain state reorientation terminology is used when speaking about transitions between two domain states. When the reorientation is between ferroelectric domain states with different P_s vectors, the process is called polarization reorientation. When both P_s vectors are antiparallel the process is called polarization reversal. Domain state reorientation may occur in the whole sample or in its part. Therefore full or partial reorientation (or switching) can exist.

Domain structure of the material may be changed by application of electric field, mechanical stress or temperature gradient [14], [15], [16]. Geometrical preference for the direction of spontaneous polarization is the direction along the applied electric field. According to Curie's principle spontaneous polarization direction is preferred in the plane perpendicular to the direction of mechanical stress application. It is possible to change the preferred direction of P_s by using different dopants (Fe, Co, etc.). Sometimes there is a situation when the reversal process is not possible (e.g. potassium iodate KIO_3 with no antiparallel domain states, species $3m \rightarrow 1$) or some materials exist with preferred direction of spontaneous polarization like L-alanine doped triglycine sulfate (TGS, where P_s is given by crystallography of chemical bond, species $2/m \rightarrow 2$).

It is possible to observe two thermodynamically saturated states for uniaxial ferroelectric single crystal (crystal is uniaxial when it has only one axis for P_s orientation dependent on ferroelectric species) placed in a capacitor with the ferroelectric axis parallel to the direction of applied electric field. These states are represented by spontaneous polarizations $+P_s$ and $-P_s$. The response of the sample depends also on the waveform of applied field. It can be unipolar pulse, set of pulses of alternating polarity, AC field, etc. For example, the crystal response to single pulse and to DC field was observed in Merz circuit (Fig.1.2.1) [17]. The voltage across the small resistor in series with the sample gives the opportunity to observe the current flow. If the process of polarization reversal takes place the typical shape of the switching current is shown in Fig. 1.2.2. The charge density transferred during polarization reversal is equal to $2P_s + \Delta P$, where ΔP is the induced polarization under the applied DC field. The i_{max} and t_s values are dependent on the electric field amplitude.

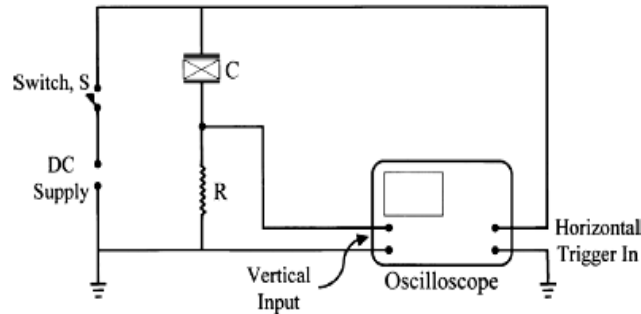


Fig.1.2.1. Merz circuit to measure switching in a ferroelectric capacitor [17].

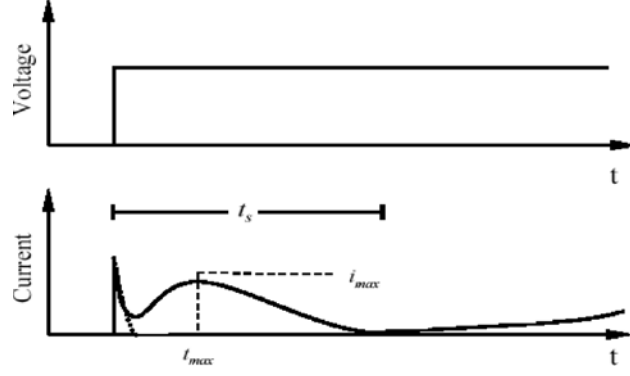


Fig. 1.2.2. Voltage trace (top), and current trace (bottom) showing the switching (solid line) and non-switching (dashed) components [17].

The switching time t_s is defined as a time needed to decrease the current to the certain fraction of maximum current value i_{max} , for example to 5% of it. For antiparallel domain reorientation it was found in case of BaTiO₃ [18]:

$$i_{max} = i_0 \exp(-\alpha/E) \text{ or } t_s = t_0 \exp(\alpha/E) \quad (1)$$

where α is the activation field for switching.

There is the alternative scheme (Sawyer-Tower circuit – Fig. 1.2.3) for the observation of polarization reversal – hysteresis loop, during switching of the crystal with a low frequency [19]. This method defines the dependence of polarization on the applied field and shows the maximum polarization P_{sat} and the remanent polarization P_r (Fig. 1.2.4). The value of P_{sat} or P_r depends on the frequency and amplitude of the applied voltage. It is possible to detect clearly the coercive field (E_c). A typical value of E_c considered for single crystals and ceramics is in the range from 10^4 to 10^6 V/m.

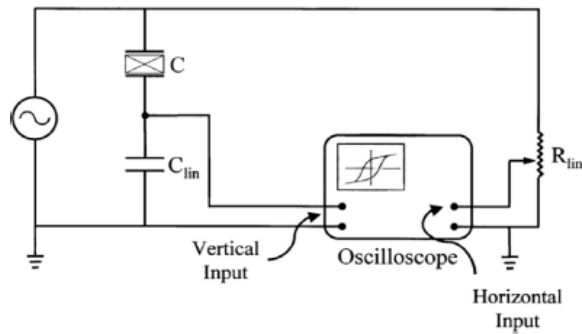


Fig. 1.2.3. Sawyer-Tower circuit for the polarization vs. electric field hysteresis measurement in ferroelectric materials [17].

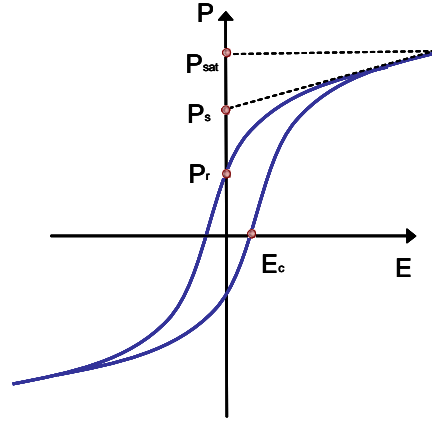


Fig. 1.2.4. Typical hysteresis loop diagram.

Processes in the ferroelectric sample, which define the shape of the switching current or hysteresis loop and characteristics like t_s or E_c , depend on material.

Area of hysteresis loop represents the quantity of dielectric energy loss density after running one full hysteresis loop cycle. This will affect the size of the loop. For example, “hard” piezoelectric ceramics has more rectangular hysteresis loop. “Soft” ceramics has less rectangular loop [20]. Shape of hysteresis loop depends also on loop rate frequency. Loop is slimmer at higher frequencies. Comparison of single crystal and ceramics form of the same material shows that ceramics has usually higher coercive field and lower remanent polarization. Saturated polarization of the sample will appear under high values of electrical field with saturated DW movements. Domain walls movement occurs mainly under lower fields (close to E_c value). The rectangular shape of hysteresis loop was explained by the sideways expansion of domains growing from fixed residual nuclei [21].

There are two different cases for ferroelectric single crystals: when P_s reverses its sign (180° processes) or processes with more domain states involved than only those with antiparallel P_s . 180° reorientation is the only reorientation possibility in uniaxial ferroelectrics, but 180° domain reversals can also occur in multiaxial ferroelectrics when the antiparallel domain states are involved. Polarization reversal starts with a nucleation process (i.e. formation of small domain nuclei). They grow by forward and sidewise movement of domain walls. This reversal stage shows at the steep shoulders of the hysteresis loop. It is further followed by combination of domains when P achieves its saturated value. Finally the single domain state will be reached.

If another reorientation of polarization is allowed by crystal symmetry (not only 180°), the switching process will be rather complicated. It will be influenced by electrical and mechanical boundary conditions. These processes involve motion of non- 180° walls and these walls are always ferroelastic. Such kind of local changes of strain take place in parts of the crystal traversed by these walls.

Ferroelectric domain walls interact with structural defects. Application of electric field is necessary to move the pinned wall from its position. Assemblies of defects may lead to the preference in P_s orientation through the whole region. Material behaves as under internal electric bias. These interactions of domain walls with defects and the internal bias may influence the shape of the loop and other processes. Defects may impel the existence of frozen-in nuclei (small regions with the preferred direction of P_s which is never changed and which serves as cores for

the reorientation process). Defects with preferred particular orientation of P_s can undergo the backswitching [17, 22].

The ferroelectric material domain structure untwisted after traversing hysteresis loop may not be stable in time. The process of material property change in time without influence of external fields (electric field, stresses or temperature changes) is called aging. It is the result of pinning of domain walls by local fields (dipole alignment due to lattice defect influence, change in the resolution of internal deformations caused by crystal anisotropy or defects accumulation on domain walls).

1.3. Velocity of domain walls.

The measurements of the sideways velocity of domain walls define an exponential dependence of the velocity upon the applied field in BaTiO₃ crystals [23] in the form:

$$v = v_{\infty} \exp\left(-\frac{\delta}{E}\right) \quad (2)$$

where the value of δ , was found to be nearly equal to the value of the activation field α for metal-electroded crystals. Parameter α depends on the crystal thickness as it was given by Merz [24] in the following equation (see Eq. 1):

$$\alpha = \alpha_{\infty} \left(1 + \frac{d_0}{d}\right) \quad (3)$$

where α_{∞} is the value of activation field α for very thick crystal, d is the crystal thickness and d_0 is approximately equal to 10^{-2} cm. Switching time/current is proportional to $\exp(-\alpha_{\infty}/E_b)$, where E_b is the actual field existing in the bulk of the crystal. E_b is smaller than the average applied field E because the dielectric constant of the surface layer is considered to be smaller than in the bulk. Therefore an appreciable portion of the applied voltage lies across the surface layer. The thickness of this layer was of the order of 10^{-4} – 10^{-5} cm according to Merz's estimate.

Miller and Savage defined, that parameter δ depends on the thickness of BaTiO₃ crystal in the following way:

$$\delta = \delta_{\infty} \left(1 + \frac{d_0}{d}\right), \quad (4)$$

where $d_0 = 5 \times 10^{-3}$ cm. The similarity of these results (Eqs. (3) and (4)) becomes significant when we compare applied fields in both experiments. Fields used by Merz were higher than by Miller and Savage. The longest switching time measured by Merz was about 10msec, while the shortest switching time measured by Miller and Savage was 1sec.

1.4. Goals of Ph.D. thesis.

There are some main reasons for poling conditions improvement, which make the push effect for thesis creation. First one is the achievement of desired value of material properties including the aging behaviour. Second one is reduction of production costs for ceramics products (PZT components amount decrease), and possible poling temperature decrease.

Main practical aims of these Ph.D. theses are:

- try to find optimal poling conditions for inspected ceramics material,
- observe the influence of different poling methods on material properties (various sample geometry),
- study of poling dynamics in PZT ceramics (switching current behavior),
- analyze electric field influence on material properties of PZT ceramics.

This work is connected with investigation of PZT ceramics poling conditions and its influence on material properties of samples with different geometry.

Introductory part of this work represents an overview of ferroelectric materials theory, their main characteristics including domain state reorientation types and velocity of domain walls. Basic definitions used in theory of ferroelectric materials are described in introduction to unify such items for further application.

Chapter II and Chapter III describe the theoretical study of poling dynamics in ferroelectric crystals and ceramics respectively. Investigation of current status of poling procedure in case of different materials helps to understand background of this topic. Poling conditions influence of PZT ceramics material properties were analysed in literature in consequence with the further ceramics applications. Such literature study did not only map the actual state of topic but also help to establish some of initial conditions for future experimental work. Material properties depend on manufacturing parameters, doping and electrical poling. Mainly this information was used as basis for further investigation. Poling is related to the microstructure (grain size), ferroelectric domain structure and switching behaviour. The current displacement observation was used for the poling dynamics definition on ferroelectric crystals example. The domain structure of crystals was described and domain switching kinetics gave the first facts to explain the more complicated polarization in the case of ceramics materials.

The complete experimental procedure is described in Chapter IV. The experiment consists of two main research topics: 1) investigate the influence of poling conditions on material properties of samples after application of electric field; 2) poling dynamics study in PZT ceramics through switching current observation. First experimental topic includes the description of three methods of poling applied to the samples (de-poling, re-poling, cross-poling). To start the experimental work appropriate sample geometry has to be selected first. Thin bar, plate and disc geometry were chosen as suitable for resonance method of measurement. Sample dimensions were fitted to the measurement technique requirements. The poling conditions were selected to ensure the saturated material properties. Three poling methods were suggested to investigate completely the influence of poling conditions on material properties of PZT ceramics. These methods cover all possible orientations of electric field application on resonators with selected geometry. As a result, the optimum poling conditions for selected PZT samples were set up and electric field applicability limits of studied PZT ceramics were defined.

Switching current observation was connected with sample geometry definition and with voltage pulse waveform as well. Disc samples were selected for such experiment. Design of voltage pulse was selected after a lot of trials as the most suitable for such measurement. Bipolar triangular, square, trapezoidal pulses and their series were tested. Maximum switching current amplitude was observed for trapezoidal bipolar pulse. Pulse design was adjusted to the measurement conditions. The temperature and electric field influences on switching current value were demonstrated in this work. Values of spontaneous polarization were defined experimentally by nonlinear fitting of measured current curve with the Gaussian function. The hysteresis loop measurement was done to compare the results from pulse poling measurement. Values of spontaneous polarization were compared. The activation field value was defined.

Final chapter describes main conclusions of the experimental part and its contribution to the research field.

Chapter 2.

Poling dynamics of ferroelectric crystals.

It is very important to know the mechanisms involved in the polarization switching and conditions which may influence the material properties in ferroelectrics. Barium titanate (BaTiO_3) was the first crystal which was studied in details. Initially BaTiO_3 single crystals were studied by Merz [25]. Switching polarization was mainly described in terms of antiparallel domains nucleation followed by domains growth due to the domain walls motion. The investigation of such crystals gave the opportunity and methods for further study of other single crystals and ceramics.

2.1. Barium titanate (BaTiO_3).

BaTiO_3 single crystal (with sequence of ferroelectric phases $m\bar{3}m \rightarrow 4mm$ (P_s [001], 6 domain states (DS), domain walls (DW) $\{110\}$ 90° , 180°) or $m\bar{3}m \rightarrow mm2$ (P_s [110], 12DS, DW $\{100\}$, $\{110\}$, $\{11k\}$ S-walls) or $m\bar{3}m \rightarrow 3m$ (P_s [111], 8DS, DW $\{100\} + \{110\}$ 71° , 109° , 180°)) was very interesting for investigation due to its high dielectric permittivity. Piezoelectric and elastic coefficients were observed in [26] for single crystal barium titanate. Spontaneous polarization, dielectric constants and optical properties of these crystals were investigated in [27] as a function of temperature. Dielectric constant increased if domain walls are present and the piezoelectric effect decreased. Changes in dielectric constant were dependent also on changes in domain structure. Such behavior was observed in [28]. 90° and 180° domain walls existed in as-grown barium titanate single crystal prepared by the top-seeded solution growth (TSSG) method. In order to remove 90° domain walls sample was mechanically poled and only 180° domain walls remained. DC field was applied in [001] direction to the sample after that and growth of domains with P_s [001] was possible in the same direction as field. As a result polarizations were gradually aligned in the same direction as field and single domain state occurred. Stepwise poling was applied to the sample (500V/cm, 1kV/cm, 2kV/cm – all at RT, and 2kV/cm at 125°C). Resulted dielectric spectrum demonstrated several peaks due to electrical poling. Presence of antiparallel domains affects the piezoelectric oscillation before electrical poling. The positive and negative directions of domain orientation have the same volume. This equilibrium between antiparallel domains is destroyed by poling. Dielectric constant below the mechanical resonance includes the contribution of piezoelectric oscillation (unclamping). Such oscillations (clamping) do not contribute to the dielectric permittivity above piezoelectric resonances. Existence of domain walls increased the value of dielectric constant (Fig. 2.1.1) and

decreased the piezoelectric effect in barium titanate single crystal. Such changes are dependent on changes in domain structure. 180° domain walls were observed after etching by immersing the sample in concentrated HCl solution [29].

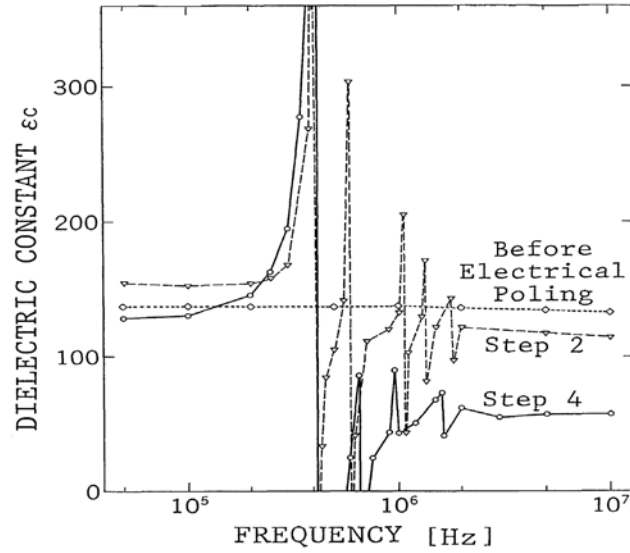


Fig.2.1.1. Dielectric spectra in BaTiO_3 crystal in $[001]$ direction [28].

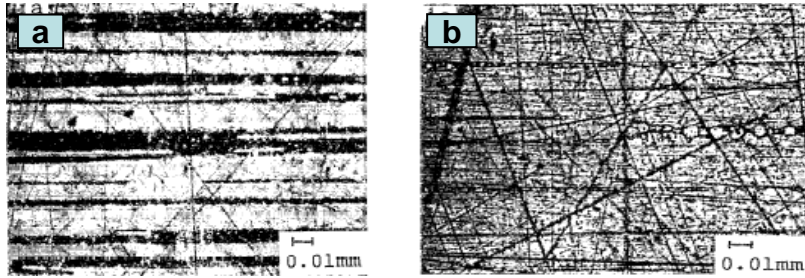


Fig.2.1.2. Etching pattern of (001) surface of BaTiO_3 crystal: a) before poling, b) in step 3 [29].

Sidewise motion of 180° domain walls in BaTiO_3 single crystal was described by two models [30]. Nucleation model described wall motion as the nucleation of triangular steps along existing 180° domain wall. Such assumption successfully explained a lot of data. This model predicts wall velocity $v = v_\infty \exp(-\delta/E)$. Second model (dislocation) had two restrictions. Crystal was treated as isotropic medium and influence of depolarizing energy was ignored. The presence of screw dislocation may affect the motion of domain walls. Such mechanism of domain walls propagation is similar to certain types of crystal growth.

2.2. Lithium niobate (LiNbO₃).

Periodically poled lithium niobate (ferroelectric species $\bar{3}m \rightarrow 3m$, P_s [001], 2DS, antiparallel DW 180°) crystals are used in different applications such as optical parametric oscillators [31] or second harmonic generators [32].

Creation of bulk periodically poled lithium niobate single crystals with antiparallel domain structure may be done during growth process by influence of electric field of alternating polarity. The period of the domains corresponds to the frequency of applied alternating electric current. Some limitations of period dimensions must be taken into account. They are defined by growth velocity and temperature accuracy [33]. Main merits of periodically poled lithium niobate structure production during crystal growth process are the possibility of obtaining thicker and wider structures and the elimination of the subsequent poling process.

Electric field poling through structured electrodes is the conventional method of producing periodically poled lithium niobate crystals. The main disadvantage of it is the small period length due to inhomogeneities of electric field.

The investigation example of the poling dynamics of LiNbO₃ is presented in [34] by an electro-optic observation technique. Observation of the displacement current may provide information about the poling dynamics and strictly define end of the poling process. But this method characterizes only integrated behavior of poling under the electroded area. On another hand the electro-optic interferometric method gives more details about the spatial dynamics of poling. The voltage was ramped linearly with time (15 V/s) on Z-cut LiNbO₃ crystals (15×15×0.5 mm³). After achieving the coercive field the domain inversion started. Charge redistribution in the crystal causes the displacement current occurrence. At the beginning of the poling process displacement current arose, but then it decreased almost to zero when the whole area had been poled (Fig. 2.2.1). The domain walls may be observed in the interference pattern when the voltage is applied. Switching started at some point and then randomly spread in the crystal.

These inversion seeds then grow along certain preferred crystallographic axis with three-fold symmetry.

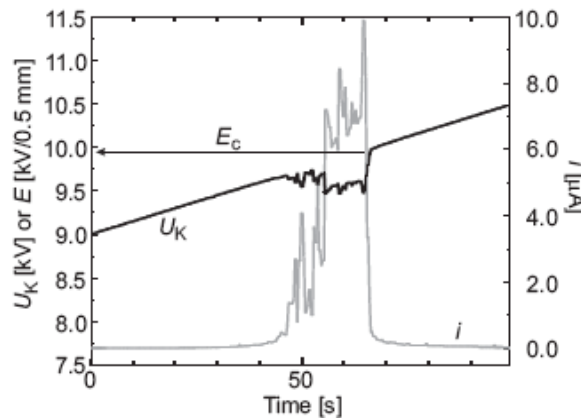


Fig.2.2.1. Displacement current i and voltage U_k applied to LiNbO₃ crystal vs. time t [34].

Poled area can be seen as a hexagon-shaped discontinuity within the interference rings in Fig.2.2.2. Poled area growth has been done step-wise during twenty seconds poling period. This kind of domain growth is explained not only by preferred domain walls orientation, but also by the repetitive reduction and increase of the electric field.

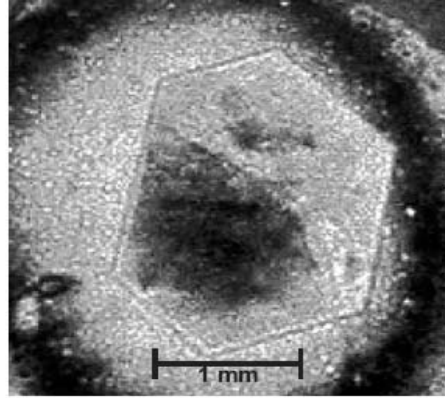


Fig. 2.2.2. The spatial dynamics of a poling process 7,5 s after start [34].

Production of high quality periodically inverted domain arrangement in bulk crystal is limited to longer periods due to high aspect ratio of instabilities. The successful fabrication of large scale uniform inverted domain gratings is usually limited to 6-10 μm in case of commercially available lithium niobate. The fabrication method of periodically inverted fine period ferroelectric domain distributions in lithium niobate crystals is based on conventional electric field (E -field) poling with an intentional “overpoling” step [35]. As in conventional E -field poling the crystal is covered with photolithographically patterned photoresist provided on one of the two Z faces. The patterned photoresist provides electric field contrast, so the areas with higher value of electric field than the coercive one will invert their polarity. In this experiment the voltage was controlled to keep the current constant. The amount of charge which is needed to invert domain of an area A is: $Q=2 \times A \times P_s$, where Q is the calculated charge, P_s is the spontaneous polarization of lithium niobate ($0.72 \mu\text{C}/\text{mm}^2$). External empirical factor (EF) must be considered for correction of the variations in supplier dependent material stoichiometry, precise values of thickness in the sample and specific electrical characteristics of the power supply. The modified calculated Q value is $2 \times A \times P_s \times EF$. The EF factor defines the sample state after poling. If the factor value is less than 1 the sample becomes underpoled. Only a portion of the patterned area is successfully domain inverted. Sample becomes overpoled if factor value is higher than 1. The sample appears uniformly poled regardless of any initial photoresist patterning.

Domain inversion as a function of EF is shown in Fig. 2.2.3. When EF is equal to 1, good quality of domain inversion can extend through the crystal. If EF is higher than 2, complete domain inversions has occurred with exception of the small regions directly under the photoresist which have the original polarization state. It is possible due to the presence of compensating charges, which are trapped between the insulating photoresist and lithium niobate surface. A local electric field occurred in the direction opposite to the externally applied field.

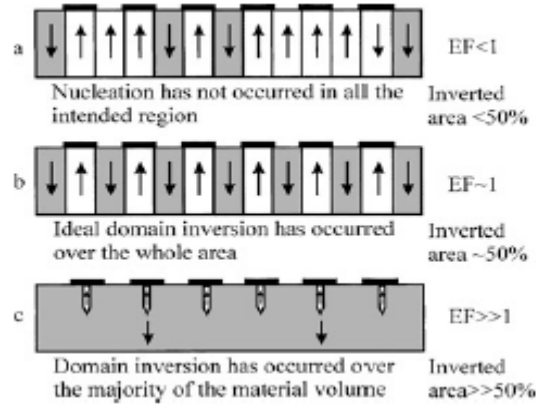


Fig. 2.2.3. Schematic of the resultant inverted domain structures as a function of the empirical factor EF [35].

Poled areas are observed unevenly distributed across the surface in the underpoling state. This happened due to domain nucleation which began from randomly distributed surface defects. In the overpoling state the sample shows a surface relief pattern corresponding to the initial photoresist period. Portion of the areas under the photoresist have carried their original polarization state. Figure 2.2.4 shows an SEM picture of an overpoled sample patterned with the period of $\sim 2.5 \mu\text{m}$ where the inverted ferroelectric domains have been made visible after etching in HF acid. The measurements show that the depth of the surface domains decreases with decreasing domain period. Domain periods down to $1 \mu\text{m}$ have so far been achieved using this method.

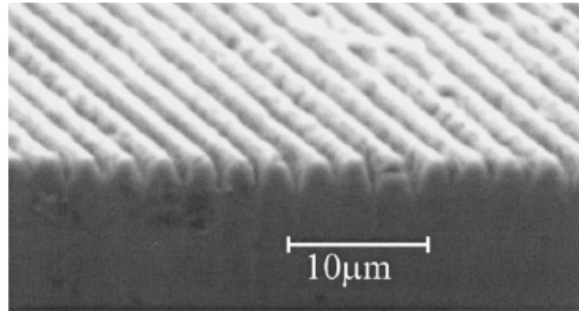


Fig. 2.2.4. SEM picture of surface domains revealed by HF/HNO₃ acid etching. The period of the domain inverted structure is $2.5 \mu\text{m}$ [35].

Calligraphic poling is one more method for domain engineering of LiNbO₃. Micron sized electrode which drags charge across the surface of the crystal causes domain reversal in real time (Fig. 2.2.5). In this method domain reversal occurs rather fast. This makes calligraphic poling useful for the measurement of domain wall growth and domain flipping dynamics [36]. Domain reversal takes place locally under the pen's position. The arrows represent the polarization direction for local regions on the crystal.

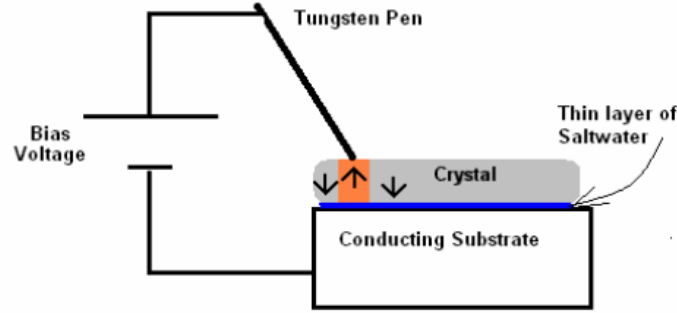


Fig. 2.2.5. A diagram of the calligraphic poling machine [36].

When the pen is in contact with the upper surface of the crystal, excessive pressure applied to it may cause the break of the crystal or the pen. The optimal radius for pen electrodes was defined as 1 μm . Larger radius of the electrodes automatically excludes straightforward engineering of small domains. This method was used for congruent crystals that are less than 200 μm thick and stoichiometric crystals less than 250 μm thick. The coercive field for domain inversion was reduced drastically in these crystals. The coercive field value for the congruent samples was 22kV/mm, it makes impossible to produce single domain samples at room temperature because of dielectric breakdown. In stoichiometric crystals this field is reduced down to 3 kV/mm. Influence of polarization gradients at pre-existing 180° domain walls on coercive fields for domain wall motion was explained deeply in [37] in LiTaO_3 and LiNbO_3 . Main merit of calligraphic poling is in repeatable poling procedure possible in single crystal with different patterns.

The phase diagram of the system $\text{LiO}_2\text{-Nb}_2\text{O}_5$ (Fig. 2.2.6) presents a solid solution area close to 50% of the component cations. Crystal growth process starts with this melt composition (called congruent - eutectic point at 48.5% mol. of Li). The crystal grows exactly with the same cationic ratio and the liquid composition remains unaltered during the process. Growing of crystals with other liquid composition leads to compositional inhomogeneity along the pulling direction [38].

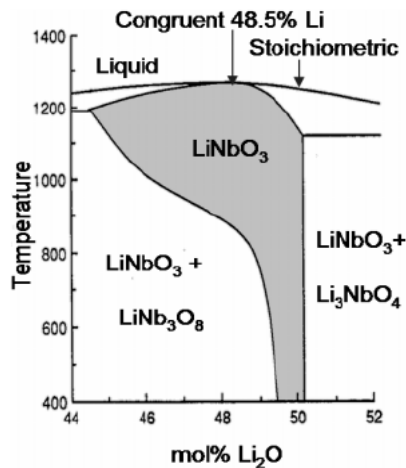


Fig. 2.2.6. Phase diagram of the $\text{LiO}_2\text{-Nb}_2\text{O}_5$ system [38].

Generally, the size and shape of fabricated domains is influenced by the magnitude of the voltage bias between pen and substrate and by the duration of applied voltage. Poling dynamics is influenced by the crystal thickness. The resultant domains in thick crystal are smaller than in thin one when the same voltage is applied for the same period of time. Creation of large domain structures (or creation of small domain structures in thicker crystals) is carried out by increasing time of the bias field application on the crystal, rather than the bias voltage increasing.

2.3. Lithium tantalate (LiTaO_3).

Interest in engineering ferroelectric 180° domain wall structures in LiTaO_3 ($\bar{3}m \rightarrow 3m$, 2DS, 180° DW) crystals was born due to their applications in the fabrication of solid state electro-optic devices and in frequency doubling to obtain a blue light source. There are a lot of techniques of domain switching in this material which combine the heat treatment, chemical patterning and electric field application. There is number of similarities and differences in the kinetics of 180° domain wall structures in LiTaO_3 and LiNbO_3 materials. Among the similarities there are the coercive fields for creating 180° domain wall structures, exponential behavior of switching times with external field, defined stabilization time for domain walls. The differences are in the internal field's magnitude, the shape of the transient current pulse during domain creation and the shape of the nucleated domains. Systematic study of the switching and stabilization times of 180° domain structures in congruent LiTaO_3 and LiNbO_3 crystals was given in [39]. Two main differences in the switching kinetics of LiTaO_3 and LiNbO_3 were defined: the kinetics of domain reversal (transient currents and shape of domain nuclei observation) and the difference in 180° domain wall stabilization times.

The peak current value reached more than 10 mA for LiNbO_3 while it was 1mA for LiTaO_3 for similar switching time 25ms. Under the constant electric field, the sideways wall velocity of independently growing domain was constant with time in LiTaO_3 and much varies in LiNbO_3 . Anisotropy of domain wall motion will be visible in formation of the domains, which sides are oriented along crystallographic direction. In congruent LiTaO_3 there is higher density of pinning centers than in congruent LiNbO_3 . The spikes in transient current correspond to depinning events and quick movement of the domain wall segment before meeting the next pinning site. Optical micrographs of 180° domains in LiTaO_3 and LiNbO_3 crystals can be observed in Fig.2.3.1. The nucleating domains are triangles in LiTaO_3 and hexagons in LiNbO_3 . It is observed that the triangles in LiTaO_3 are equilateral. The hexagons in LiNbO_3 don't have equal lengths on all six sides. The orientations of walls are a subset of orientations of the six sides of the hexagon. Detail investigation of the domain kinetics in LiTaO_3 and LiNbO_3 was described in [40]. As a result, same shapes of domain walls were observed.

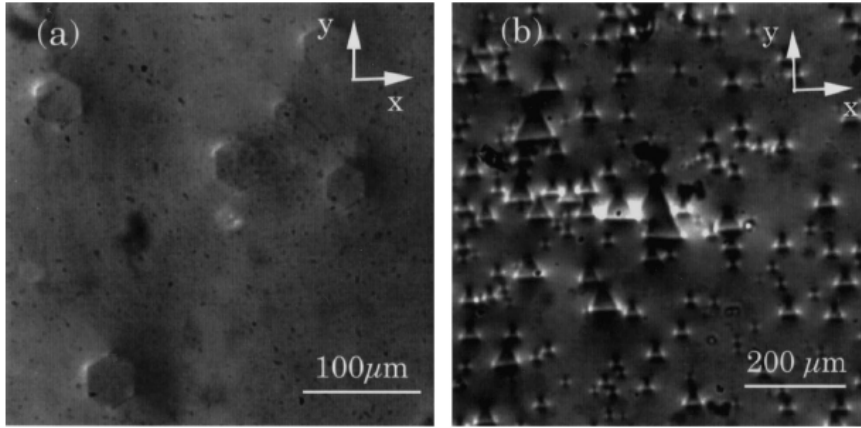


Fig. 2.3.1. Optical micrographs of 180° domain walls in a) LiNbO_3 and b) LiTaO_3 [39].

The stabilization times were measured by applying square voltage pulses of different magnitudes, pulse width and zero voltage delay to the crystals. As a result, stabilization was complete above pulse widths 2s in LiTaO_3 and 30ms in the case of LiNbO_3 . The stabilization time is closely connected to the non-stoichiometric point defects. When the domain wall moved to the new location the defects at the original position have the tendency to relax. This can be observed on disappearing trace behind the domain wall. New wall location defects have to adapt to the presence of the polarization gradient in this area, which shows as stabilization time.

Optical periodic poling is the alternative method for the fabrication of periodically patterned domain structures in LiTaO_3 [41]. This technique involves the simultaneous application of combined electrical and optical fields. Electric field is applied through planar electrodes and the light is used to define regions of domain inversion occurrence. The periodicity of optically induced domain structures is dependent on laser wavelength and intersection angle of two interfering beams. Submicron periodicities can be achieved, by generating interference patterns using UV light and by adopting counter propagating standing wave geometry. Periods of less than 100 nm can be realized.

2.4. Lead Germanate $\text{Pb}_5\text{Ge}_3\text{O}_{11}$ (PGO).

Detailed study of domain structure at phase transition in PGO ($\bar{6} \rightarrow 3$, 2DW, 180° walls), the dependences of the domain shape under reversal conditions, the dependences in forward and sidewise growth of domains in electric field were shown in [42]. The crystals 100 mm in length and transverse dimensions up to 20 mm were used. In PGO single crystals domain pattern with unique features known as as-grown domain structure (ADS) is formed during the cooling down to room temperature. The electric field was not applied to the crystals after crystal growth. The existing domain structure was changed after heating above Curie point and further cooled down under electric field. As a result optically visible domains were observed. The peculiarities of ADS can be explained by the existence of domains and the pinning of domain walls by space charges or by mechanical stresses. This structure consists of prolonged cigarlike domains (10-20 μm long, transverse size of 2-3 μm) organized in composite labyrinth structure along polar axis. The surface layer consists of small domains whose concentration is much smaller then in the bulk. The application of

constant electric field along polar axis when cooling from paraelectric phase led to the increase of the thickness of single domain layer at one of the electrodes and to the decrease of such layer at another one. It is possible to conclude that arising of small domain structures have been done due to the composition fluctuations and charged defects.

Main stages of domain structure change during complete switching by rectangular bipolar pulses were observed: 1) arising of cylinder domains; 2) increasing of domain diameters as a result of sidewise motion of domain walls; 3) union of cylinder domains with subsequent formation of large irregularly shaped domains; 4) disappearance of remanent domains with non-preferred wall orientation.

Switching from the multidomain state can be seen in Fig. 2.4.1. After application of switching pulse, the domain wall moves from the equilibrium position and stops. The chain of cylinder domains appears due to the sidewise motion till they join with primary domain.



Fig. 2.4.1. Arising of domains at the primary domain wall during partial switching from the multidomain state. Delay from the front of switching voltage pulse: A-0 ms; B- 40 ms. Scale bar – 100 μm [42].

The initial displacement of domain wall has been created due to the lower energy of nucleation at the wall than in the bulk. Domains arisen directly at the wall are also restricted because of depolarization field. As a result cylindrical domains are created in some distance from the wall and from each other because of decrease of interdomain interaction energy.

There are different mechanisms of sidewise motion of domain walls in strong and weak fields. In strong fields traditional 2-dimensional nucleation occurs at the wall as a result of exponential dependence of domain velocity on the field. In weak fields it is 1-dimensional nucleation. In PGO the trigonal anisotropy of the surface energy must lead to the preferred motion of the steps in three directions. Thus hexagonal domains are obtained in the weak fields (Fig.2.4.2, picture A.).

The 2-dimensional nucleation at the wall leads to the isotropic domain growth and then preferable domain wall orientations disappear. If short pulses of strong field are applied to the sample both mechanisms of domain wall motion may exist. If the strong field is switched on, 2-dimensional nuclei are formed at the wall. During the break between pulses the walls are smoothened as a result of motion steps. The wall motion in three directions is orthogonal to the direction of hexagonal domain wall movement. In this case triangular domains are created (Fig. 2.4.2, picture C).

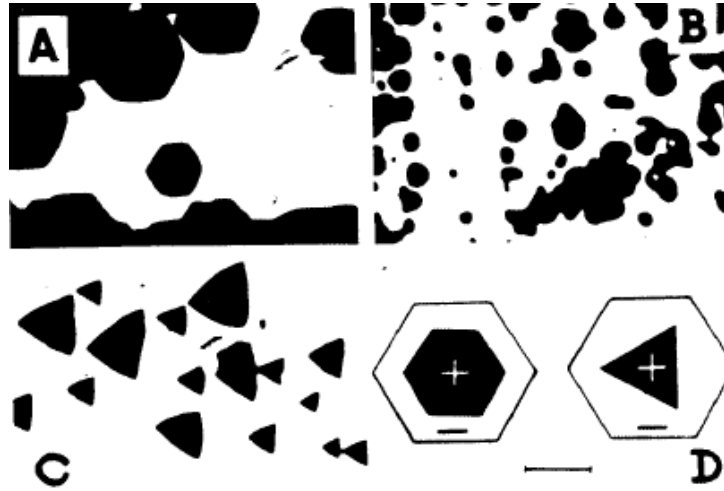


Fig. 2.4.2. Microphotographs of domains arising during the switching process in the same PGO sample: A – hexagonal domains; B – irregular-shaped domains; C – trigonal domains; D – schematic of regular shape domains of PGO single crystal [42].

2.5. Potassium niobate (KNbO_3).

Potassium niobate is an orthorhombic crystal with the point group $mm2$ at room temperature (species $m\bar{3}m \rightarrow mm2$, 12DS, DW 60, 120°, 90°, 180°, S -walls). The crystal undergoes three phase transitions, at 418°C (cubic to tetragonal $4mm$), at 203°C (tetragonal to orthorhombic $mm2$) and at -50°C (orthorhombic to rhombohedral $3m$), when it is cooled from the growth temperature. The orthorhombic phase is both ferroelectric and ferroelastic. Crystals usually exhibit 60°, 90°, 120°, and 180° domain walls. Single-domain crystal may be observed after poling at elevated temperature [43].

Integrated structures or boundaries of the domain structures other than 180° domain walls can be used in new applications. The dependence of electric poling directions for domain generation in KNbO_3 single crystals have to be investigated for better artificial control of these domain structures. The application of electric field in several different directions gave the optimum direction for poling. This direction is coincident with the direction of the difference of the spontaneous polarization vectors between the original and controlled domain. Such poling concept was called “differential vector poling” (Fig. 2.5.1) [44]. This method allows production of 60° domain structures by the application of 240 V/mm and 90° domain structures by application of 140 V/mm.

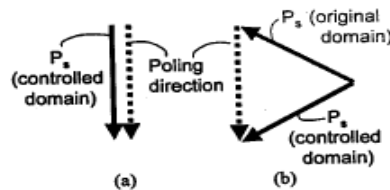


Fig. 2.5.1. Concepts of electric poling: (a) Polarization vector poling; (b) Differential vector poling concept [44].

KNbO_3 crystal was grown by the top seeded solution growth (TSSG) method. Cubic block samples parallel to a -, b -, and c -axis were used (size $15\text{mm} \times 15\text{mm} \times 15\text{mm}$). These blocks were poled by applying the electric field 200V/mm at 215°C and then annealed for 120 hours at 195°C to make it single domain. Proper poling direction has to be chosen. Pseudocubic axes were used to define the spontaneous polarization direction. Their direction $[110]_{\text{pc}}$ corresponds to spontaneous polarization direction (c -axis) of KNbO_3 [45]. Fabrication of 60° domain was done by differential vector poling. KNbO_3 $(10\bar{1})_{\text{pc}}$ -cut single crystal plate (2mm in thickness) was used. The electrodes were coated parallel to theoretical $(1/0.3/1)_{\text{pc}}$ -wall orientation. Electric current was used to monitor the domain generation. Inversion process was observed by optical images from $[0\bar{1}0]_{\text{pc}}$ direction using video camera (Fig.2.5.2.).

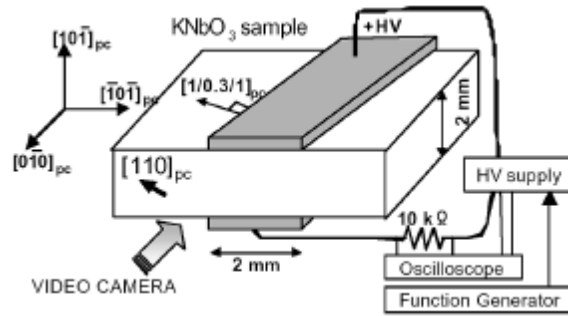


Fig. 2.5.2. Schematic view of experimental setup [45].

Different voltage patterns (DC, pulse) were applied with changing its amplitude and duration at the room temperature. Triangle or trapezoid voltage patterns gave the good performance in artificial fabrication of 60° domain structures without the generation of unwanted domains. It was found from the current waveform that the threshold voltage of 60° domain walls was from 230V/mm to 250V/mm . The current peak width was several hundred milliseconds. Optical microscope images and surface profile of $(10\bar{1})_{\text{pc}}$ plane were measured to confirm the fabricated domain structures.

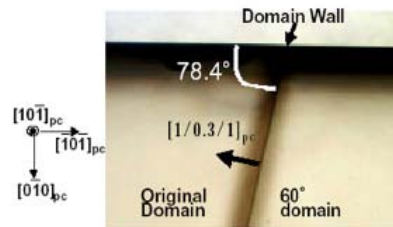


Fig. 2.5.3. Optical microscope image of $(10\bar{1})_{\text{pc}}$ plane at generated domain boundary [45].

From optical microscope image Fig. 2.5.3, direction of generated domain wall was tilted at an angle of about 78.4° to $[\bar{1}01]_{pc}$. Such wall direction is coincident with the theoretical 60° domain S-wall direction $((1/0.3/1)_{pc})$.

Fabricated 90° domain structures were confirmed by (101) surface profile measurement with help of the optical interferometer. The coercive electric field of 90° domain walls is low (140 V/mm) compared with the same of 180° domain structures (250 V/mm). It was possible to fabricate 90° domain structures with 200 μ m period without generating unwanted domain structures. While domains in 90° domain wall structures differ in the refractive index, new applications of these structures will be possible in principle [46]. Comparable 180° domain wall structures with antiparallel P_s orientation show that the domains do not differ in refractive index. In “differential vector poling” case for 120° domain walls, sample area under electrodes became milky color when threshold voltage (about 215 V/mm) was applied. In this region 60° domain walls were observed by optical microscope image. After using of etching technique, 180° domain walls were observed in most of milky color region. Permissible 120° domain walls were only rarely observed. They were located in the region, which was not under control. The creation of 120° domain structures without generation of other domain structures by electric poling method is difficult.

Using “differential vector poling” and consider permissible domain wall directions, it is possible to control 60° , 90° and 180° domain structures of KNbO_3 single crystal artificially.

Chapter 3.

Poling dynamics of ferroelectric ceramics.

3.1. External fields and microstructure influence on the electromechanical properties of piezoelectric ceramics.

Ceramics, by definition, comprise inorganic, non-metallic, non-water-soluble compounds that show ionic contributions in their chemical bonds. Various issues of texture, electric and mechanic field, temperature will be discussed in this chapter with respect to their influence on the material property.

3.1.1. Mechanical pressure.

One-dimensional pressure (T_2 , T_3). The effects of uniaxial stress on the properties of piezoelectric ceramics are important in the design of some types of underwater transducers. In PZT ceramics, external stresses can cause substantial changes in the piezoelectric coefficients, dielectric constant, and elastic compliance due to nonlinear effects and stress depoling effects. It is also important to realize that aging and deaging processes may play a significant role in modifying the material properties.

Static stress perpendicular to the polar axis (T_2). In this case the transversal stress T_2 which is perpendicular to the polar axis was applied. The resonance method was used for the measurement of changes in the material properties of PZT ceramics under the influence of T_2 . It was possible to observe the great changes of resonance and antiresonance frequencies with increasing static stress from measured impedance characteristics of bars samples. In hard PZT (APC 840, 841, 880) ceramics the growth of d_{31} (2-3 %) was observed at low mechanical stress, finally it decreased in the range 10-20 % for different ceramics types. Soft PZT (APC 850, 856) showed the decrease of d_{31} by about 30 % (Fig. 3.1.1.1). The effect on the permittivity is fairly small. In hard PZT the change was in the range 1-8 %, but in soft it was about 10%. It is possible to observe the stress stability of d_{31} coefficient in the range near 8 MPa [47].

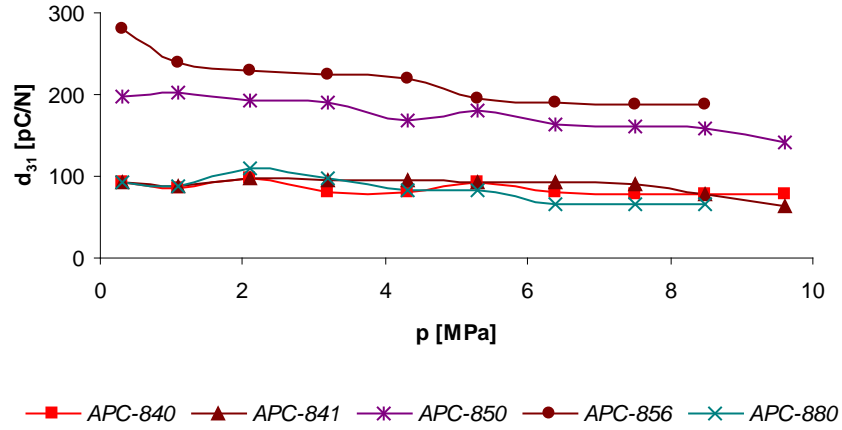


Fig.3.1.1.1. Piezoelectric coefficient d_{31} as a function of static pressure perpendicular to the polar axis (samples – bars: APC 840, 841, 850, 856, 880) [47].

The changes in the permittivity, loss and piezoelectric constants under the application of 14MPa (1psi = 6894,8Pa) stress were observed in [16]. Bars of hard ceramics PZT-4, PZT-8 and soft ceramics PZT-5A, PZT-5H were tested. Permittivity generally decreases with stress. d_{31} (in the direction of stress application) decrease markedly with stress, while d_{32} (in the direction perpendicular to the stress application) generally rises (Fig.3.1.1.2). The effects are less severe for hard ceramics.

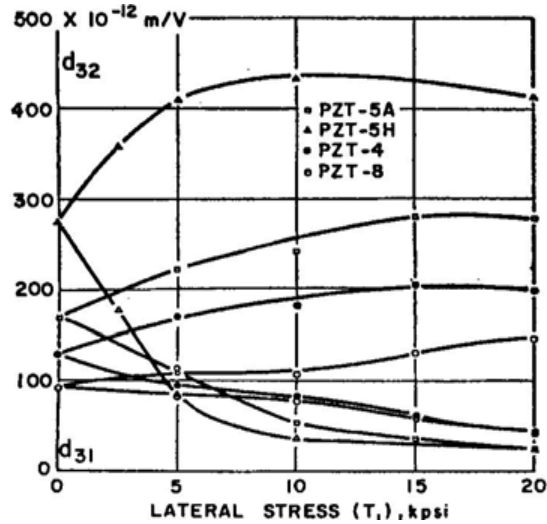


Fig.3.1.1.2. d_{31} and d_{32} vs. lateral stress perpendicular to the polar axis [16].

Stress perpendicular to the polar axis tends to create rather few additional domain walls in a poled material and does not drastically affect domain alignment. The effect on the permittivity is therefore small.

Static stress along the polar axis (T_3). Method of measurement of induced charge on the electrodes of the ceramics sample was chosen to show the influence of the mechanical stress on the material properties of PZT. The applied pressure was up

to 40 MPa. This pressure application gives the opportunity to define the stress limits of ceramics, which are very important for device design.

In soft ceramics (sample – ring) the increase of d_{33} value was the biggest in the range 0-8 MPa, it was more than 50% of the original zero-stress value [47]. The motion of domain walls and sample anisotropy value was the reason of this change. Above 8 MPa saturation and moderate growth of the value was observed (Fig. 3.1.1.3).

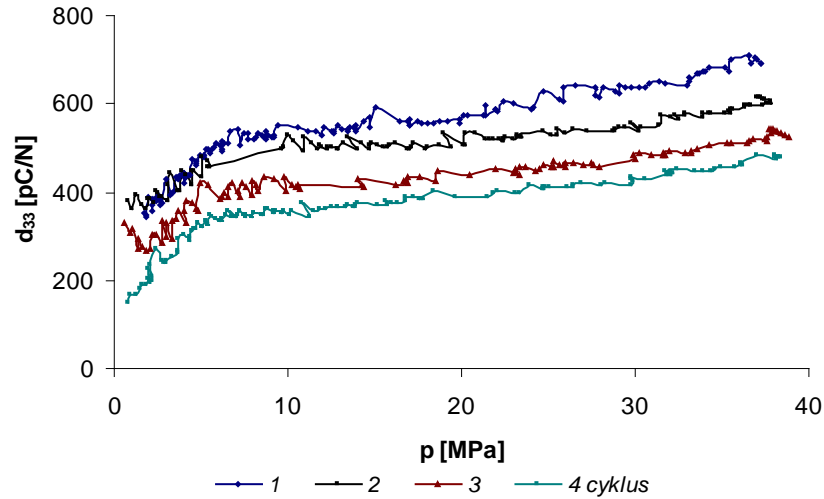


Fig.3.1.1.3. The dependence of d_{33} coefficient (sample – ring APC 850) from cyclic stress application along the polar axis [47].

Mechanical stress along the polar axis tends to increase permittivity drastically because anisotropy of the permittivity and creation of additional domain walls act together.

Compressive stress T_3 can significantly increase the piezoelectric activity and coupling factor in hard PZT ceramics. The piezoelectric coefficient and dielectric constant return to the zero stress state with 40% higher values after a stress cycle of 150MPa was applied. This increase involves a change of domain orientations with respect to the external field and applied stress and the coupling of the local polarization to the local defect fields [48]. For hard PZT, no stress depoling was observed in the time scale of the current experiment, because the depoling stress is higher than 90MPa for PZT-8.

The experimental results reveal that soft PZT ceramics can be depoled easily by the compressive mechanical stress T_3 . The depoling stress was defined as 50MPa for soft PZT-5H and 60MPa for soft PZT-5A. This is connected with the fact, that PZT-5A has a higher coercive field. As a result, it is more difficult to be stress depoled. Soft PZT can be stress depoled easily, by applying a DC bias electric field. These ceramics can be used to high stress levels without being depoled. Fig.3.1.1.4 shows the change of d_{33} of PZT-5H with stress. DC electric field of 5kV/cm, which is parallel to the original poling direction, is applied to the ceramics. The ceramics still retains 90% of the original piezoelectricity after 150MPa stress cycle.

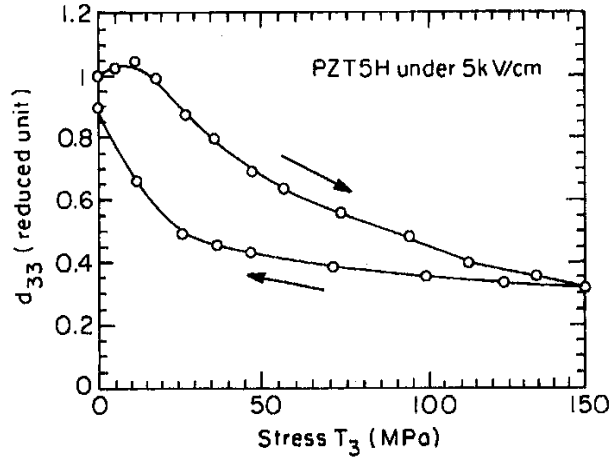


Fig.3.1.1.4. The dependence of d_{33} on the compressive stress T_3 while under the 5kV/cm DC bias electric field that is parallel to the original poling direction for PZT-5H [48].

The coercive field E_c for PZT-5H is 9 kV/cm, so the result indicates that a field below E_c can be used to stabilize a ceramics from the stress depoling. It is a memory of the original poling direction. That is why, a small electric field parallel to the original poling direction can repole the ceramics back to the high polarization level.

The piezoelectric state in PZT ceramics is a result of poling. When a high mechanical stress is applied to the ceramics, it will reorient the polarization directions at each grain and may cause depoling of the piezoceramics. This will certainly impose a limit on the maximum stress level that can be applied to piezoceramics. Some typical electrical and mechanical limits are given in Table 3.1.1.1 for Philips PZT ceramics [49].

| PZT type | Electric field strength (V/mm) | Mechanical pre-stress (MPa) |
|----------|--------------------------------|-----------------------------|
| PXE 59 | 350 | 5 |
| PXE 52 | 100 | – |
| PXE 42 | 400 | 25 |
| PXE 41 | 300 | 10 |
| PXE 43 | 500 | 35 |

Table 3.1.1.1. Some typical electrical and mechanical limits [49].

Hydrostatic pressure. The effect of hydrostatic pressures up to 70 MPa on the piezoelectric strain constants (d_{33} and d_{31}), permittivity and dielectric loss at non-resonant driving fields up to 3 kV/cm is presented for two commonly used projector materials – a modified barium titanate ceramics (Ba, Ca, Co)TiO₃ containing 5% calcium and 0.75% cobalt (tetragonal) and a commercially available lead zirconate titanate PZT-4 (rhombohedral) [50].

The piezoelectric strain constants were determined by measuring the strains produced in the ceramics by an applied field directly. Fields up to 1.5kV/cm at 25Hz were applied at constant pressure. The permittivity and dielectric loss were determined from the equivalent series capacitance and resistance of the sample with

a high-voltage substitution resonance bridge at the frequency of 10kHz measurement. Plates of poled ceramics were driven at fields up to 3 kV/cm and constant pressure.

The effect of hydrostatic pressure on the piezoelectric strain constants and the permittivity and dielectric loss of the two studied materials was found to be small, the total change at 70MPa for PZT-4 was 6% for d_{33} and 7% for d_{31} (Fig.3.1.1.5). Figure 3.1.1.6 shows the increase in permittivity over the initial low-field value at atmospheric pressure with increasing hydrostatic pressure and field. The dielectric loss showed no change with pressure for (Ba,Ca,Co)TiO₃ and for PZT-4 showed only a slight increase in the case of higher fields. Comparison of these results with those of one- and two-dimensional stresses shows that the changes in the material parameters due to hydrostatic pressure may be up to one order of magnitude smaller than those due to the directional stresses. Stress aging at high fields was found to be negligible after a few minutes. The pressure effects were found to be greater in PZT-4 than in (Ba,Ca,Co)TiO₃ in the case of all studied properties.

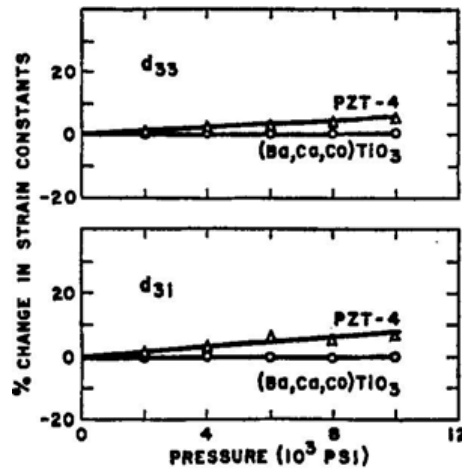


Fig.3.1.1.5. Variation of piezoelectric strain constants with hydrostatic pressure [50].

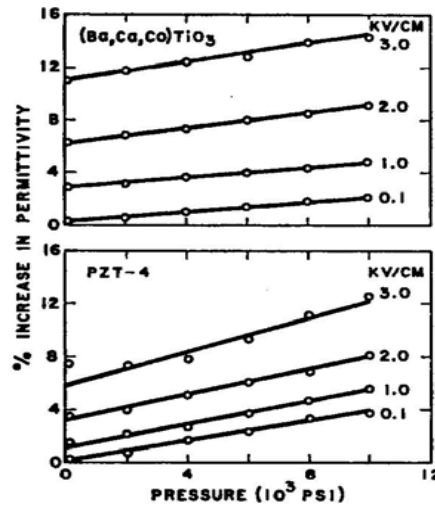


Fig.3.1.1.6. Variation of permittivity with hydrostatic pressure [50].

The thermodynamic theory of ferroelectricity predicts the linear increase in permittivity with hydrostatic pressure. Changes in the tetragonal distortion and the motion of the domain boundaries, both of which are not taken into account by the thermodynamic theory, may also contribute to some of the observed pressure effects.

3.1.2. Electric field.

A polycrystalline ceramics that has not been subjected to static field behaves macroscopically as non-polar material even though the crystals comprising it are polar. One of the most valuable features of ferroelectric behaviour is that ferroelectric ceramics can be transformed into polar material by applying strong static field. This process is called “poling”. The ceramics can be depoled by the application of appropriate electric fields. Another typical behaviour of ferroelectric ceramics is change of its properties with time without influence of electric field, stress or temperature – “aging”.

The electromechanical response of PZT ceramics as a function of amplitude and frequency of large electric fields and effects of DC bias field were investigated in [51]. The strains of ferroelectric ceramics were measured directly by modified ZMI2000 laser interferometer. The strain of PZT ceramics was determined as a function of electric fields and as a function of frequency in the low frequency range. Piezoelectric coefficients have been determined after these measurements.

The piezoelectric coefficient d_{33} was defined by measurement of the longitudinal strains developed under an applied electric field with the laser beam incident on the electrode surface of PZT samples (Fig.3.1.2.1). The piezoelectric coefficient d_{31} was found from measurements of the transverse strain with the laser beam incident on the side surface of the sample, which was perpendicular to the poling direction. In order to find the shear coefficient d_{15} , the original electrodes were removed, new electrodes were applied on surfaces parallel with the poling direction, and the laser beam was used to measure the shear displacement.

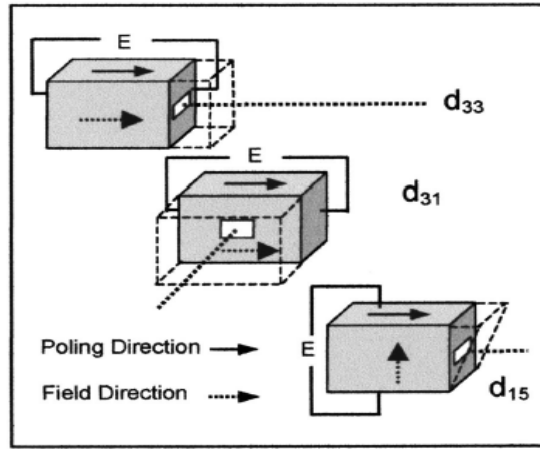


Fig.3.1.2.1. Schematic of the measurement system for determining the various piezoelectric coefficients [51].

A.C. field. The variation of d_{31} , d_{33} , and d_{15} for two PZT types as a function of AC electric field (applied in the same direction as the poling one) at 100 Hz is shown in Fig.3.1.2.2. It is possible to see that d coefficients increase with electric field. This effect is more significant in case of soft ceramics. Hard PZT EC-69 is characterized by low piezoelectric constants. The domain walls in hard PZT are pinned by impurities and structure discontinuity. The small increase in d_{15} is perhaps due to some depinning. Soft PZT EC-65 is characterized by high piezoelectric constants and mobile domain boundaries. Extrinsic contributions are inherently more important and their effect increases in higher fields. The d coefficients increase in soft PZT due to

the large extrinsic contribution resulting from higher domain switching under the influence of large fields.

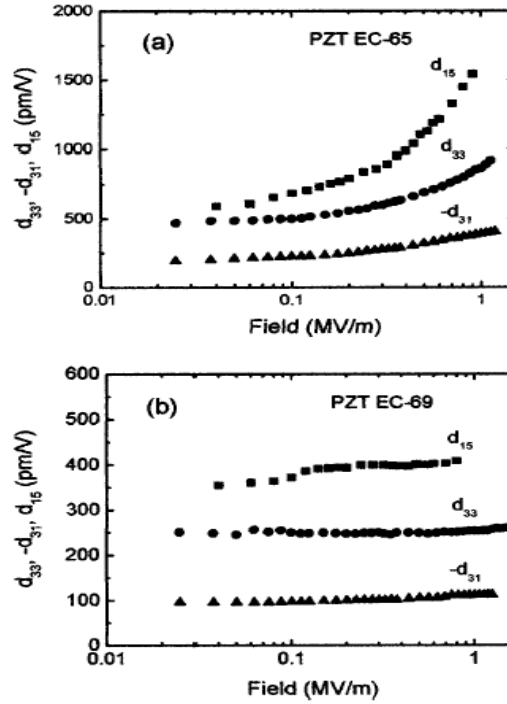


Fig.3.1.2.2. Piezoelectric d coefficients of two types of PZT as a function of an applied 100 Hz AC electric field [51].

The piezoelectric coefficient showed significant nonlinearity with increasing field strength for both hard and soft PZT.

AC field dependence for various DC bias fields was measured when DC bias was applied opposite to the polar direction. Fig. 3.1.2.3 (picture a) shows the result for hard PZT. The d_{33} increased in nonlinear fashion until the combined AC and DC fields are sufficient to induce depoling when the negative bias increased from 0 up to -1.5 MV/m. The DC bias field causes depinning of domain walls. Curve corresponding to DC bias -2.1 MV/m shows decrease in d_{33} due to depoling and the repoling that occurs at higher fields. In case of soft PZT the behavior of d_{33} is more nonlinear (Fig.3.1.2.3, picture b).

D.C. field. If positive DC bias (along the poling direction) is applied to the hard PZT EC-69 ceramics, small decrease in d_{33} is observed (Fig.3.1.2.4). Positive DC bias field does not increase the total polarization but contributes to the pinning of the domains. Negative bias caused a field-induced deaging (depinning of the domain walls). The extrinsic contribution to the piezoelectric response will increase. The d_{33} shows small increase as a function of negative bias field until the sample is depoled (about 1 MV/m) in soft PZT EC-65. If negative bias further increases it causes a repoling of the sample. Piezoelectric constant d_{33} rise at low DC bias can be attributed to the depinning and deaging phenomenon. It is clear that the field dependent nonlinearity plays an important role in applications where large driving fields are applied to piezoelectric materials.

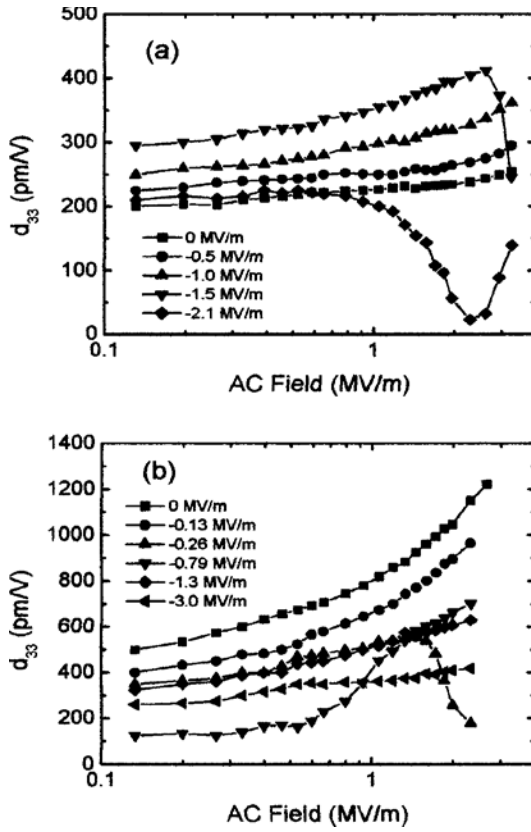


Fig.3.1.2.3. AC field dependence of d_{33} for hard (a) and soft (b) PZT under negative DC bias fields.

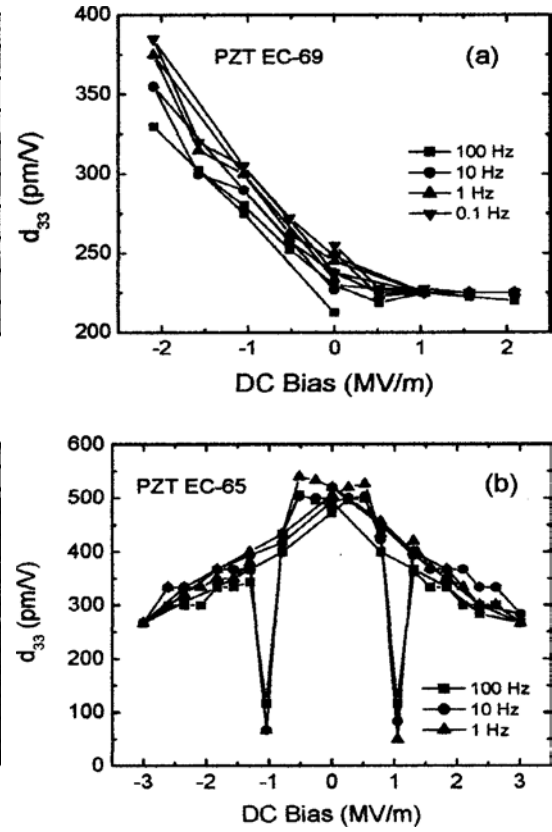


Fig.3.1.2.4. DC bias dependence of d_{33} for PZT at various frequencies [51].

3.1.3. The peculiarities of the temperature influence.

Pure PZT ceramics. The temperature influence on piezoelectric properties of PZT ceramics was observed on bar samples with gold electrodes, which were poled by electric fields of 20-40 kV/cm for 4-30 min. The samples were cooled down to 4.2K first and then measured during heating to 300K [52]. The dielectric constant of $\text{Pb}(\text{Zr}_{0.52}\text{Ti}_{0.48})\text{O}_3$ samples increased and decreased by poling for the tetragonal and rhombohedral compositions, respectively. The increase in tetragonal phase was explained due to the elimination of the effect of compression of 180° domains. Dielectric constant decrease exists because the dielectric constant contribution dominates due to the 71° (109°) domain reorientation for the rhombohedral compositions. Fig.3.1.3.1 shows the temperature dependence of d_{33} and k_{31} in tetragonal phase. The compositions near the morphotropic phase boundary show the larger temperature dependence.

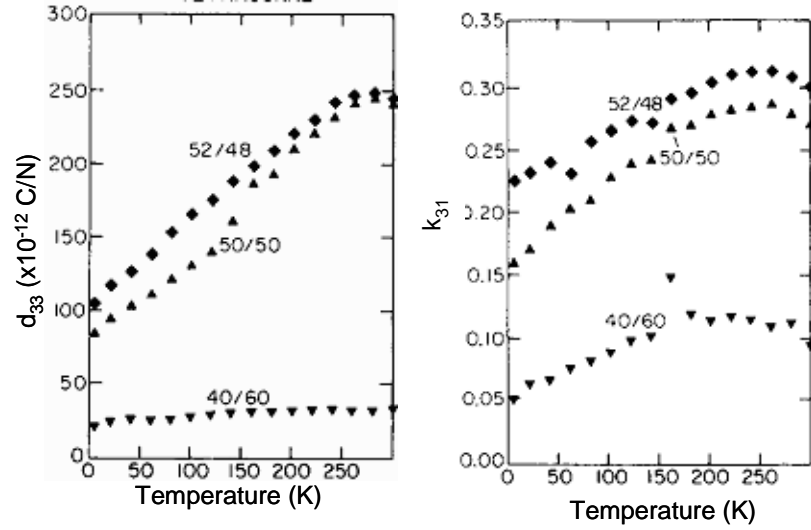


Fig.3.1.3.1. PZT coupling factor k_{31} and strain coefficient d_{33} versus temperature [52].

PLZT ceramics. Temperature dependences of the remanent polarization and the coercive field were obtained for 8/65/35 PLZT ceramics from the ferroelectric hysteresis loops in the temperature range 20-140°C. [53]. Temperature dependencies of the complex piezoelectric and dielectric constants, the complex elastic compliance, the electromechanical coupling factor, and mechanical quality factors were determined from the piezoelectric resonance data. Temperature dependences of the real and imaginary parts of complex material constants determined from piezoelectric resonance data are shown in Fig.3.1.3.2. It should be pointed out, that only absolute values of the real and the imaginary part of the complex piezoelectric constant and their product can be determined from the piezoelectric resonance data.

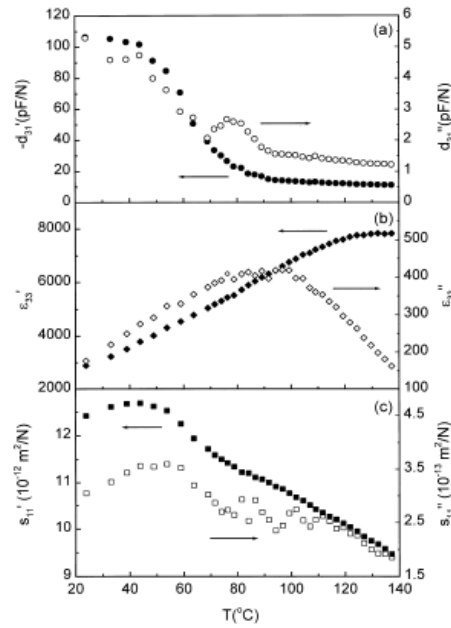


Fig.3.1.3.2. Temperature dependences of the real and imaginary parts of (a) piezoelectric constant, (b) dielectric constant, and (c) elastic compliance [53].

Temperature dependences of other material properties are shown in Fig.3.1.3.3. Saturation of electromechanical coupling factor k_{31} confirms that below 50°C the ferroelectric order is established in the presence of a DC electric field in PLZT ceramics. Both the piezoelectric resonance peak and the slim ferroelectric hysteresis loop originate from the existence of polar clusters above 90°C. The second order phase transition between these two states is reflected in the changes of the real part of the complex piezoelectric constant, the electromechanical coupling factor and the mechanical quality factor.

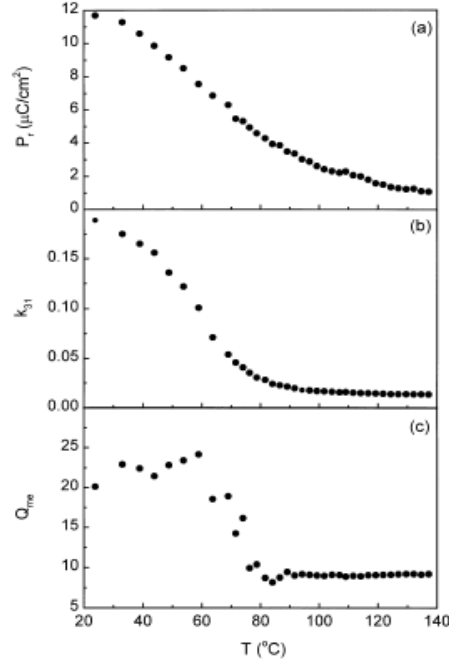


Fig.3.1.3.3. Temperature dependences of the (a) remanent polarization P_r , (b) electromechanical coupling factor, and (c) mechanical quality factor [53].

3.1.4. Texture: grain-oriented ceramics.

In recent years new fabrication techniques made possible the production of ceramics with textured microstructures. One way is to combine the method of templated grain growth (TGG) with the fused deposition of ceramics (FDC) process to fabricate net-shape electromechanical components with grain orientation and superior properties. Nucleation and growth of the required crystal on aligned single crystal template particles results in an increased portion of oriented material with heating in TGG [54]. There are some criteria for templates selection for TGG. At first, template particles must possess a similar crystal structure, have a suitably high aspect ratio morphology (like whisker, platelet), so that it can be mechanically oriented under an applied shear force during forming. Template particle must be also thermodynamically stable within the environment at which it is supposed to function (template must not react or dissolve into the matrix material before stable growth). For example, epitaxial thin films of $\text{Pb}(\text{Mg}_{1/3}\text{Nb}_{2/3})\text{O}_3$ (PMN), PZT, PMN-PT may be grown on MgO , SrTiO_3 , MgAl_2O_4 , LaAlO_3 . BaTiO_3 and SrTiO_3 could also be template materials. Fig.3.1.4.1 shows a number of the template particles that have been considered for TGG of ferroelectrics.

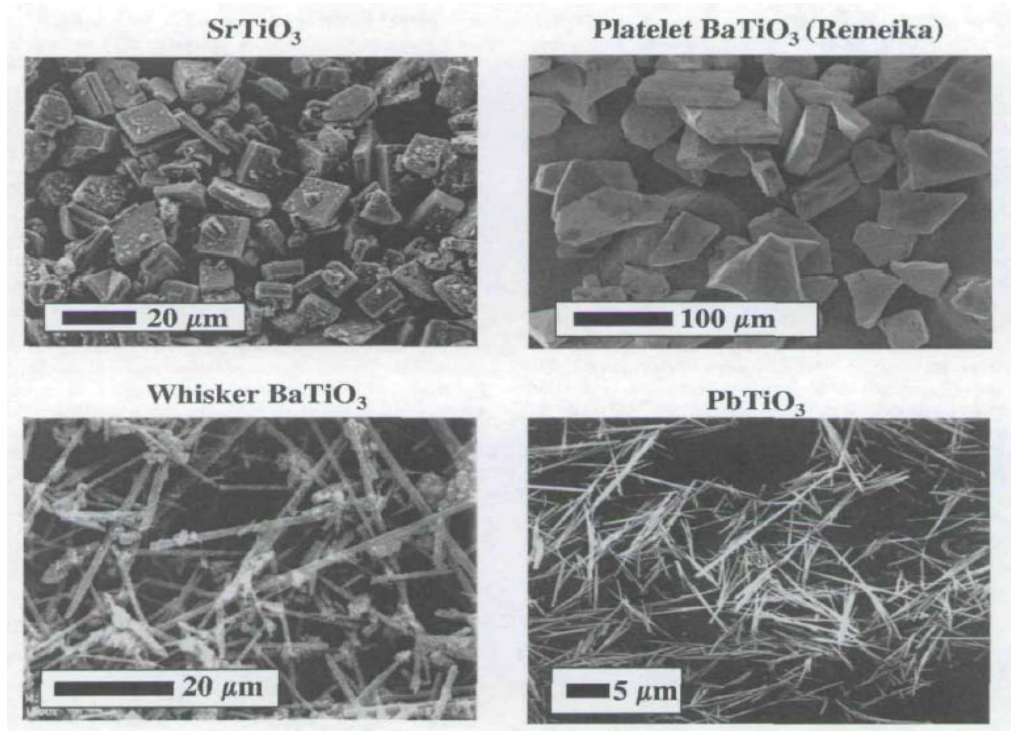


Fig.3.1.4.1. SEM micrographs of template particles grown by molten salt or hydrothermal synthesis methods [54].

PbNb₂O₆. Lead metaniobate (PbNb₂O₆) ($4/mmm \rightarrow mm2$ species) is used commercially in piezoelectric transducers because of three attractive properties: high Curie point (570°C), low mechanical quality factor ($Q_m=20$), and large d_{33}/d_{31} ratio. Mainly the large ratio results in large hydrostatic piezoelectric effect $d_h=d_{33}=2d_{31}$. PbNb₂O₆ is used for hydrostatic pressure detectors. The lower dielectric constant of PbNb₂O₆ (PN) increases the voltage sensitivity. Grain alignment is expected to improve some of ceramics properties [55]. Needle-shaped particles of PN were prepared by Molten Salt Solution (MSS). Conventional ceramic processing was used for PN equiaxed particles preparation. Equimolar ratios of PbO and Nb₂O₅ were chosen and heated with one mole of KCl at 1150°C and one hour in MSS. Scanning electron microscopy and X-ray diffraction results showed a needle-shaped orthorhombic phase with K⁺ ion substitution. Same equimolar ratio of PbO and Nb₂O₅ was chosen and calcined at 800°C for 2 hours for PN matrix. The rhombohedral phase was observed in PN matrix. FDS deposition of eight 254μm thickness layers was created. Densification process appeared in temperature range 1100-1200°C. The majority of grains were oriented parallel to the deposition direction near 1250°C.

When samples were poled under an electric field 40 kV/cm at 140°C and 30min electromechanical measurements were done. The values of d_{33} coefficients were near 80pC/N for grain-oriented samples. Such low coefficients were observed due to the presence of non-ferroelectric phases and microcracks, which were formed during sintering at 1300°C. Table 3.1.4.1 also shows some electromechanical properties of grain oriented PN samples made by the FDC process [56].

| ϵ_{33} (ϵ_0) | $\tan\delta$ (%) | k_{31} (-) | d_{33} (pC/N) | g_{33} (10^{-3} Vm/N) | ρ (g/cm ³) | Q_m (-) |
|-------------------------------------|---------------------|-----------------|--------------------|-------------------------------|--------------------------------|--------------|
| 210 | 9.5 | 0.44 | 80 | 43 | 5.6 | 10.6 |

Table 3.1.4.1. Some properties of grain-oriented PbNb_2O_6 made by FDC [56].

Sintering experiments were carrying out with starting powders of various particle sizes and different modifications (rhombohedral and orthorhombic structures) for obtaining of dense PbNb_2O_6 ceramics. The phase transformation from the rhombohedral to tetragonal structures raise grain growth, which brings the formation of intragrain pores and cracks and the reduction in densification rate. Crack formation may be explained by grain growth and phase transformation. Starting powder with orthorhombic structure increased sintered density, because the phase transformation was detained. The strong dependence of dielectric and piezoelectric properties on microstructure was confirmed. The intragrain pores and cracks relaxed the internal stresses and increased the depolarization, which is caused by the space charge effect. That is why, intragrain pores and cracks increased Curie temperature and decreased the dielectric constant. Maximum dielectric constant and the Curie temperature showed dependence on the morphology of pores and the magnitude of crack density. Same dependence was in case of the grain size and pore volume. The starting powder improved the piezoelectric properties, what brought the absence of intragrain pores and the reduction in crack density. The electromechanical coupling factors (k_p and k_t) and piezoelectric charge constant (d_{33}) increased because of better domain reorientation during poling [57].

PMN-32.5PT ceramics. Ferroelectric ceramics which display a high degree of grain orientation (texture) possess directionally dependent dielectric, pyroelectric, and piezoelectric properties similar to single crystal. Therefore, it is possible to obtain an inexpensive substitute for single crystals and display similar dielectric, pyroelectric and piezoelectric properties by texturing ferroelectric ceramics by conventional ceramic processing routes. This is especially important for PMN-PT composition ($m\bar{3}m \rightarrow 3m$ or $m\bar{3}m \rightarrow 4mm$ species) since single crystal growth is limited by high production costs, low production efficiency, long growth time, small product size, limited shape forming capability, and compositional heterogeneity.

Described $0.675\text{Pb}(\text{Mg}_{1/3}\text{Nb}_{2/3})\text{O}_3-0.325\text{PbTiO}_3$ (PMN-32.5PT) ceramics (with 1 wt.% excess PbO) were fiber textured in the $\langle 001 \rangle$ direction by the templated grain growth (TGG) process using a low concentration (≤ 5 vol %) of oriented $\{001\}$ - BaTiO_3 crystals as the template particles [58]. The orientation of anisotropic template particles in fine-size powder is carried by shear-forming technique in the TGG process. The template particles have to be relatively large and anisometric in shape, in this case they can be effectively oriented during forming and they grow preferentially during sintering. The difference in surface free energy between the templates and the matrix grains induces the driving force for TGG process, which increases with the relative difference in the size between the templates and the matrix. PMN-32.5PT ceramic samples showed increased piezoelectric, electromechanical coupling and compliance coefficients with an increase in texture. Unipolar strain–electric field curves of PMN–32.5PT ceramics containing 5 vol% BaTiO_3 templates (PMN–32.5PT–5BT) and displaying various degree of texture are given in Fig.3.1.4.2. The d_{33} piezoelectric coefficient of highly textured PMN-32.5PT ceramic was ~ 1.2 times greater than for randomly oriented samples Fig.3.1.4.3. The enhancement in the electromechanical response was limited

by its relatively low dielectric constant ($\epsilon_{33}^T < 3000$) caused by the presence of the residual intergranular PbO phase, which was intentionally added to enhance the texturing kinetics.

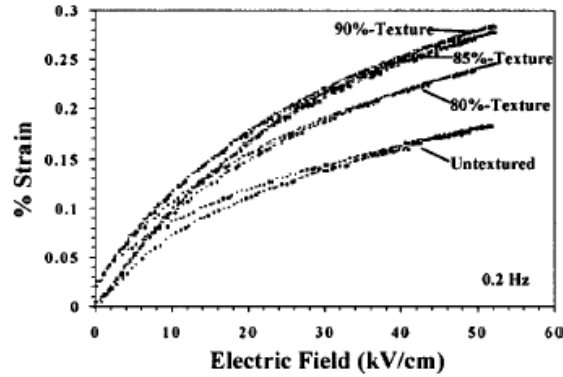


Fig.3.1.4.2. Unipolar strain–electric field curves of PMN–32.5PT ceramics containing 5 vol% BaTiO₃ templates (PMN–32.5PT–5BT) displaying various degree of texture [58].

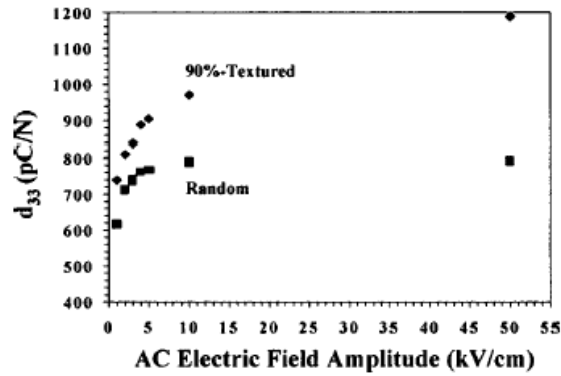


Fig.3.1.4.3. Low-field (< 5 kV/cm) d_{33} coefficients measured from unipolar strain–electric field curves of ~90% textured PMN–32.5PT–5BT ceramics and a random PMN–32.5PT ceramics measured up to maximum unipolar fields between 1 and 50 kV/cm [58].

3.1.5. Grain size effect.

BaTiO₃ ceramics. Small additions of TiO₂ together with controlled firing could give increase to BaTiO₃ ceramic capacitors with permittivity close to 3000 over a broad temperature range (1950). The merits were found later in a liquid phase densification which inhibited grain growth in the ceramics. Residual boundary phase which reduced the Curie peak permittivity was left. Both these effects have been studied separately.

The measurements of the pure grain size effect were done by Kinoshita (1976) [59]. Hot pressing of a weakly dysprosium doped BaTiO₃ was used for production of samples with controlled grain size from 1.1 μm to 53 μm, which showed no suppression of Curie peak. Such samples demonstrate a continuous increase of weak field permittivity near the room temperature to values above 5000 with the reduction in grain size at 1.1 μm (Fig. 3.1.5.1).

The frequency of occurrence of 90° domain walls was decreased with grain size reducing. Another model for the grain size effect was proposed by Arlt (1976). This model would require that the fine grain ceramics have higher density of twins. Experimental evidence is proposed for this hypothesis. The main benefit of the twin (domain) model is that it accounts well for the higher dielectric losses ($\tan\delta$) in the fine grain system, but it does not explain the phase transition shift [60].

One possible item for study would be to bottle up 0°C transition in BaTiO_3 for example by calcium doping. The grain size effect should become lower rapidly as ε_a intrinsic contribution is lowered for the internal stress model.

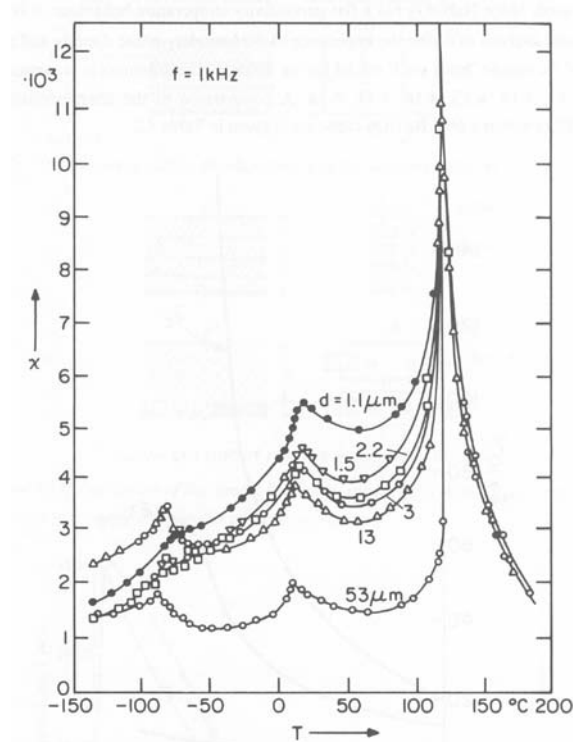


Fig.3.1.5.1. Dielectric susceptibility of BaTiO_3 as a function of grain size [60].

Pure nanocrystalline barium titanate ceramics. Advantages of the nanocrystalline ferroelectric ceramics application are based on new effects important to this class of materials caused by change of particle size of ceramic grains. Phase transitions and dielectric characteristics are depend on grain size. The reduction of grain size below $1\ \mu\text{m}$ is causing the changes in ferroelectric domain structure and it is resulting in the change of phase transition temperatures. That gives a restriction on desirable miniaturization of ceramic products [61].

Measurement of dielectric properties has shown that the permittivity of ceramics strongly depends on the grain boundary structure, which in turn is a function of material processing method (Fig.3.1.5.2). The calculated grain boundary for the pure barium titanate ceramics was 3-10 times wider than the actual grain boundary width, which was measured directly under microscope. The possible rootcause of this discrepancy can be the contribution of depolarization field. This field is appeared due to the existence of uncompensated charge layers near the grain boundaries.

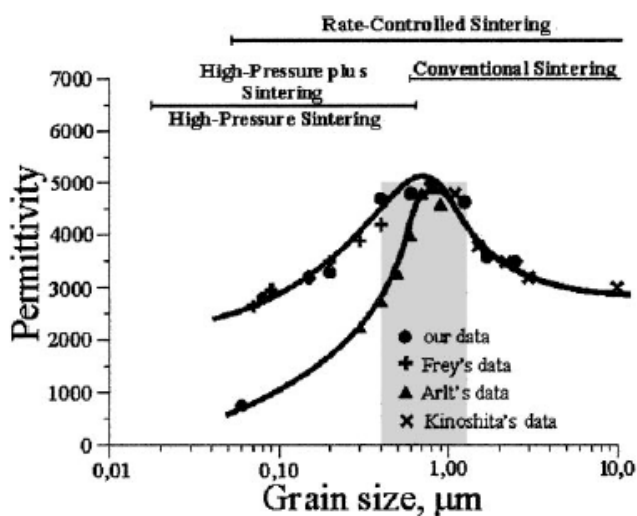


Fig.3.1.5.2. Permittivity of barium titanate ceramics obtained by different methods [61].

Fine-grained PLZT ceramics. Diameter of grains in the lanthanum-modified lead zirconate titanate (PLZT) ceramics was significantly reduced to the nanometer size due to using mechanical alloying (MA) for powder synthesis and hot pressing for densification. The grain size effects influence on ferroelectric and photostrictive properties of PLZT ceramics were systematically investigated within an extensive grain size range. The observed results are important for the next reasons: rather high photoinduced voltage was detected in the PLZT ceramics with submicrometer grains, photoinduced strains may rapidly increase by optimizing the microstructure.

Ferroelectric hysteresis loops of PLZT samples with various grain sizes and their comparison is shown in Fig.3.1.5.3 [62]. The remnant polarization and coercive field gradually decreased when the grain size was lower. The decrease of remnant polarization has been explained in terms of the increased difficulty for the domain reorientation due to microstructure refinement. But, as shown in Fig. 3.1.5.3, the coercive fields of PLZT samples remained almost without any change. The grain size reduction did not bring the increase of coercive fields as obviously expected. The reason for this is the polarization of the sub-micrometer-grained PLZT ceramics. It was not saturated within the same range from -40 to $+40 \text{ kV}\cdot\text{cm}^{-1}$. Changes in the value of remnant polarization with applied electric field at different grain sizes are shown in Fig.3.1.5.4.

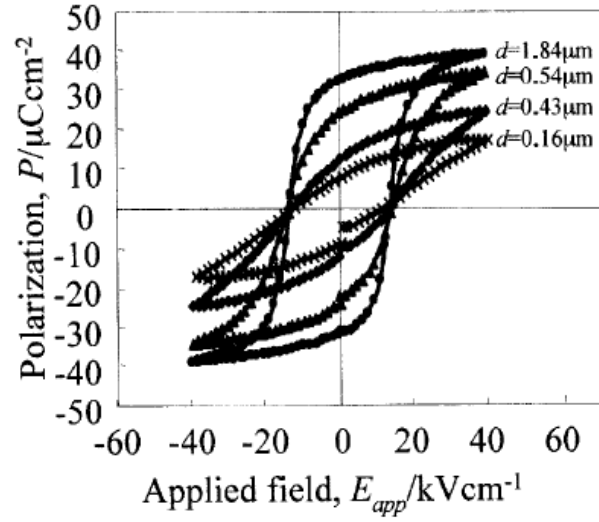


Fig.3.1.5.3. *P-E hysteresis curve of the PLZT ceramics with various grain sizes [62].*

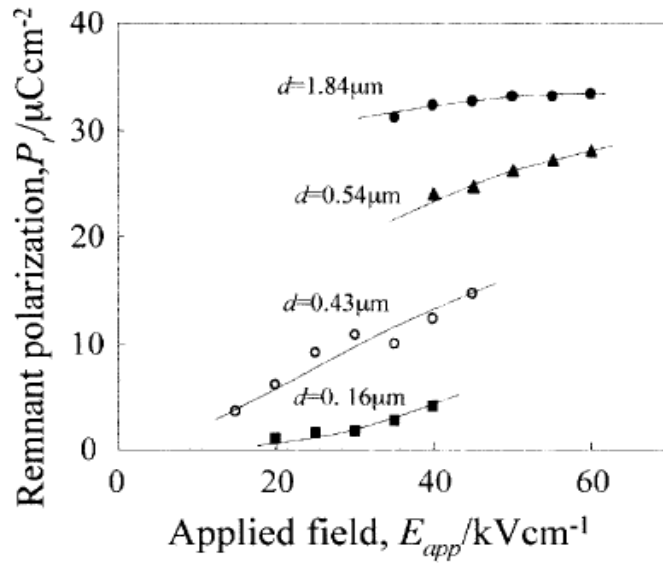


Fig.3.1.5.4. *Relationships between the remnant polarization and applied electric field at different grain sizes. The values are obtained by the P-E hysteresis measurement [62].*

3.1.6. Domain structure.

The formation of domains in ceramics and single crystals are different. The domain structure of the grain is formed under mechanically clamped conditions but single crystal is mechanically free. The spatial domain configuration in BaTiO_3 ceramics has been identified by analysis of the observed domain patterns. There are two types of domain configurations, both of them having three kinds of domain walls. Two kinds of walls in both configurations are elementary 90° walls. The third kind is a mixed wall of alternating stripes of 90° and 180° walls Fig.3.1.6.1. In addition, pure 180° walls have been observed in all regions [63].

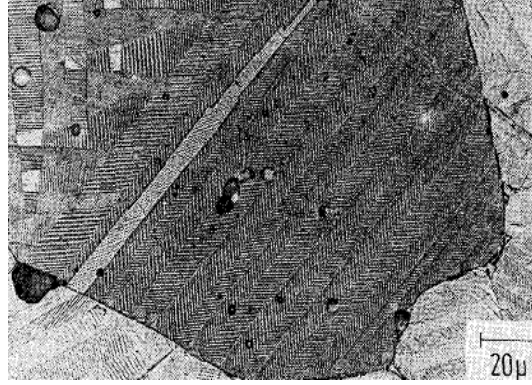


Fig.3.1.6.1. Etched surface of BaTiO_3 ceramics herringbone and square net pattern [63].

Both configurations permit the grain to remain underformed in the cubic-tetragonal transition. By the motion of 180° walls, of 90° walls, of mixed walls, and of the boundaries between the various regions, however, the grain can be deformed and polarized. A process in which the crystal is divided into many oppositely polarized regions (the energy associated with the polarization in the depolarizing field is minimized by twinning) is shown in Fig.3.1.6.2. The whole configuration shown comprises 180° domains [64].

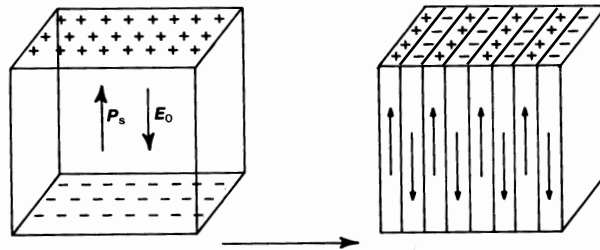


Fig.3.1.6.2. (a) Surface charge associated with spontaneous polarization; (b) formation of 180° domains to minimize electrostatic energy [64].

This multidomain state can usually be transformed into a single domain by applying a field parallel to one of the polar directions.

Microstructure observations show that the domain structures of BaTiO_3 ceramics are stabilized by aging. Once stabilized, the original domain structures reappear even when the stress conditions during phase transformation are changed [65]. Thin BaTiO_3 specimens (discs with diameter 12.7mm and thickness 1mm)

which had been aged for more than 2 years for this investigation were used. By applying DC voltage 6V/mm, the samples were heated above the Curie temperature, and phase transition from tetragonal to cubic phase occurred. The disappearance of the domain structures (detwinning process) could be observed. The velocity of the transition front was ~ 0.5 mm/s. The formation process of domains (twinning process) could also be observed by shutting off the electric current. In Fig. 3.1.6.3, the transition fronts observed during heating (during detwinning process) are shown. For Fig. 3.1.6.3(a), the temperature of the left part of the grain was higher than that of the right side. The left side of the specimen was about to transform from the tetragonal to the cubic phase so that the domains disappeared. The wall bands of the large grain in the centre were parallel to the heating direction and the transition front exhibited a saw-toothed shape. The transition was retarded at the region close to the wall bands compared with that inside the band. It is possible to resume that the Curie point in the region close to the wall band was higher than that of the bulk. The shape of transition front was changed when the specimen was rotated to 90° compare to Fig. 3.1.6.3(a). In Fig. 3.1.6.3(b) the transition front was relatively straight and the transition was observed to occur step by step. The transition front stayed at the wall band for a while and then advanced quickly to the next wall band. Such kind of local delays in phase transition were also observed at the pores as well as at the grain boundaries. The delay in growth of the transition front at the pores during heating cannot be explained in terms of the elastic fields [66].

During the progress of the transition front with the formation of domains, i.e., during the twinning process, the transition was observed to occur earlier than inside the bands.

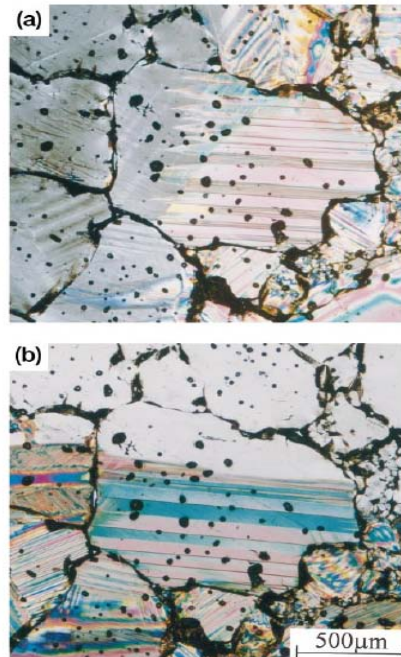


Fig.3.1.6.3. Detwinning process observed during heating of the BaTiO₃ specimen. The heating direction is (a) parallel and (b) perpendicular to the wall bands [65].

3.2. Lead zirconate titanate (PZT) ceramics.

Lead zirconate titanate (PZT) ceramics is widely used in sensor and actuator applications as the popular piezoelectric material. Most of the technically important PZT ceramics have compositions in the vicinity of morphotropic phase boundary (MPB) to reinforce electro-mechanical coupling. There are two ferroelectric phases: tetragonal and rhombohedral, coexisting inside material (Fig.3.2.1) [67]. PZT ceramics (species $m\bar{3}m \rightarrow 4mm, m\bar{3}m \rightarrow 3m$) is usually modified with dopants to meet the requirements for specific applications. Higher-valent additives (donors) induce “soft” piezoelectric behavior, while lower-valent additives (acceptors) induce “hard” behavior [68]. Higher piezoelectric coefficients of soft compositions are used in actuator applications, while hard PZT ceramics are particularly suitable for ultrasonic motor applications [69].

Polycrystalline ferroelectric ceramics consists of crystals subdivided into domains, which are separated by domain walls. Domain is a spatially connected region of unit cells within single crystal. Unit cells in one domain share the same spontaneous polarization direction. The angle between polarization directions in neighboring domains is important for domain walls description. Domain walls can be divided into two categories: 180° walls separating domains with opposite polarization vectors, and non- 180° walls separating the remaining domains (90° for tetragonal symmetry and $71^\circ/109^\circ$ for rhombohedral symmetry). The polarization directions of domains may be reoriented by application of an electric field or mechanical load. This behavior is called switching or domain wall motion. Domain switching induced by field electric is ferroelectric switching; both 180° and non- 180° reorientation can occur in this case. Piezoceramics also exhibits ferroelasticity. The non- 180° domain switching can be induced by mechanical stress load of proper magnitude [70]. The consequence of domain switching is the occurrence of non-linear hysteresis behavior. When large-signal influences (electric field and/or stress) are applied, the real responses of piezoceramics are dominated by significant non-linearity and hysteresis due to the ferroelectricity and ferroelasticity. Consequently, the conventional linear assumptions for small-signal loading conditions are inadequate in representing accurately the practical behavior of materials. Experimental efforts are focused on the evaluating the large-signal non-linear behavior of ferroelectric piezoceramics in the context of domain switching for optimization of device design and components reliability assessment.

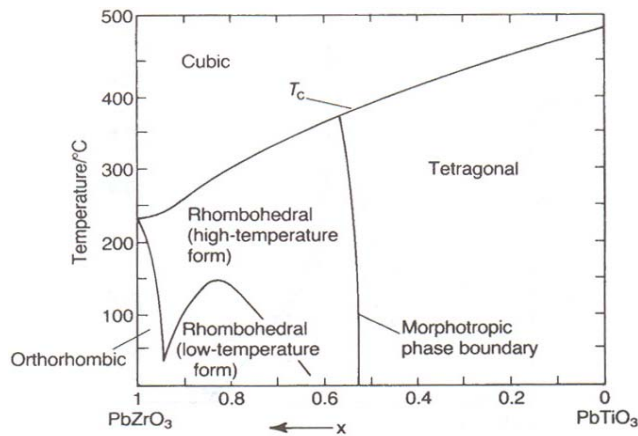


Fig. 3.2.1. Phase stabilities in the system $Pb(Ti_{1-x}Zr_x)O_3$ [64].

Application of strong alternating electric field to the mechanically unclamped piezoelectric ceramic specimen causes the polarization to reverse. As a result, the dependence of polarization and strain versus the field applied are recorded by the so-called dielectric and “butterfly” strain hysteresis loops [71]. It was found that the hysteresis response of piezoceramics depends significantly on the amplitude and frequency of the field applied.

A special method of samples preparation and an improved experimental setup were demonstrated to investigate reliably large-signal electromechanical response of piezoceramics [72]. Bipolar high electric field-induced polarization and “butterfly” longitudinal/transverse strain hysteresis loops were measured for commercial soft PZT material under various compressive stress preloads up to 400 MPa. The elastic deformation is induced by mechanical preload and ferroelastic domain switching significantly changed the shape and amplitude of the strain curves. When the prestress increase, the strain curves become much smoother and non-linear changes in the residual strain (strain values at zero electric field) were observed. Slopes of the polarization and strain curves at zero electric field were measured to evaluate the influence of prestress on the permittivity and piezoelectric coefficients (d_{33} and d_{31}) of piezoceramics (Fig. 3.2.2.). After values reached the maximum at definite stress level these parameters decreased rapidly as compression preload is further increased.

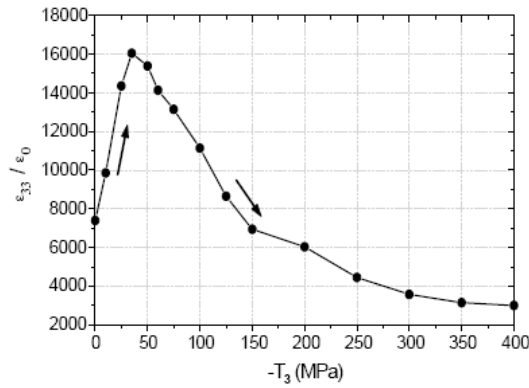


Fig. 3.2.2. Change in the relative dielectric constant (measured from the slope of P - E curves as E field passed through 0 kV/mm) with increasing preload stress [72].

The effect of prestress on the nonlinear dielectric (polarization) and piezoelectric (strain) response of PZT-5H piezoelectric ceramics was studied in [73]. The response to bipolar (-2/+2 MV/m) and unipolar (0/+2 MV/m, -0.4/+2 MV/m) electric field under constant prestress (up to 175 MPa) was described. Prestress mainly influences non-180° process first in the bipolar regime. In the unipolar case, the dielectric and piezoelectric response achieves maximum values near 50-60 MPa due to higher number of available non-180° domains which were caused by prestress. The dielectric and piezoelectric response of the material is proportional to the value fraction of non-180° domains and to the difference in domain wall pressure created by mechanical and electrical loads.

New electromechanical method of poling PZT ceramics was suggested in [74]. This method allows for significant decrease of the electric field necessary for poling, while simultaneously increasing the piezoelectric coefficient. Commercial PZT PIC 151 samples were used. The ferroelectric coercive field of such material is about 1000V/m, the ferroelastic coercive stress is about 40MPa. Cylindrical samples

dimensions were 6 mm height and diameter 5.85 mm. Both circular faces of each sample were sputter coated with thin (100 nm) Au/Pd layers serving as electrodes (Fig. 3.2.3).

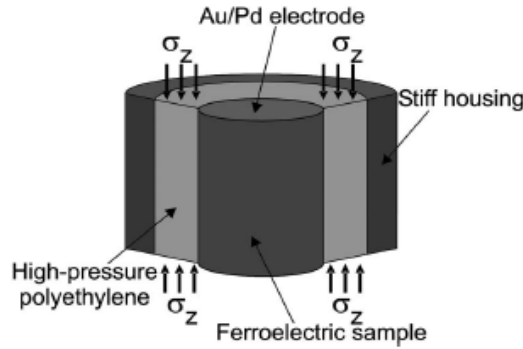


Fig. 3.2.3. Schematic sketch of a cut through the sample holder used for electromechanical poling [74].

Sample holder consists of stiff cylindrical steel housing containing high pressure polyethylene (HDPE) tube. The sample was placed inside the HDPE tube which transfers axial compressive stress σ_z into uniform radial compressive stress σ_r due to the lateral expansion of the HDPE tube. Three different poling protocols were used. The first protocol (only E_{pol}), consisted of the linear increase of the external electric field E from zero to certain poling field E_{pol} within 25 s, followed by linear decrease back to zero in the same span. Mechanical load was not applied for the first protocol. For second protocol (first σ_z , then E_{pol}), force $F = 12.7$ kN corresponding to stress $\sigma_z = 100$ MPa was applied to HDPE tube, which transformed it to radial stress $\sigma_r = 90$ MPa on the sample. Then an electric field cycle identical to the first protocol E_{pol} was performed before the mechanical stress was removed. In third protocol (first E_{pol} , then σ_z), E was first applied to E_{pol} , then σ_z was increased from zero to 100 MPa within 20 s. The sample was kept under this condition for 60 s, then the mechanical load was removed within 20 s, and E was turned down within 25 s. The charge in the sample was measured by detecting changes in surface charge during poling. The application of σ_z strongly increases the effectiveness of the poling, gives the higher values of the remnant polarization P_r . The samples may be poled with lower fields and reach higher values of P_r when the mechanical load is applied. This process is more effective when the load is applied when the electric field already influences the sample (protocol 3). The improvement of the piezoelectric properties with electromechanical poling is connected to the ferroelastic properties of PZT and to the possibility of non-180° domain reorientation. The application of single low electric field causes only very little domain reorientation, and thus very small ferroelectric polarization and piezoelectric response. When σ_r is applied without external field, some non-180° domains are aligned along the axial direction of the cylindrical sample. If an electric field is missing, the orientation is random and no macroscopic polarization develops. When the external field is applied to this sample under mechanical load, the remaining non-180° domains switch very easily in the direction of the electric field. If the field is high enough, some of the domains that were oriented down prior to electric field application are oriented by 180° switching. These processes lead to higher remnant polarisation and higher d_{33} value at low poling fields (Fig. 3.2.4). At high poling fields, the advantage of this method over the

all-electrical poling decreased. Second poling protocol is much more effective than protocol 1 for low electrical fields, but not at high fields. In the protocol 3, the external field is applied first, resulting in the first switching of 180° domains as well as non- 180° domains into the poling direction.

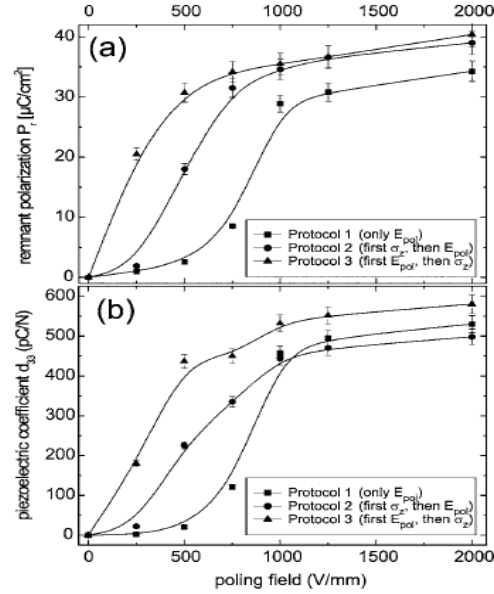


Fig. 3.2.4. Remnant polarization P_r (a) and piezoelectric coefficient d_{33} vs. poling field for three poling protocols [74].

The polarization switching in PZT ferroelectric bulk ceramics undoped (pure) and doped with donor Nb (PZTN) or acceptor Fe (PZTF) was studied by means of both hysteresis loops and transient current measurements at room temperature (Fig. 3.2.5) [75].

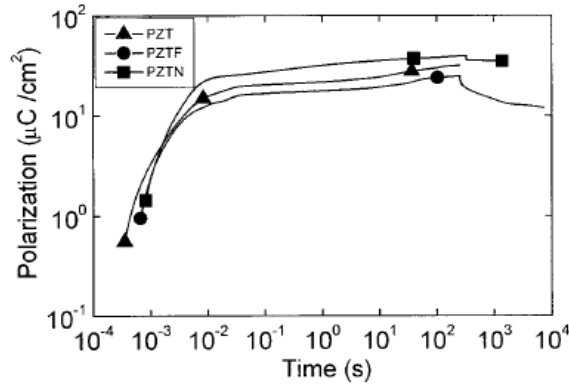


Fig. 3.2.5. Time dependence of polarization for the PZT, PZTN, and PZTF obtained from switching integration while applying and after removing a poling electric field [75].

It revealed that during the poling process in PZT ceramics, the reorientation of the polarization may be interpreted as resulting from two contributions: 90° domain wall reorientation followed by 90° domain wall rearrangement, resulting in higher reorientation of 90° domain walls. 90° domain wall rearrangement enabled an increase of about 40% of the total polarisation in the samples. The reorientation behaviour of domains showed to be strongly influenced by the type of impurity and by the electrical field strength.

The polarisation reversal in ceramics is extremely slow spending long time to be completed in comparison with single crystals. Multidomain crystals can be convert into single domain ones by the electrical field application in single crystals. Their dynamics might be well understood, but this is not the case in polycrystalline ferroelectrics. The polarization switching in ferroelectric bulk ceramics is located at the beginning near the surface of the grains where domains are nucleated and grow to meet each other. Such behaviour was observed by electron microscopy. When the polarization is switched under high bipolar electric field it may decrease with the gradual increase of the number of the cycles. Also the coercive field increase is observed [76].

Domain switching and rotation in PZT ceramics may be caused by mechanical stress or electric field application, because the ceramics possess ferroelastic and ferroelectric properties. It was found that space charge field was generated while applying pulse. Direction of the field was fixed independently of the pulse cycles. The possibility of bipolar pulse poling was investigated in [77]. Disc samples were 14 mm in diameter and 1 mm thick. The bipolar pulse with the periods T of 800 msec and 12 s as shown in Fig. 3.2.6 was applied up to 10 times.

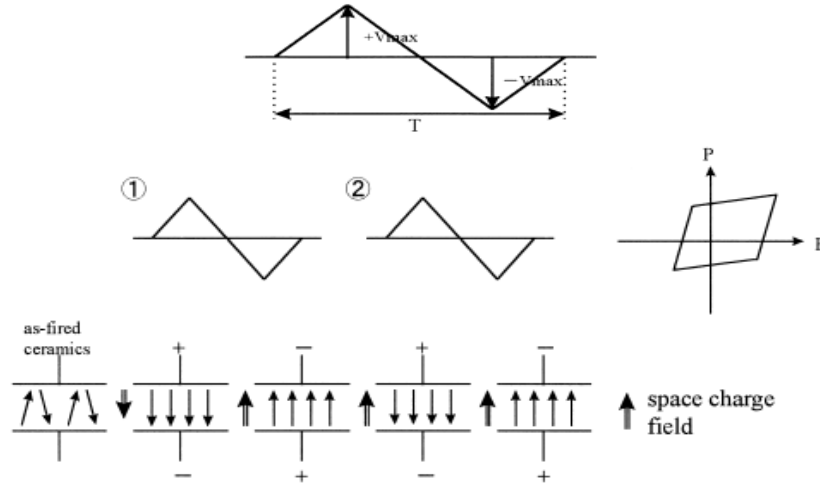


Fig. 3.2.6. Bipolar pulse for the measurement P - E hysteresis in PZT ceramics and generation of space charge field by applying bipolar pulses [77].

The comparison (Fig. 3.2.7) between bipolar poling (open circles) and DC poling (closed circles) in the case of soft and hard PZT ceramics was observed after 10 times repeated bipolar pulses ($E = \pm 3.0$ kV/mm, $T = 800$ ms) application. The DC poling at 80°C , 3.0 kV/mm and 30 min was done. Electromechanical factor k_p in hard PZT composition, was less than half of k_p obtained by DC poling. The difference in the poling effect was occurred due to the difficulty of 90° domain rotation in tetragonal phase and 71° or 109° domain rotation in rhombohedral phase. The pulse cycle dependence of k_p was investigated, each time the pulse was applied on soft and hard PZT ceramics.

Value of k_p decreases with the first pulse application in poled soft PZT ceramics. It is possible to explain the decrease in k_p by the first pulse corresponding to 90° domain walls rotation (Fig. 3.2.7) k_p was independent of the number of pulse cycles. 180° domain switching is mainly occurred. It was during subsequent cycles.

In case of poled hard PZT ceramics, k_p took minimum at the first pulse application. This phenomenon was thought that by DC poling the oriented 90° domain walls were irritated by the bipolar pulse. Result value of k_p became smaller if compared with depoling. Further increase of the number of pulse cycles brought that k_p increased with the cycle numbers due to the poling again. First pulse application effect may be compared in soft and hard PZT. It can be mentioned that 180° domain walls mainly affected k_p in soft PZT ceramics. Both 90° domain walls as well as 180° domain walls affected k_p in hard PZT ceramics.

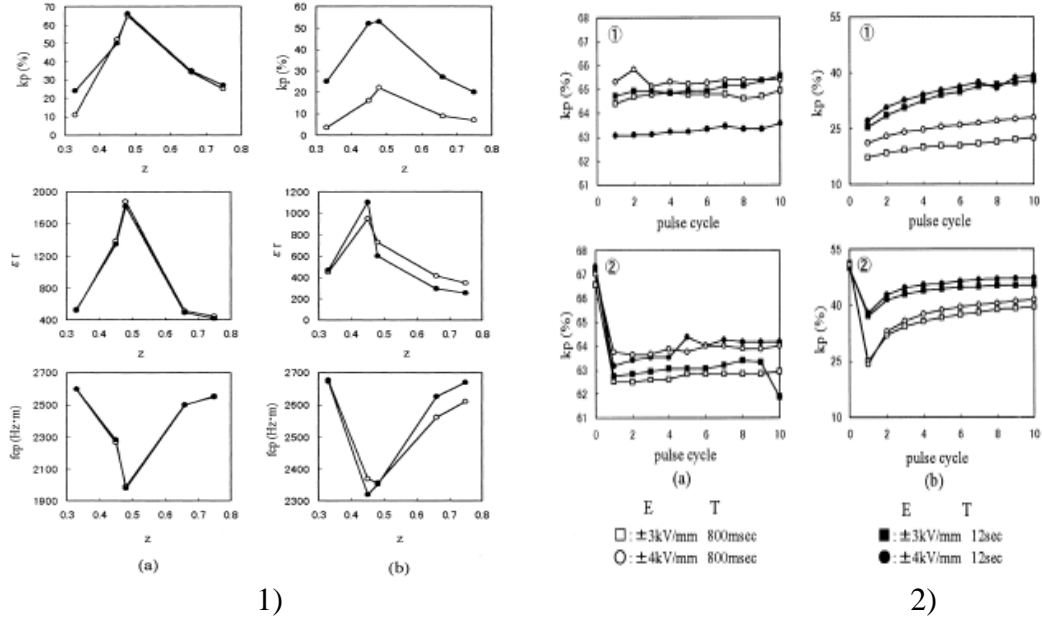


Fig. 3.2.7. 1) Comparison of ferroelectric properties in (a) soft and (b) hard PZT ceramics between pulse poling (\circ) and DC poling (\bullet).
2) Bipolar pulse cycle dependence of k_p when the pulses were applied to (1) as-fired and (2) DC poled (a) soft and (b) hard PZT ceramics [77].

If the material is heated above the Curie temperature, aligned domains return to random state in poled piezoelectric ceramics. This behaviour is called thermal depoling. This process brings changes in electrical and mechanical properties. The elastic anisotropy and fracture toughness anisotropy dependence on depoling temperature were investigated using ultrasound and Vickers indentation in PZT piezoelectric material. Depoling is also evident through changes in domain character revealed by X-ray diffraction. Effects of thermal depoling on elasticity and fracture toughness of PZT ceramic and the relationship between anisotropy and preferred domain orientation were discussed in [78]. Vickers indentation was applied to measure the fracture toughness of the unpoled and poled PZT ceramics. For poled samples (rectangular bars $23 \text{ mm} \times 7 \text{ mm} \times 6 \text{ mm}$), the experiments were performed on the side surfaces parallel to the polar direction. Care was taken throughout sample preparation to minimize thermal effects during cutting or polishing by the generous use of coolants. Applied loads were varied from 9.8 to 196 N. Figure 3.2.8 shows typical indentation cracks on the side surfaces of unpoled (a) and poled (b) PZT. Thermal depoling treatment demonstrated that anisotropy transition is gradual and begins prior to reaching manufacturer's designated Curie point, suggesting that some grains undergo depoling prior to others.

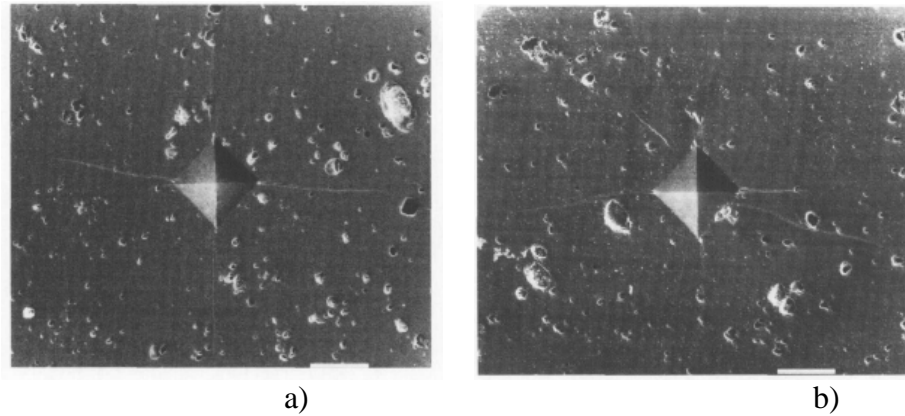


Fig. 3.2.8. Typical indentation cracks under an indent load of 49 N on polished side surfaces of (a) unpoled and (b) poled PZT samples [78].

Poling of ferroelectric ceramics in order to produce biased domain state is usually taking to the account the respect to single domain direction. Subsequently, all property assessments are made with respect to this unique direction. Motion of 90° and 180° domain walls caused the changes of the average orientation state within the crystals during poling of piezoelectric ceramics with the tetragonal crystal structure. The most investigations of reorientation within 90° domain walls focus on the ceramics either aligned with the initial poling direction or orthogonal to it [79].

Domain orientation distributions (DOD) were measured in PZT Navy VI piezoceramics poled subsequently in two orthogonal directions. Such measurement demonstrates potential of domain orientation, which is further responsible for the anisotropy of electromechanical properties. Samples were cut into parallelepipeds and finely polished by $0,1\text{-}\mu\text{m}$ alumina grinding media. The samples were electrically poled by the electric field located in range from 0 to 24 kV/cm (Fig.3.2.9). Poling was done in silicone oil for 30 min.

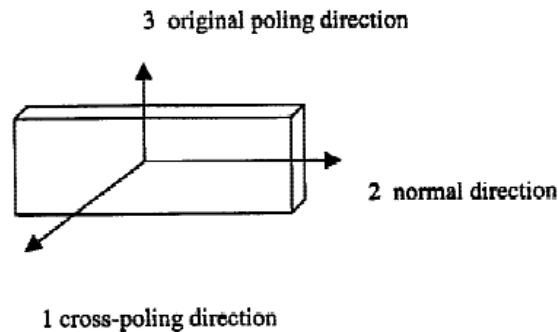


Fig. 3.2.9. Poling directions [79].

The poling process was resulted in an initially axisymmetric texture with $[001]$ or long c-axis orientations aligned with the original poling directions. By use of the same electric cross-poling along direction orthogonal to the original poling direction, DOD changes are possible. Partial cross-poling produced partial reorientation of domains such that two maxima can be recovered in the DOD. It will be visible in multiaxial orientation distribution wherein the proper anisotropy is no longer axisymmetric but orthotropic. Poling process can be completed to produce single maximum in DOD by the continued cross-poling. This final orientation distribution is not entirely axisymmetric and retains the effects of the starting poling. Such poling

treatment has one interesting aspect. The degree of orientation in the new poling direction is stronger than the original poling treatment. But the cross-poling treatment might not be as severe as original poling treatment. This thing may have important implications on piezoelectric performance and design of poling.

Preferred domain orientation of piezoelectric ceramics develops through domain switching under electric poling. In previous investigations the critical free energy required for domain switching has been assumed as constant. This assumption leads to overestimation of the poling-induced texture and provides no explanation for the switching reversal in ferroelectric ceramics after the poling field is removed. Domain switching fraction dependent model has been proposed to evaluate 90° domain walls switching in piezoelectric ceramics. The overall domain switching energy includes intrinsic threshold energy and interaction energy. Under electric field, both inhabit domain switching. The interaction energy increases with 90° domain walls switching fraction. Upon removal of the poling field, the interaction energy is the driving force for switching reversal. The switching reversal will not stop until the interaction energy decreases to the value smaller than the intrinsic threshold energy. This greatly weakens the texture. Computer simulation was performed to calculate the domain orientation distribution for the tetragonal ferroelectric ceramics during the various poling stages. This model predicts well the texture for piezoelectric ceramics under electric field and the remanent texture after poling when compared with experimentally measured pole figures. The remanent domain switching after poling is the result of the balance between the interaction energy and intrinsic threshold energy [80].

3.3. Lead lanthanum zirconate titanate (PLZT) ceramics.

Ferroelectric PLZT ceramics have to be poled for presentation of their piezoelectric properties, since only then it presents remnant polarization P_r , which must be as big and stable as possible. P_r also depends on the electric process of poling. Polarization data systematically obtained on PLZT 8/65/35 and 12/40/60 ceramics from hysteresis loops and P-T diagrams were reported [81]. Results are matching to the classical concept of domain switching. It has been proved that application of 20 kV/cm during cooling from 100° C to room temperature is suitable poling method for PLZT ceramics. Discs 0.8 mm thick and 46 mm² of surface area were prepared for the experiment. P_r values which correspond to different poling operations were obtained by the charge integrating method.

Fig.3.3.1 a)-b) show the thermal variation of P_r in four PLZT 8/65/35 samples poled using different ways. All of them were heated to 100° C and field of 20 kV/cm was applied during 15 minutes: in sample 1, the electric field was removed allowing the sample to cool in 60 minutes; sample 2 was cooled in 15 minutes with the field removed; sample 3 was also cooled in 15 minutes with the field applied and sample 4 was cooled in 60 minutes with the electric field also applied.

Fig.3.3.1 shows well known results from hysteresis loops: apart from an electric field equal to the coercive field for the rhombohedral PLZT, P_r values become quite large. Therefore, if 20 kV/cm is used as poling field, the increase of P_r is small at larger temperatures and poling times.

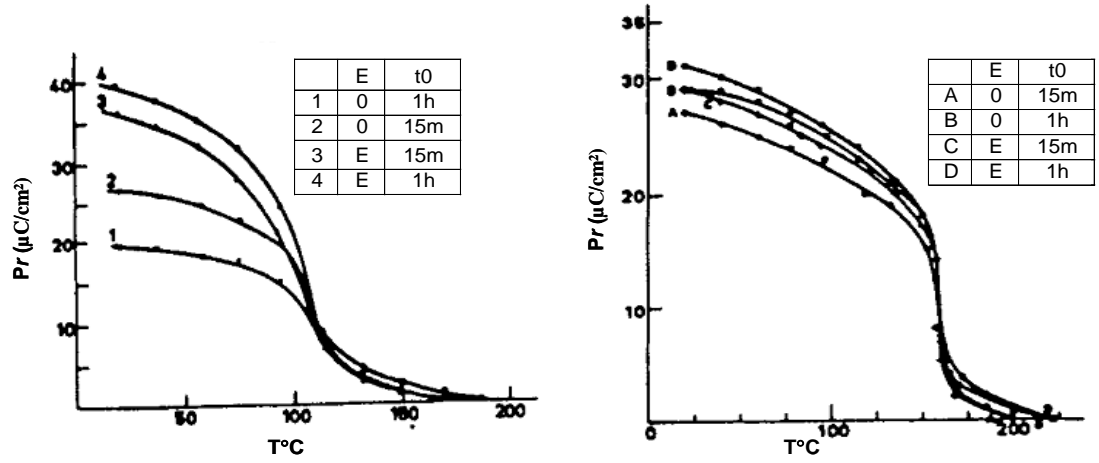


Fig. 3.3.1. a) PLZT 8/65/35 poled at 100 $^\circ\text{C}$ and 20 kV/mm and b) PLZT 12/40/60 P_r for different poling [81].

Fig.3.3.1.a) illustrates the importance of the electric field application during cooling down, as well as the cooling time effect. It is known that if ferroelectric ceramics is cooled with an electric field applied, successive domain configurations are very similar to each other and P_s grows up since 90° and 180° domain walls already lined up remain at that state. Cooling must be applied on at certain rate and a slower rate is more useful. Curves 1 and 2 show the necessity to maintain the electric field applied while cooling to prevent thermal relaxation effects. These effects are larger when cooling rate is smaller.

So, good strategy to pole PLZT ceramics is to warm up the sample to 100 $^\circ\text{C}$ and to apply electric field of 20 kV/cm during cooling down to room temperature.

Chapter 4.

Experiment procedure and results.

Generally the poling process must take into account the material texture, domain geometry and switching behavior. Poling conditions are very important for further achievement of defined material properties for commercial application. PZT ceramics is commercially poled by the strong D.C. voltage at elevated temperatures, but the poling conditions are not usually known to the customers. In applications, alignment of the dipole moments in ferroelectric ceramics is influenced by the electric field in the direction opposite to the poling field. If it is strong enough, such electric field could completely destroy the polarization orientation and therefore also the piezoelectric properties. While poling (as well as following application of electric field, i.e. so called depoling) process is basically the dynamic process, different poling (and depoling) results are supposed from D.C. or pulse-poling voltage. Poling-dependent material properties were recently studied in soft and hard lead zirconate titanate (PZT) [82, 83], lead titanate (PbTiO_3) [84] and barium titanate (BaTiO_3) [85] ceramics for the electric fields exceeding the coercive field.

Experimental investigation of different poling methods and their influence on material properties of PZT ceramics samples of specific shape was the main task of this work. Switching process characteristics (maximum current value and switching time) were investigated during pulse poling of PZT ceramics. These parameters were observed under the influence of electric field and temperature.

4.1. Samples material description.

Samples for the experiments have been supplied by the American Piezo Ceramics International Ltd., Mackeyville, PA, USA and Piezokeramika, s.r.o., Libřice, Czech Republic. Samples include soft (APC 850 and 856) as well as hard PZT (APC 840, 841 and 880) ceramics (Tab.4.1.1). Due to the resonant method used for the material properties measurement [86], sample shapes were bar and disc (Fig.4.1.1). There are a lot of contributions which describe the methods for material constants determination [87, 88, 89]. Dimensions of bar-shaped samples were – length 15mm, width 4mm and thickness 1mm. Plate dimensions were – length 14mm, width 7mm and thickness 1mm. Discs were 15mm in diameter and 1mm in thickness. Main faces of the discs and bars were electroded by the fired silver paste.



Fig.4.1.1. Disc and bar samples used for depoling.

| | APC840 | APC841 | APC850 | APC856 | APC880 |
|---------------------------------|--------|--------|--------|--------|--------|
| Curie temperature T_c (°C) | 325 | 320 | 360 | 150 | 310 |
| Density (kg/m ³) | 7793 | 7830 | 7639 | 7609 | 7757 |
| Coercive field (kV/mm) | 1,44 | 1,42 | 1,4 | 0,8 | 1,27 |
| Mechanical quality | 500 | 1400 | 80 | 72 | 1000 |

Table 4.1.1. Basic properties of PZT ceramics [100].

Mainly the further investigation involves de-poling, re-poling, cross-poling and bipolar pulse application techniques for poling procedure. Fig.4.1.2 shows the sum of components in definition of methods due to the orientation of electric field and spontaneous polarization vectors. Any other arbitrary electric field direction is a composition of these field directions studied in re-poling, de-poling and cross-poling.

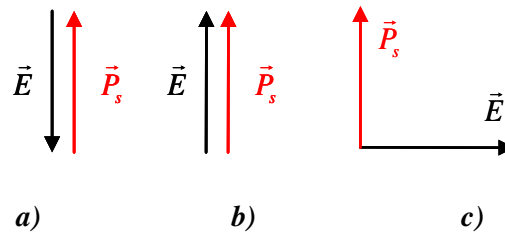


Fig. 4.1.2. Depoling – a), re-poling – b), cross-poling – c) methods.

4.2. Crystallographic orientation and material properties.

Selected polarization directions represent the complete set where possible contribution to the enhancement of material properties could be expected with respect to chosen sample geometry and material symmetry (which could be rhombohedral or tetragonal for PZT ceramics with composition close to MPB). For example, the length-extensional vibrations of a thin bar could be affected much less by an application of transversal poling field. In this case, the cross-poling method was applied to a plate vibrating in the thickness-shear mode. Experimental setup was created with respect to detailed investigation of piezoelectric and dielectric properties near the MPB region [90]. The theoretical expectation of crystal orientation dependence of piezoelectric properties was studied for tetragonal and rhombohedral

compositions [91]. Physical properties of PZT single crystals are dependent on the crystal orientation. The estimation of PZT ceramics practical usage may be prognosed if single crystal properties are known. It is necessary to know the anisotropy of material. For example, to define the spontaneous polarization in ceramics we need to know the average cosine value of angle between direction of spontaneous polarization in single grains and polar axis of ceramics. Possible directions of spontaneous polarization in ferroelectric materials were described in [92]. The anisotropy of material properties in ferroelectric materials was described for $3m$, $4mm$, $6mm$ crystallographic classes. The minimum value of dielectric permittivity was found in the direction along the poling one for tetragonal PZT crystal [91]. The maximum values of d_{33} occur along the polarization direction. The maximum permittivity in rhombohedral PZT crystal was calculated in the direction perpendicular to the poling direction. Maximum values of d_{33} and k_{33} were obtained in the directions 56.7° away from the poling direction respectively. Such direction is not the same as direction in the tetragonal state (Fig.4.2.1).

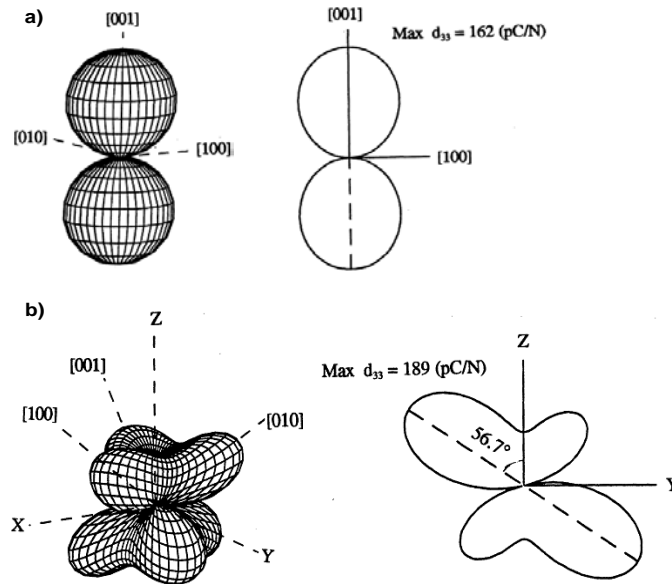


Fig. 4.2.1. Piezoelectric constant d_{33} of tetragonal (a) and (b) rhombohedral PZT [91].

The most enhanced value of d_{33} and k_{33} are located along the direction close to cubic perovskite [100] one. If PZT composition approaches the morphotopic phase boundary from the rhombohedral side, the d_{33} increases drastically. Such crystallographic dependences gave the optimal directions in which material property changes may be observed.

4.3. Resonance method.

The resonance method of measurement [93] was used in depoling, re-poling and cross-poling experiments. This method lies in complex impedance measurement of sample electrical circuit, which depends on frequency of weak electric field (converse piezoelectric effect is used).

Material properties of PZT ceramics were obtained from impedance spectrum measured by HP4192A analyser. The programme software application Agilent VEE Pro was used [94]. Scheme of connection is shown in Fig.4.3.1. Parameters of components or circuits are measured by analyser in the range of adjustable frequencies (5Hz-13MHz), test signal level ($5 \text{ mV}_{\text{rms}}$ - $1.1 \text{ V}_{\text{rms}}$) and DC bias level (from -35V to +35 V).

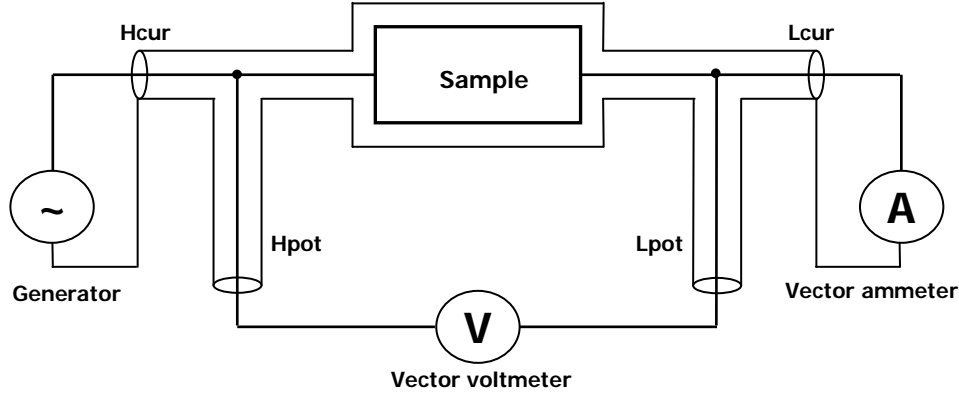


Fig. 4.3.1. Four terminal pair measurement principle [95].

The four terminal pair configuration helps to the higher accuracy in the measurement in high frequency range and avoids measurement limitations in inductance, interference of measurement signals and residual factors in connection method [95]. The current terminals (high current H_{cur} and low current L_{cur}) reduce the measurement current flow through the sample. The potential terminals (high potential H_{pot} and low potential L_{pot}) are detecting the voltage across the sample. Two independent parameters are measured in each cycle. The combination of these parameters describes both resistive and reactive (conductive and susceptive) characteristics of the sample. It is possible to measure the couple of these parameters (display A and B) as shown in Table 1 (see Appendix I). Analyser measures resistance R and reactance X in equivalent series circuit mode and conductance G and susceptance B in equivalent parallel circuit mode. Other parameters may be calculated from R and X , G and B as shown in Table 2 (see Appendix I).

Electrical impedance curve is dependent on mechanical behavior of the sample. The resonance frequency may be determined from the condition of zero impedance ($Z \rightarrow 0$), and antiresonance frequency from condition of zero admittance ($Z \rightarrow \infty$). Material properties are determined from resonance/antiresonance frequencies of sample with specific geometry. Electromechanical characteristics are calculated from theoretical formulae for these frequencies (see Appendices II-V). Vibrations distinguished piezoelectrically free and clamped (resonance frequency depends on piezoelectric properties). The vibration mode is specified by - material properties, sample geometry and electrode pattern. Electromechanical properties follow from equations:

- equation of motion

$$\frac{\partial T_{ij}}{\partial x_i} = \rho \cdot \frac{\partial^2 u_j}{\partial t^2} \quad (5)$$

- Maxwell's equation

$$\frac{\partial D_i}{\partial x_i} = 0 \quad (6)$$

- equations of state

$$\begin{aligned} S_{ij} &= s_{ijkl}^E \cdot T_{kl} + d_{nij} \cdot E_n \\ D_n &= d_{nkl} \cdot T_{kl} + \varepsilon_{nm}^T \cdot E_m \end{aligned} \quad (7)$$

4.4. Depoling method.

Disc and bar samples (APC 850, 856, 840, 841, 880) were chosen for this experiment. There is no standard setup of poling conditions for the different samples. They can be specified up to the further application. There is only one limitation, that poling electric field cannot be less than coercive field. Virgin PZT samples were poled at elevated temperature in strong D.C. electric field. According to previous tests, the poling temperatures have been selected high enough to ensure the saturated material properties with moderate aging after the poling. Soft PZT ceramics has been poled at 90°C and hard PZT at 130°C, both types by the D.C. electric field 2kV/mm for 5min in silicon oil bath. Oil (Lukosiol M50 type) was used due to the prevention of sample breakdown in surrounding air (air breakdown range 1-3 kV/mm is dependent on air humidity; oil burning point is higher than 200°C). Samples were placed into the special metal holder during poling in the oil bath (Fig.4.4.1). Heating of the oil bath was performed by magnetic stirrer/heater Heidolph MR 3001 K. Temperature control was realized by Heidolph EKT 3001 controller and detected by thermometer. Temperature changes bring the generation of electric charge on the sample electrodes which may provide the further negative impact on polarization (pyroelectric property of the sample). Samples were electrically shortened during heating before poling voltage was applied.



Fig. 4.4.1. Poling experimental setup.

Higher temperature was chosen for the hard PZT due to easier domain wall mobility. Due to the aging [96] in the material coefficients, the measurements were

done one day after the poling. Then the samples were aged for one decade (i.e. for the next ten days) and material properties were measured again. At the same time, the electric field depoling of the samples was performed. PZT aging and changes in the material properties due to the depoling process would be separated in such way. Depoling has been done by the electric fields of 250V/mm, 500V/mm, 750V/mm and 1000V/mm of the opposite direction as poling field at room temperature. Depoling field was applied either as D.C. field, or in the form of unipolar rectangular pulses (pulse shape: zero field for 1s, applied D.C. field for 1s etc. – Fig.4.4.2) for the same total time as poling field (i.e. for 5 minutes, which means approximately 150 pulses and PZT samples were subjected to the non-zero electric field for 2.5 minutes).

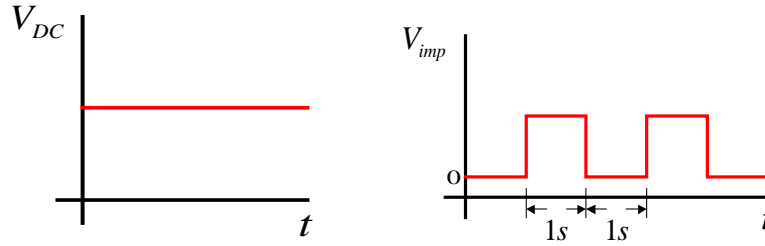


Fig. 4.4.2. Depoling voltage D.C. and pulse shapes.

Material properties measurement has been done by the resonant methods according to the IRE Standard 1961 [86]. Length-extensional vibrations of the bar (measured resonant f_r , antiresonant f_a frequency and sample static capacitance C_0 measured at 1kHz frequency) resulted in the values of material properties s_{11}^E – elastic compliance, k_{31} – transverse electromechanical coupling coefficient, d_{31} – transverse piezoelectric coefficient, ϵ_{33}^T – permittivity (Appendix II). Radial disc vibrations (measured resonant f_r frequencies for fundamental and the first overtone mode, antiresonant f_a frequency of the fundamental mode and sample capacitance C_0 measured at 1kHz frequency) give us the values of s_{12}^E – elastic compliance, k_p – electromechanical coupling factor, ϵ_{33}^T – permittivity and Poisson's ratio σ^E (Appendix IV, VI). Thickness-extensional disc vibrations could be used for c_{33} , k_t measurements (measured resonant frequencies of the fundamental f_1 and the third overtone mode f_3) (see Appendix III). Measurement scheme of the impedance spectra is shown in Fig.4.4.3. Moreover, d_{33} has been directly measured on d_{33} -meter (ZJ-3C type). Samples were pressed by harmonic force with amplitude 0.25N at 110Hz frequency and their response was compared with internal reference standard [97].

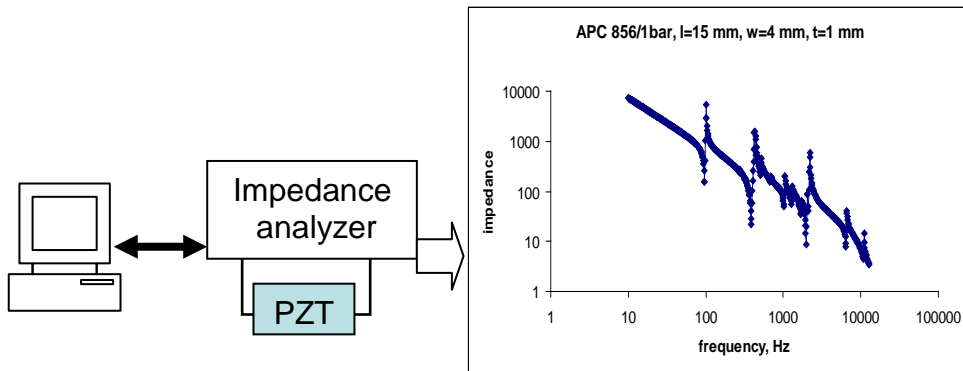


Fig. 4.4.3. Scheme of resonant spectrum measurement.

The macroscopic symmetry of poled piezoelectric ceramics is ∞m and it is independent of each grain's symmetry. At the first stage of experiment the dielectric, piezoelectric and elastic material properties of virgin PZT ceramics samples were measured. Values of material properties of the poled PZT ceramics before depoling are listed in Table 4.4.1.

| | d_{33} | d_{31} | k_{31} | k_p | k_t | ϵ_{33}^T | s_{11}^E | c_{33}^E | σ^E |
|-----------------|----------|----------|----------|-------|-------|-------------------|----------------------------|----------------------|------------|
| PZT type | [pC/N] | | [%] | | | $[\epsilon_0]$ | $[10^{-12}\text{Pa}^{-1}]$ | $[10^{11}\text{Pa}]$ | [1] |
| APC 850 | 480 | 186 | 35 | 60 | 48 | 2150 | 14.8 | 1.16 | 0.32 |
| APC 856 | 609 | 196 | 32 | 62 | 47 | 2870 | 14.4 | 0.99 | 0.45 |
| APC 840 | 274 | 97 | 29 | 55 | 46 | 1140 | 11.2 | 1.25 | 0.44 |
| APC 841 | 301 | 114 | 32 | 59 | 46 | 1284 | 11.0 | 1.31 | 0.40 |
| APC 880 | 299 | 92 | 29 | 54 | 46 | 1044 | 11.1 | 1.24 | 0.44 |

Table 4.4.1. Material properties of poled PZT ceramics before depoling.

D.C. voltage depoling

Significant changes in the material coefficients occur in soft PZT ceramics for the values of s_{12}^E , σ^E , k_{31} , k_p , d_{31} , d_{33} , ϵ_{33}^T . At certain electric field value, the piezoelectric coefficient d_{33} changes its sign (from + to –) for soft PZT. In such case, the sign of d_{33} could be directly measured by the d_{33} -meter. The change in sign means that reverse poling occurred. Similar change in the sign of d_{31} coefficient cannot be found by the resonant methods, but it is also supposed when d_{33} changes its sign. Depoling by the electric field of this magnitude would depolarize soft PZT ceramics more or less; however no virgin state will be reproduced again.

Generally, in case of homogeneous perovskite material, the antiparallel domain states (such as $\uparrow\downarrow$) have all even-rank tensors equal in all components. Odd-rank tensors, on the contrary, should have all components of the opposite sign for the antiparallel domains. Due to the ceramics non-homogeneity and non-uniform domain structure such relationship is not exactly fulfilled for the macroscopic material properties.

Depoling behavior for the measured quantities is shown in Figs.4.4.4-4.4.12 for the piezoelectric, elastic and dielectric properties. Even-rank materials tensors (e.g. the permittivity ϵ_{33}^T and elastic compliance s_{11}^E) do not change the sign by reverting the sign of polarization orientation, but just show the substantial property changes in the range of electric fields where d_{33} changes sign. Odd-rank tensors (e.g. piezoelectric coefficient d_{33}) change their signs as a result of the reverted polarization orientation as it was observed. The depinning of domain walls during

depoling caused the increase in the extrinsic contribution to the piezoelectric response.

Limits for the electric fields, not changing the properties substantially, are listed in Table 4.4.2.

| | D.C. depoling | Pulse depoling |
|---------|---------------|----------------|
| APC 850 | 700 V/mm | 500 V/mm |
| APC 856 | 200-500 V/mm | 200 V/mm |

Table 4.4.2. Electric field applicability limits for soft PZT ceramics.

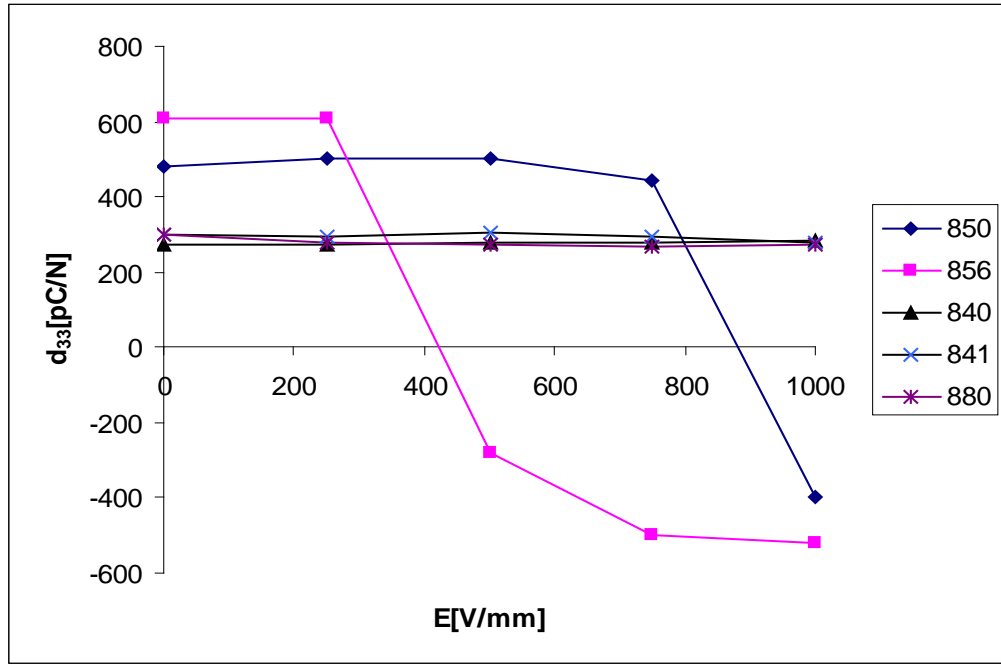
For the hard PZT ceramics, there were no significant changes of the material coefficients observed up to the electric fields of 1000V/mm. Relative changes of the material coefficients over the entire depoling electric field range studied are listed in Table 4.4.3. Relative changes are expressed as a ratio of the maximum change of the property vs. the same property value for not depoled sample (in absolute value):

$$Y' = \frac{\Delta Y}{Y(0)} \quad (8)$$

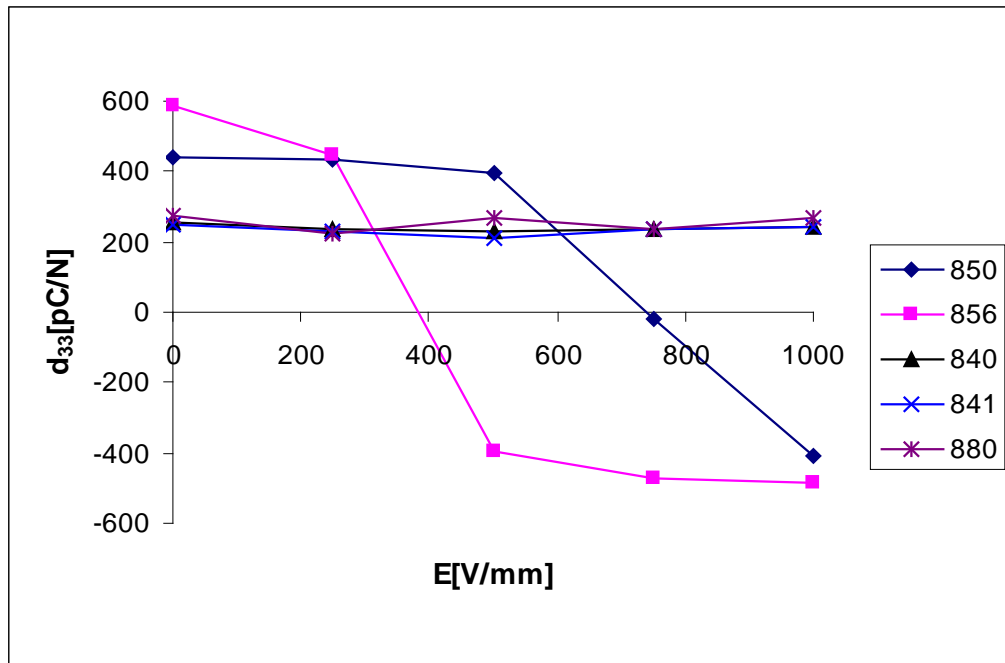
ΔY – is a change of quantity Y over 0-1000 V/mm electric field range, Y(0) – is a value of Y at 0V.

| PZT type | Relative changes of material coefficients (in %) | | | | | | | | | | | | | |
|-----------------|--|-----------|-----------|-------------|-----------|--------|-----------------------|----------------|-----------|-----------|-------------|-----------|--------|-----------------------|
| | Bar | | | | Disc | | | Bar | | | | Disc | | |
| | D.C. depoling | | | | | | | Pulse depoling | | | | | | |
| | d'_{33} | d'_{31} | k'_{31} | s'^E_{11} | d'_{33} | k'_p | ε'^T_{33} | d'_{33} | d'_{31} | k'_{31} | s'^E_{11} | d'_{33} | k'_p | ε'^T_{33} |
| APC 840 | 2.6 | 10.3 | 13.8 | 17.9 | 8.6 | 16.5 | 10.4 | 10.3 | 8.2 | 4.1 | 7.7 | 7.9 | 3.7 | 6.2 |
| APC 841 | 7.9 | 2.6 | 15.5 | 3.6 | 11.6 | 3.6 | 5.1 | 15.9 | 4.7 | 2.8 | 2.7 | 4.8 | 3.4 | 4.3 |
| APC 880 | 10.4 | 5.4 | 0.7 | 3.6 | 8.8 | 1.1 | 5.5 | 19.3 | 4.0 | 4.5 | 4.5 | 5.8 | 5.4 | 5.4 |

Table 4.4.3. Relative changes (in %) of material coefficients for hard PZT ceramics.

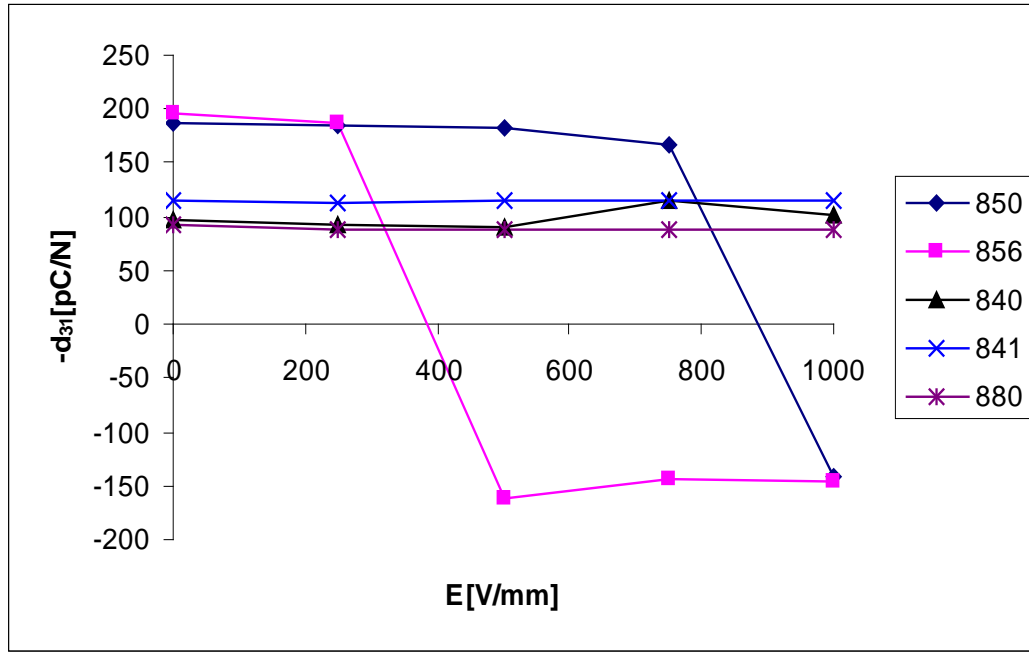


a)

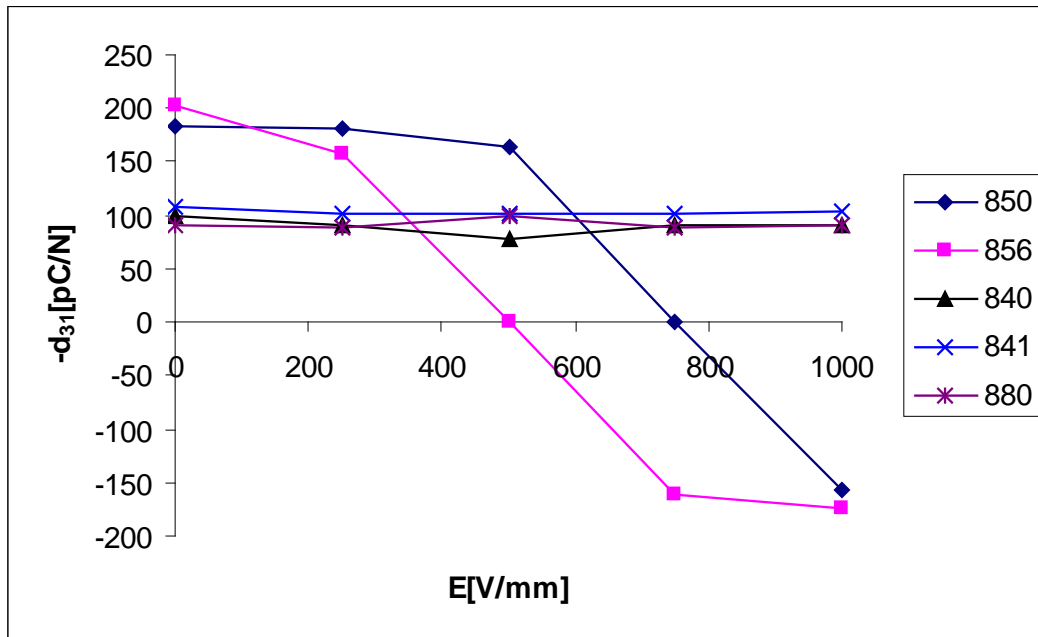


b)

Fig.4.4.4. Piezoelectric charge constant d_{33} after depoling: a) by D.C. and b) after voltage pulses applied for bar samples.

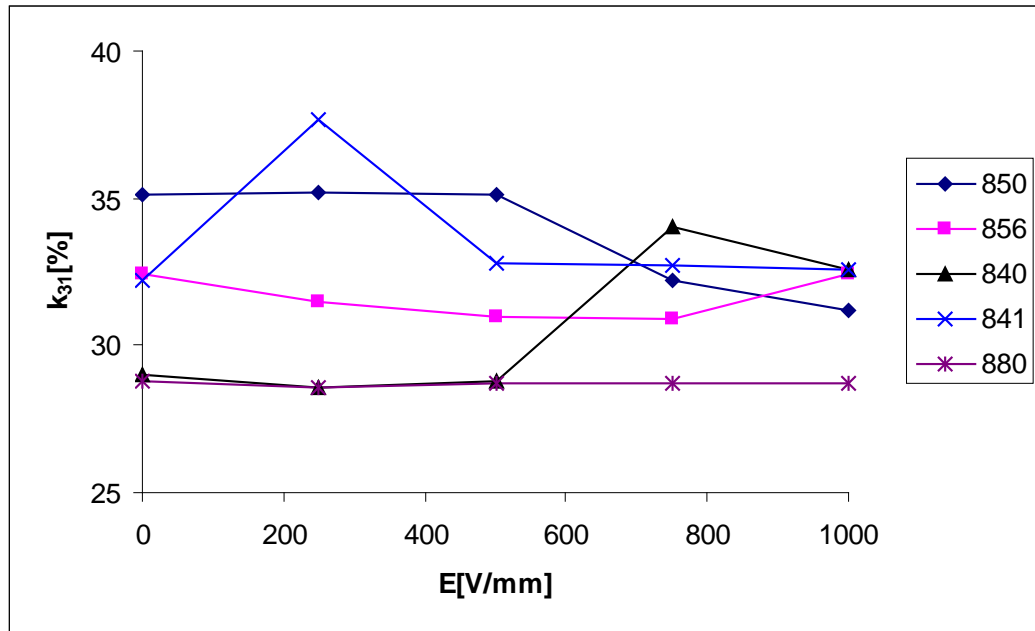


a)

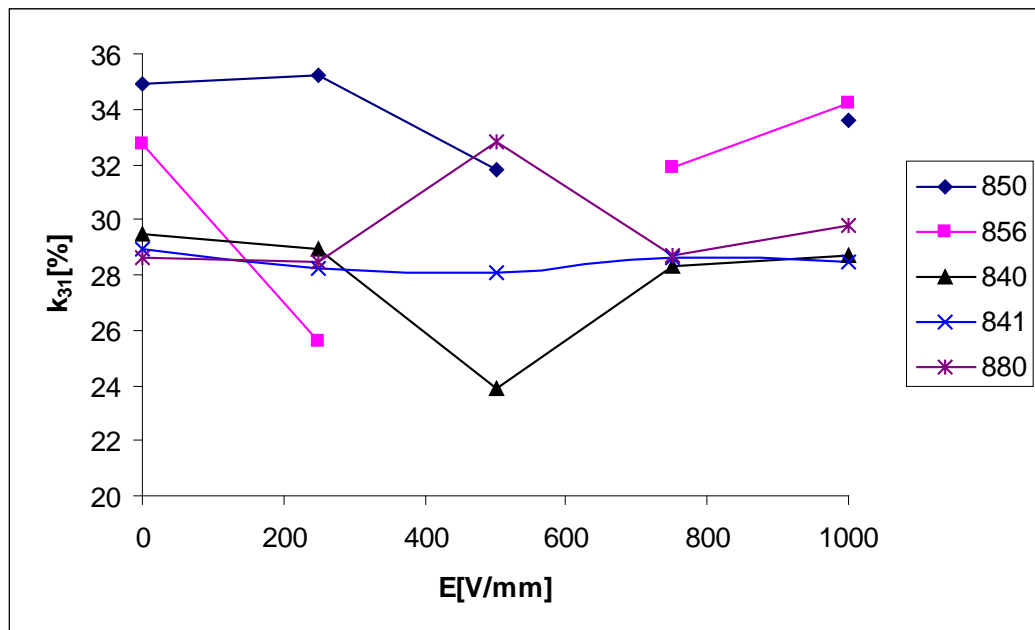


b)

Fig.4.4.5. Piezoelectric charge constant d_{31} after depoling: a) by D.C. and b) after voltage pulses applied for bar samples.

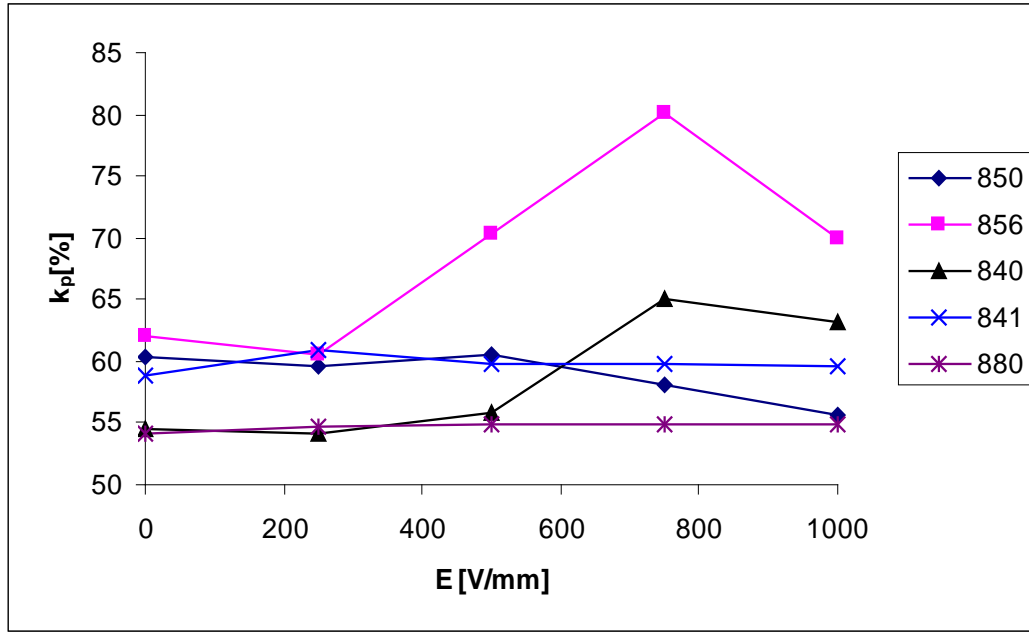


a)

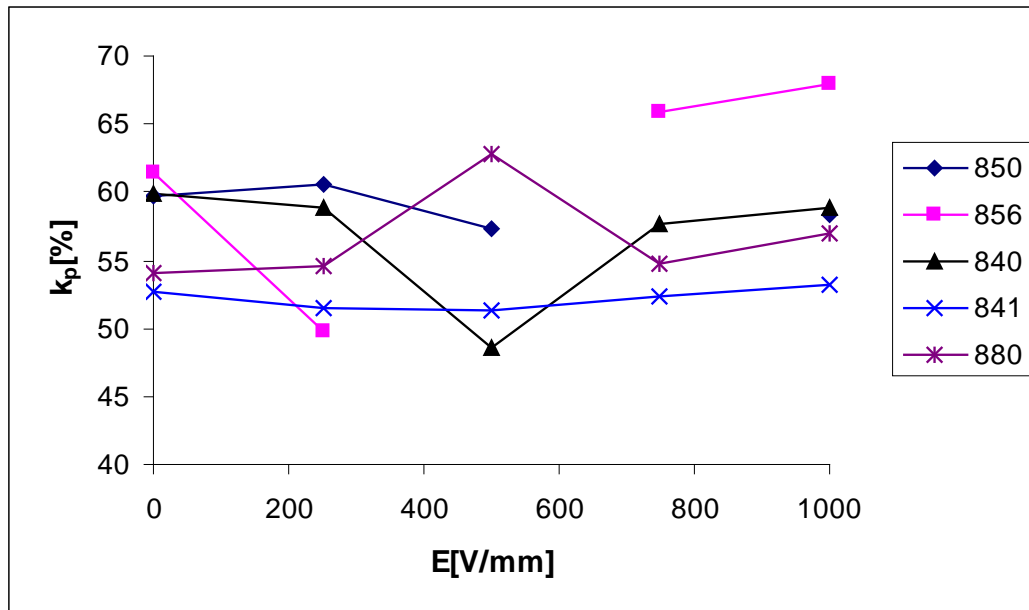


b)

Fig.4.4.6. Electromechanical coupling factor k_{31} after depoling: a) by D.C. and b) after voltage pulses applied for bar samples. Data missing in curves for APC850 and APC856 are due to the non-resonant response of samples.

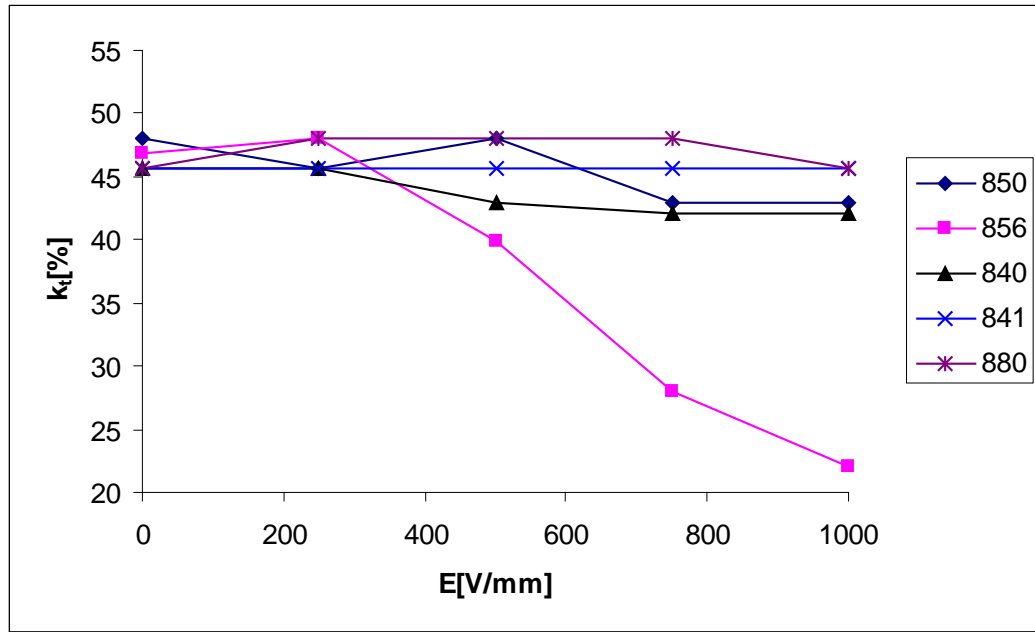


a)

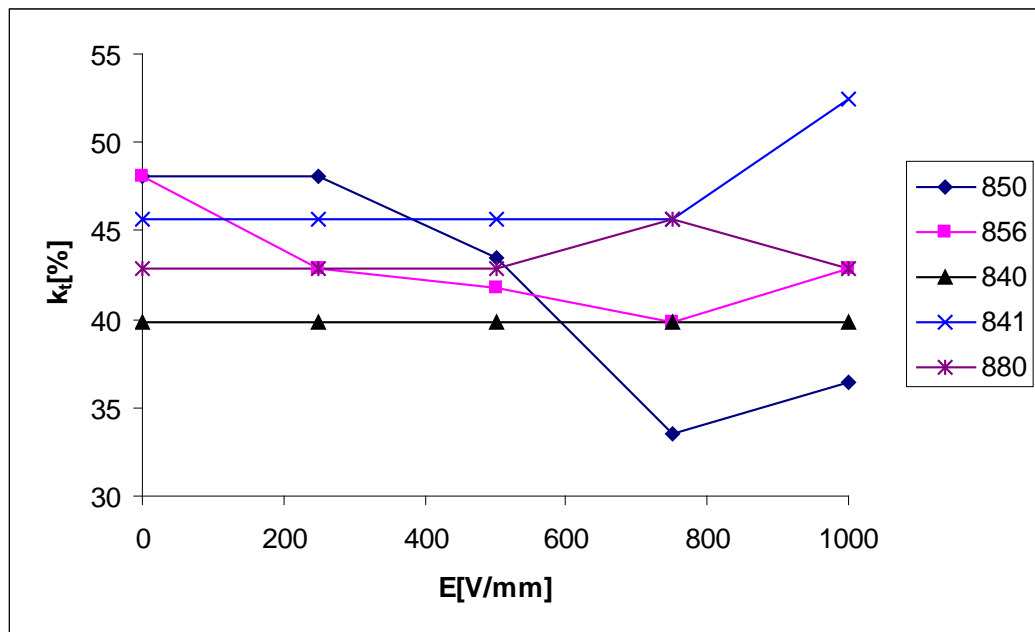


b)

Fig.4.4.7. Electromechanical coupling factor k_p after depoling: a) by D.C. and b) after voltage pulses applied for disc samples. Data missing in curves for APC850 and APC856 are due to the non-resonant response of samples.

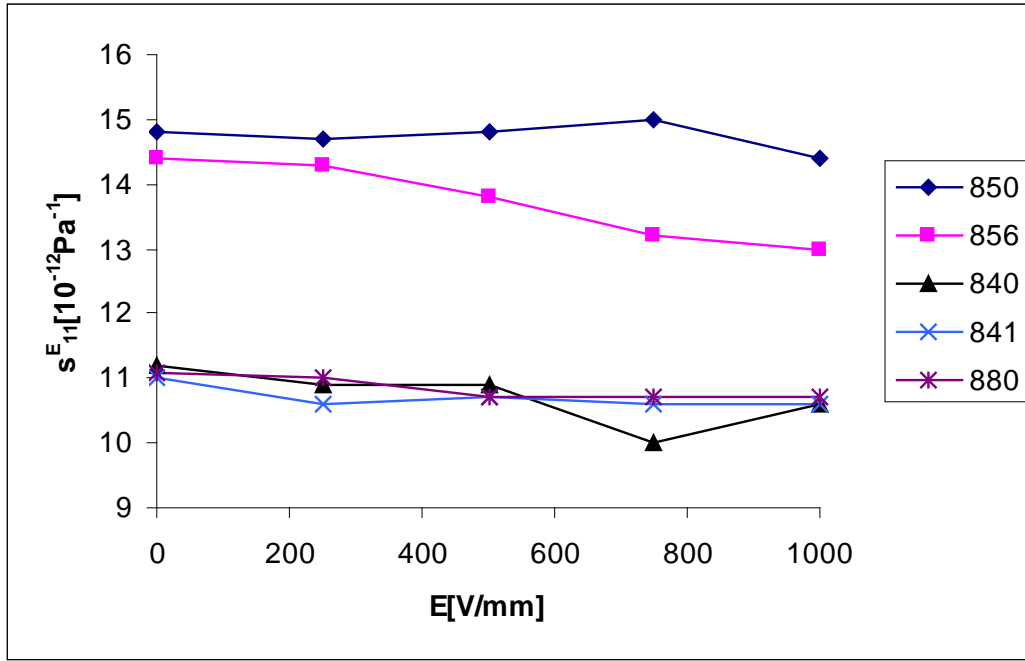


a)

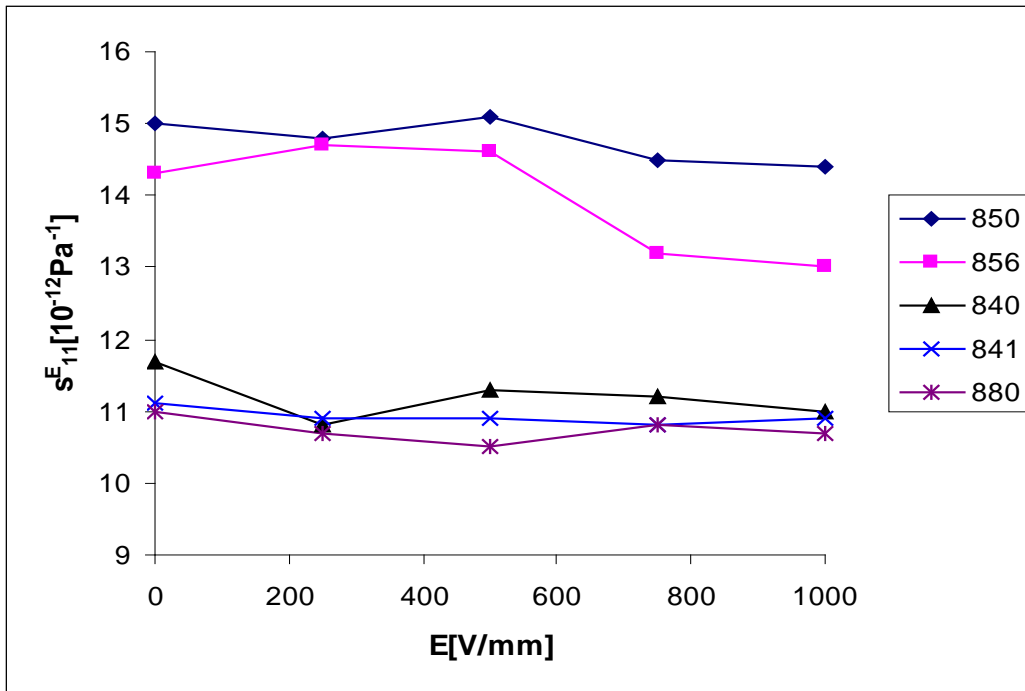


b)

Fig.4.4.8. Electromechanical coupling factor k_t after depoling: a) by D.C. and b) after voltage pulses applied for bar samples.

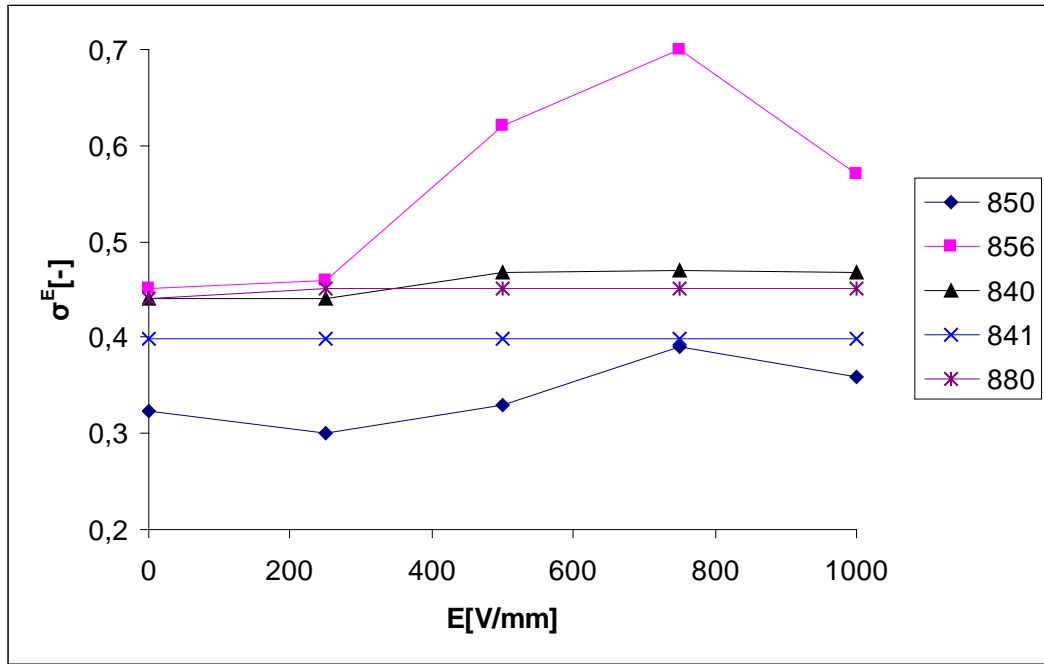


a)

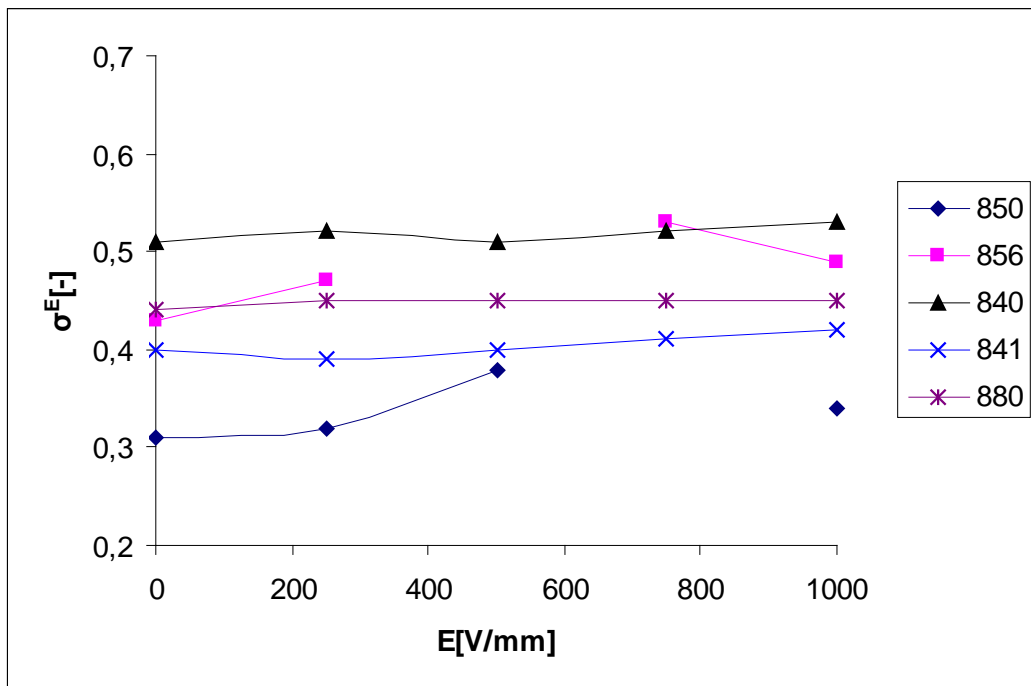


b)

Fig.4.4.9. Elastic compliance s_{11}^E after depoling: a) by D.C. and b) after voltage pulses applied for bar samples.

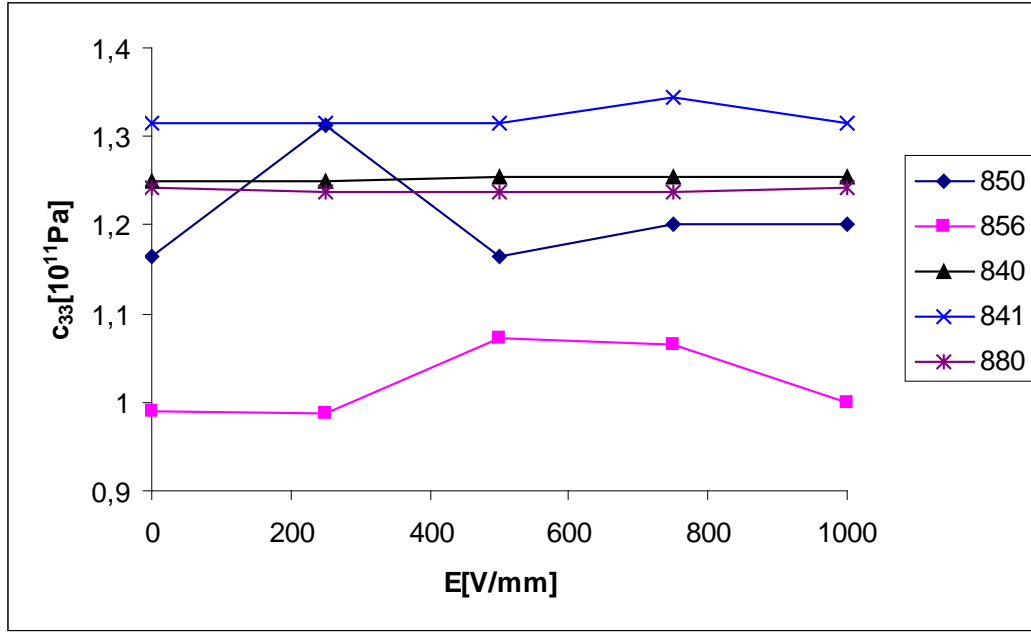


a)

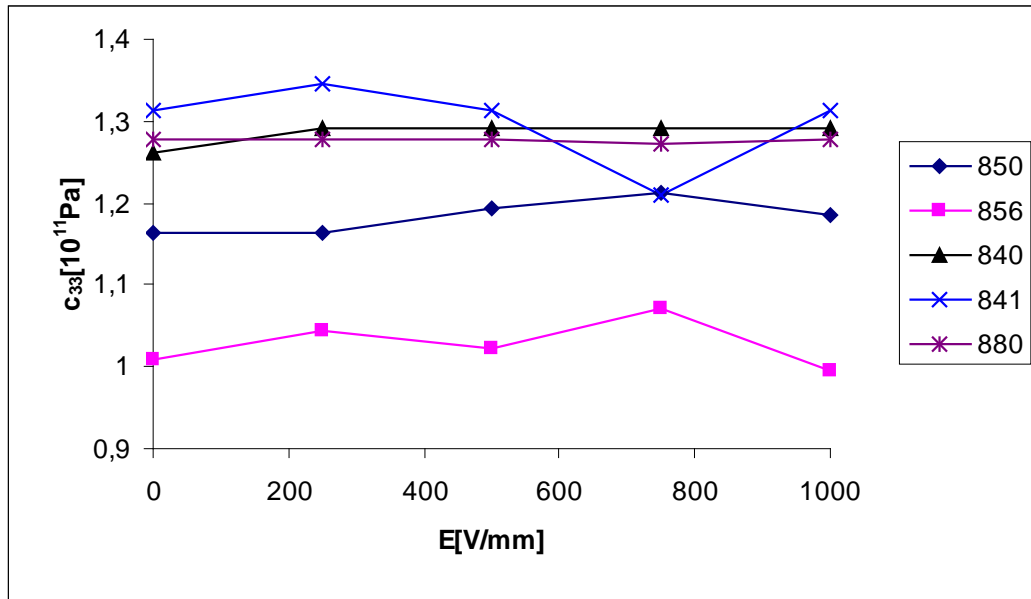


b)

Fig.4.4.10. Poisson's ratio after depoling: a) by D.C. and b) after voltage pulses applied for disc samples. Data missing in curves for APC850 and APC856 are due to the non-resonant response of samples.

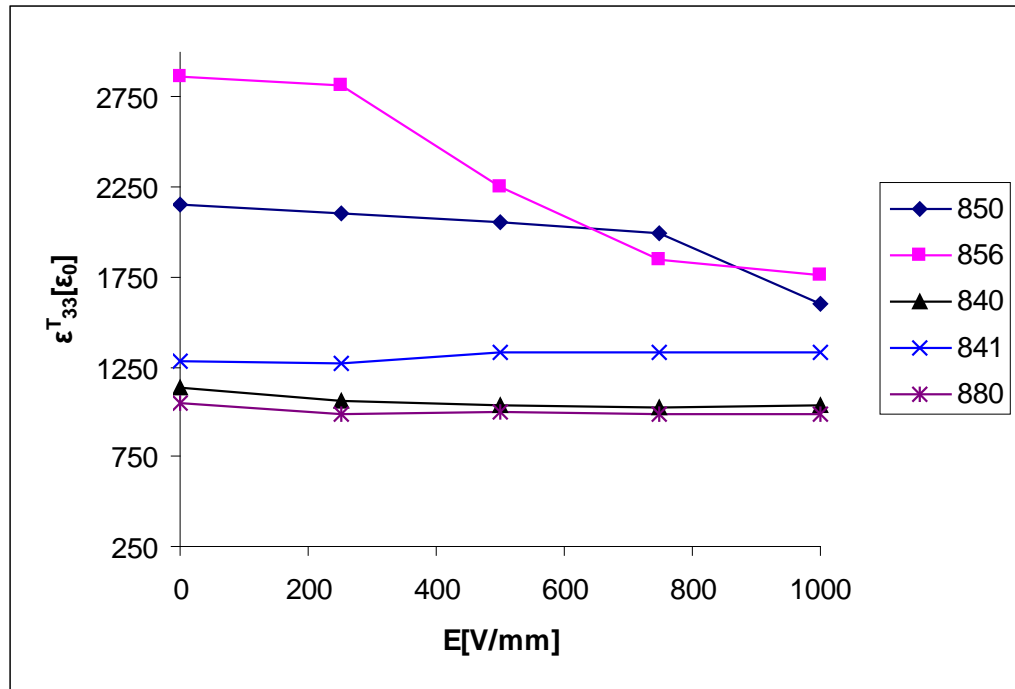


a)

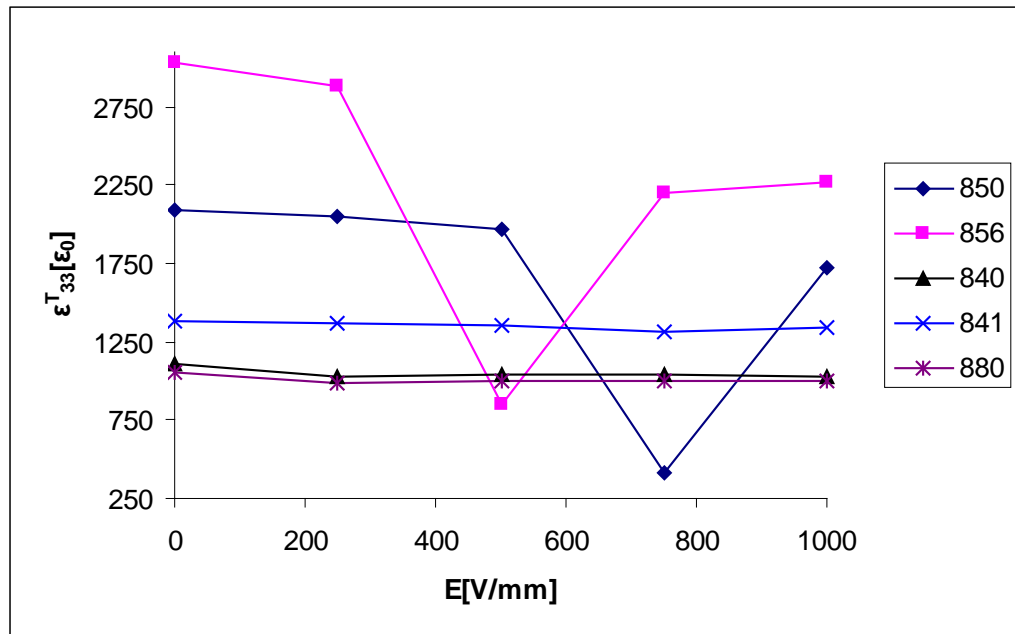


b)

Fig.4.4.11. Elastic modulus c_{33}^E after depoling: a) by D.C. and b) after voltage pulses applied for disc samples.



a)



b)

Fig.4.4.12. Permittivity ϵ_{33}^T after depoling: a) by D.C. and b) after voltage pulses applied for disc samples.

Pulse depoling

Similar behaviour as for D.C. voltage depoling occurs also in this case. Soft PZT ceramics is more sensitive to the depoling field intensity and the limit fields are even smaller than for D.C. voltage depoling. This clearly illustrates the dynamic nature of the poling as well as depoling process. Limiting fields for soft PZT ceramics are listed in Table 4.4.2. Relative changes of the material coefficients for hard PZT (listed in Table 4.4.3.) have similar magnitude (i.e. 3-20%) like for D.C. depoling (i.e. 1-18%). There is no big difference between D.C. and pulse depoling for the hard PZT's studied up to the electric fields of 1000V/mm.

Experimental results are in agreement with investigation by Ogawa et al.[83]. In his experiments, PZT ceramics (disc shape samples) was investigated statically and dynamically to observe the relationship between domain structures and electrical properties. Maximum dielectric constant and minimum planar coupling factor were obtained in rhombohedral PZT at the poling fields of $\pm 0.5\text{kV/mm}$ and $\pm 1\text{kV/mm}$, respectively. The author describes that field for minimum k_p corresponds to the coercive field [98]. The 180° switching was the dominant factor affecting k_p for both soft and hard PZT ceramics after total polarization of virgin ceramics. The bigger changes in k_p at $E=0\text{kV/mm}$ were observed in soft tetragonal PZT ceramics due to larger anisotropy of crystal structure than in soft rhombohedral PZT. Generally, soft PZT ceramics absorbs grain deformation with poling easier and maintains the deformation [83]. The ferroelectric domain structures were evaluated by poling field dependence of k_p and relative intensity of X-ray diffraction (002) peak in PZT ceramics [99]. This work proposes fifteen typical domain configurations. It was confirmed that two peaks correspond to 90° domain rotation and one corresponds to 180° domain switching. The 180° domain switching along poling field follows after the 90° domain rotation occurred.

Experimentally measured values agree well with the published data on soft and hard ceramics, namely with the limits of 100-300V/mm for soft PZT ([49], Philips, grades PXE5 or 52) under D.C. depoling and of 300-500V/mm for hard PZT ([49], Philips, grades PXE 41, 42 or 43). Data similar to such findings were published also for A.C. depoling for Morgan Matroc PZT ceramics [101], i.e. 700V/mm for soft PZT-5A type and >1000V/mm for hard PZT-4D and PZT-8 types. Manufacturer of studied PZT types (i.e. APC International Ltd.) published electric field applicability limits as high as 720V/mm for D.C. and 360V/mm for A.C. field for APC840, 600V/mm for D.C. and 320V/mm for A.C. field for APC850 and 800V/mm for D.C. and 400V/mm for A.C. field for APC880 [100]. Some tensor components are more microstructure-dependent than others, e.g. the Poisson's ratio σ^E shows bigger changes than c_{33}^E , which corresponds to the polarization orientation for elementary dipole moments in the direction parallel and perpendicular to the applied field. Such effects are related to the textures created by the external fields, grain geometry etc.

4.5. Re-poling method.

Re-poling method influence was observed on plates and disc samples (Fig.4.5.1). Soft (APC 850, 856) and hard PZT (APC 840, 841, 880) ceramics were included. Poling experimental setup was the same as in depoling experiment (Fig.4.4.3). Virgin PZT samples of all ceramics types were poled in D.C. electric field (2kV/mm) at the poling temperature 130°C for 5min in silicon oil bath. Poling temperature was selected for ensuring the saturated material properties.

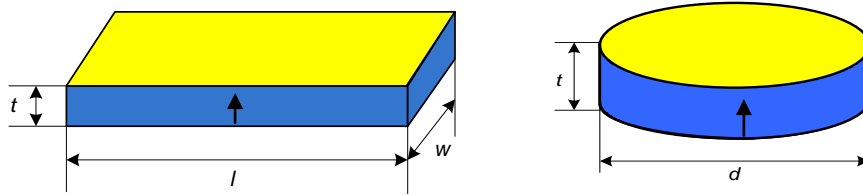


Fig. 4.5.1. Samples used in re-poling experiment.

Material properties of poled PZT before re-poling are shown in Tab. 4.5.1.

| Plate | | | | |
|----------|-------------|-------------------------------|------------------------------|-----------------------|
| PZT type | $k_{15}[-]$ | $\epsilon_{11}^T[\epsilon_0]$ | $c_{55}^E[10^{10}\text{Pa}]$ | $d_{15}[\text{pC/N}]$ |
| APC856 | 0,57 | 3817 | 2,62 | 649 |
| APC850 | 0,50 | 1604 | 2,98 | 344 |
| APC841 | 0,59 | 1513 | 2,88 | 405 |
| APC840 | 0,61 | 2033 | 2,92 | 482 |
| APC880 | 0,59 | 1717 | 2,85 | 433 |

| Disc | | | | | | |
|----------|-------------------------------|---------------|----------|-------------|----------|------------------------------|
| PZT type | $\epsilon_{33}^T[\epsilon_0]$ | $\sigma^E[-]$ | $k_p[-]$ | $k_{31}[-]$ | $k_t[-]$ | $c_{33}^E[10^{11}\text{Pa}]$ |
| APC856 | 2895 | 0,49 | 0,70 | 0,36 | 0,52 | 0,99 |
| APC850 | 2151 | 0,44 | 0,74 | 0,39 | 0,40 | 1,26 |
| APC841 | 1370 | 0,34 | 0,58 | 0,33 | 0,43 | 1,31 |
| APC840 | 1060 | 0,30 | 0,49 | 0,29 | 0,46 | 1,30 |

Tab. 4.5.1. Material properties of poled PZT ceramics before re-poling.

After poling samples were aged for one decade (i.e. for the next ten days) and then re-poled (the electric field during this poling was applied at the same direction as D.C. field). Re-poling has been done by electrical fields of 1.5kV/mm, 2kV/mm, 2.5kV/mm, 3kV/mm of the same direction as poling field at room temperature for 5 min.

Resonance measurement method was used [86]. Material properties were calculated from resonance-antiresonance frequencies. Radial disc vibrations (measured resonant f_r frequencies for fundamental and the first overtone mode, antiresonant f_a frequency of the fundamental mode and sample capacitance C_0 measured at 1kHz frequency) give us the values of k_p – planar electromechanical

coupling factor, ε_{33}^T – permittivity, k_{31} – transverse electromechanical coupling coefficient and Poisson's ratio σ^E (see Appendix IV, VI). Thickness-extensional disc vibrations could be used for c_{33}^E , k_t measurements (measured resonant frequencies of the fundamental f_1 and the third overtone mode f_3) (Appendix III).

The thickness-shear (TS) vibrations of plates (measured antiresonant frequencies of the fundamental f_1 and the third overtone mode f_3) could be used for measurement (see Appendix V) of such properties as thickness-shear electromechanical coupling coefficient k_{15} , shear piezoelectric coefficient d_{15} , elastic stiffness c_{55}^E and permittivity ε_{11}^T . The electrodes were transferred to the width surfaces on plate-shaped samples for TS mode measurement (Fig.4.5.2).

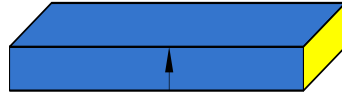


Fig. 4.5.2. Plate samples design for TS mode measurement.

Re-poling behaviour for the measured quantities is shown in Figs. 4.5.3-4.5.12 for the piezoelectric, elastic and dielectric properties. Electromechanical properties dependence on electric field was observed after re-poling.

Impact of re-poling method was found insufficient for material properties change. Increase of the re-poling field did not get a strong contribution to material properties. From the previous experience the material properties change in the plain perpendicular to the poling direction (k_p) was supposed rather less than the properties along the poling field direction (ε_{33}^T). It was found that permittivity ε_{33}^T slightly decreases with amplitude of re-poling field in case of disc-shaped samples for all PZT types. For example, permittivity of APC856 decreased by 13% after re-poling by 2kV/mm in comparison with previous value measured after poling. On the other hand, APC841 decreased only by 3% from the permittivity value measured after poling.

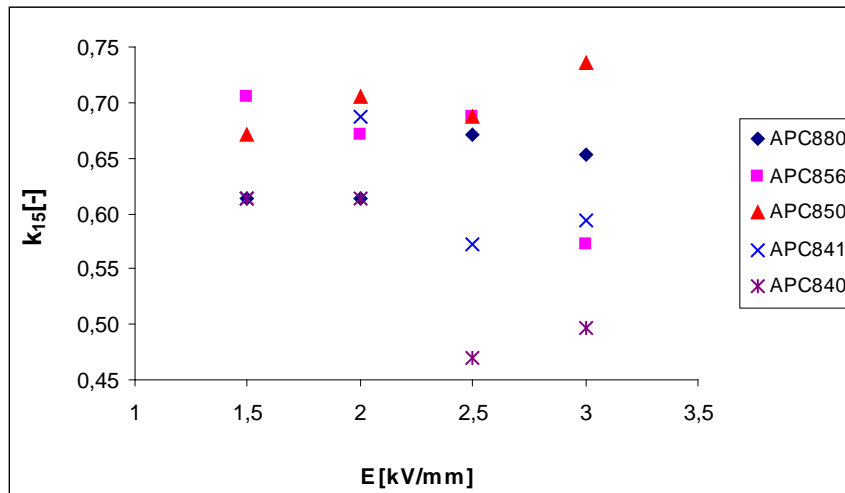


Fig. 4.5.3. Electric field dependence of electromechanical coupling factor k_{15} (plate sample).

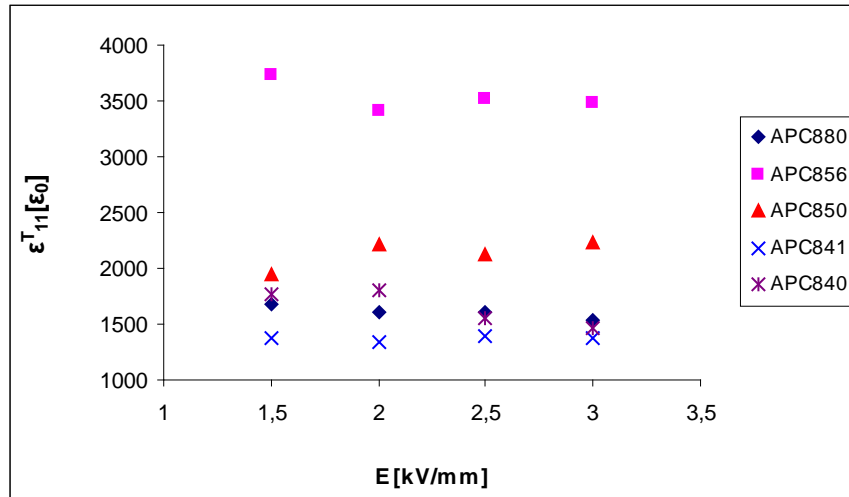


Fig. 4.5.4. Electric field dependence of permittivity ϵ_{11}^T (plate sample).

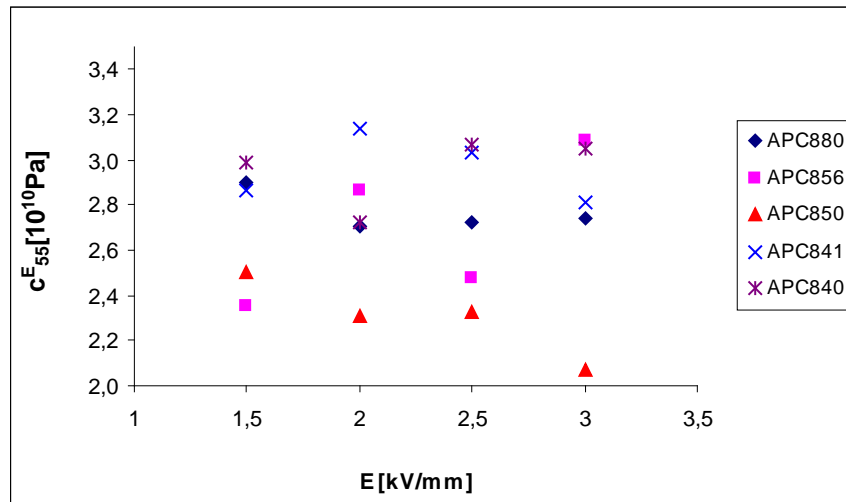


Fig. 4.5.5. Electric field dependence of elastic stiffness c_{55}^E (plate sample).

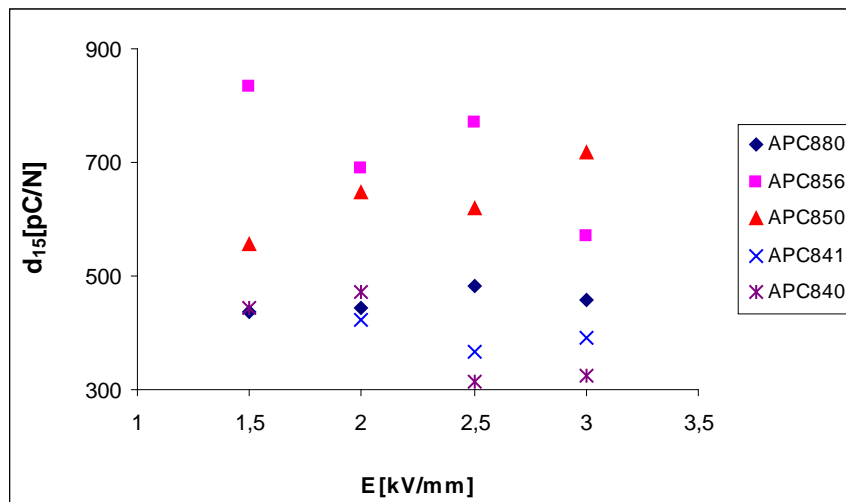


Fig. 4.5.6. Electric field dependence of piezoelectric coefficient d_{15} (plate sample).

The Poisson's ratio (σ^E) decreases when electric field amplitude was higher for soft and hard PZT (Fig.4.5.10). Soft ceramics was more affected than hard one in case of k_p value change (Fig.4.5.8). Other material properties have their values change less than 7% for disc samples. The thickness-shear electromechanical coupling coefficient k_{15} and shear piezoelectric coefficient d_{15} demonstrate the small increase in their values in plate samples. Behavior of elastic stiffness c_{55}^E and permittivity ε_{11}^T was found rather stable without occurrence of extreme changes with electric field increase. Small impact of re-poling field may be explained in the terms of domains walls motion and their pinning after first poling. Domain walls motion is pinned by structure discreteness and impurities in hard PZT. Domain structure of hard PZT is clamped by oxygen vacancies generated by acceptor doping. Domain boundaries in soft PZT have higher mobility [102]. When the poling field was removed the samples were aged for ten days. Material properties were stabilized during this time. The polarization alignment may have small changes after elimination of electric field impact. The spontaneous polarization direction may slightly change in the direction of previous orientation after electric field was eliminated. Repeatable application of electric field does not increase total polarization but contributes to a clamping of domain walls motion and reduces the piezoelectric response of the material for well-poled ceramics [51]. The 180° walls are not ferroelastic and they may influence only piezoelectric properties. But non- 180° walls are ferroelastic and they may influence both dielectric and piezoelectric properties [103]. The domain wall contribution is strongly dependent on the microstructure (intrinsic contribution - lattice) deformation and the crystal structure of the examined ceramics (extrinsic contribution – domain walls displacement and interphase boundaries) [104]. The contribution from irreversible displacement of domain walls is small in PZT ceramics. Such behaviour occurs due to internal stresses which have clamping effect on the irreversible displacement of domain walls [105]. The internal stress in the tetragonal PZT ceramics originates from the high spontaneous strain.

Poling by electrical field creates mechanical stresses in the piezoelectric samples due to the converse piezoelectric effect. Mechanical stress distribution in space is dependent on resonators shape and may influence the cracking of material. On another side, mechanical stresses have the impact on the poling of ceramics due to the direct piezoelectric effect. For example, compressive poling stresses are distributed in the radial direction in disc poled in thickness direction. Such stresses prefer polarization orientation along the disc axis. Stresses in thin plate prefer all planes perpendicular to the plate, with a special preference of plane perpendicular to the plate length. Dipole moment orientation distribution preferences are chosen due to the combination of electric field and mechanical stress influence (converse piezoelectric effect). Such behavior is in a correlation of anisotropy of the tensor coefficients discussed in [90]. The effective piezoelectric constant d_{33} achieves its maximum along the perovskite {100} direction but not in the spontaneous polarization direction.

Longitudinal components of electromechanical tensors (i.e., ε_{33}^T , k_t , c_{33}^E) do not show the strong dependence on electric field or temperature ($E > E_c$). When the certain domain wall movement related to the electric field is achieved the stable domain structure is formed during poling. Higher ratio of dipole moment alignment is not achieved by increase of electric field amplitude ($E > E_c$).

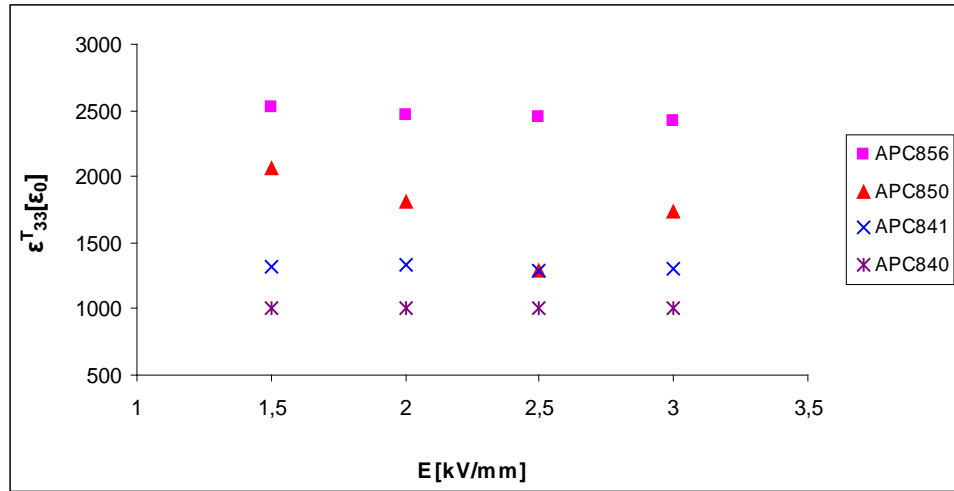


Fig. 4.5.7. Electric field dependence of free permittivity ε_{33}^T (disc sample).

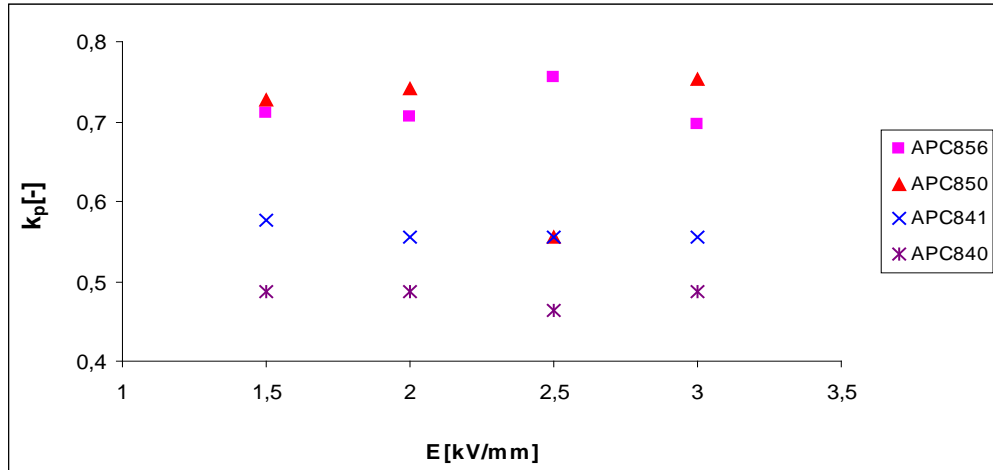


Fig. 4.5.8. Electric field dependence of planar electromechanical coupling factor k_p (disc sample).

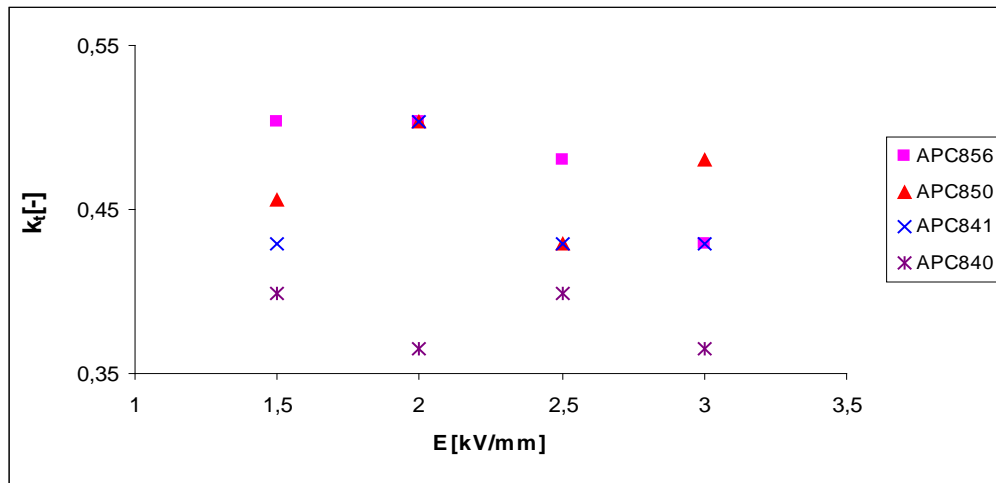


Fig. 4.5.9. Electric field dependence of thickness electromechanical coupling factor k_t (disc sample).

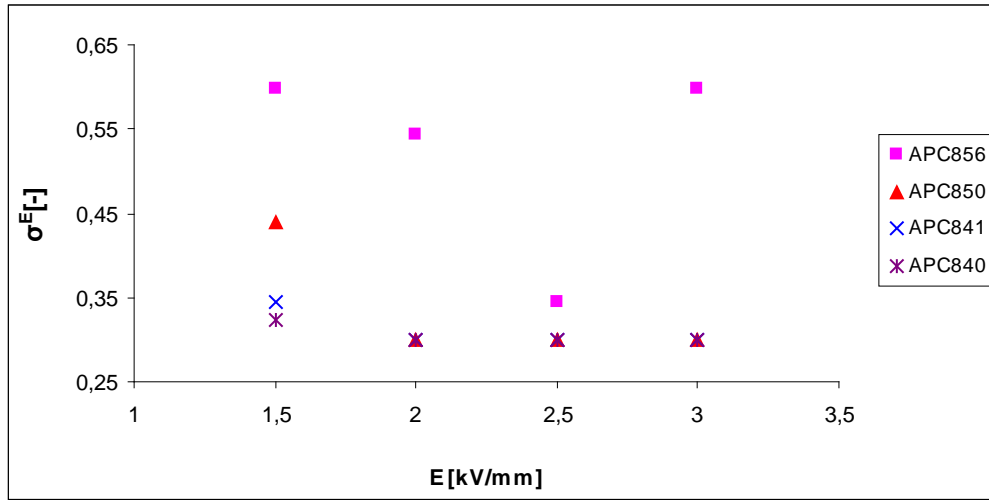


Fig. 4.5.10. Electric field dependence of Poisson's ratio σ (disc sample).

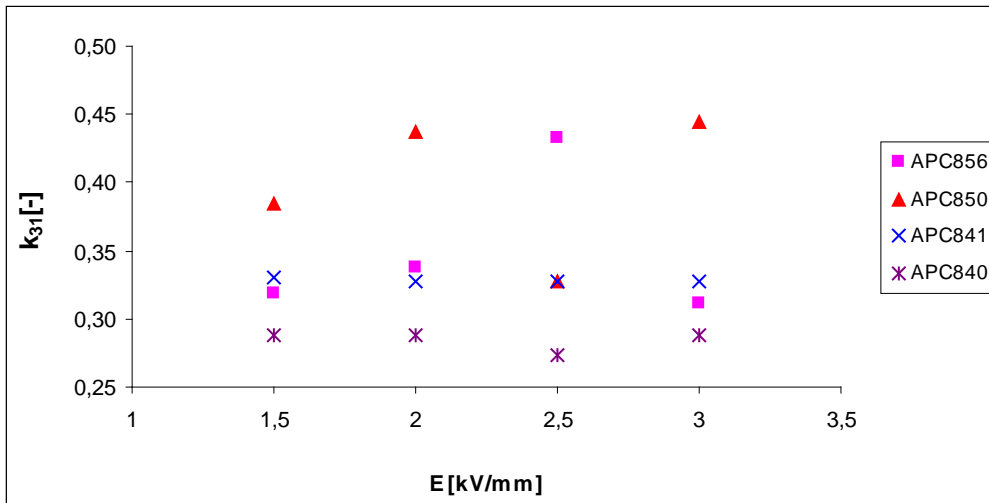


Fig. 4.5.11. Electric field dependence of transversal electromechanical coupling factor k_{31} (disc sample).

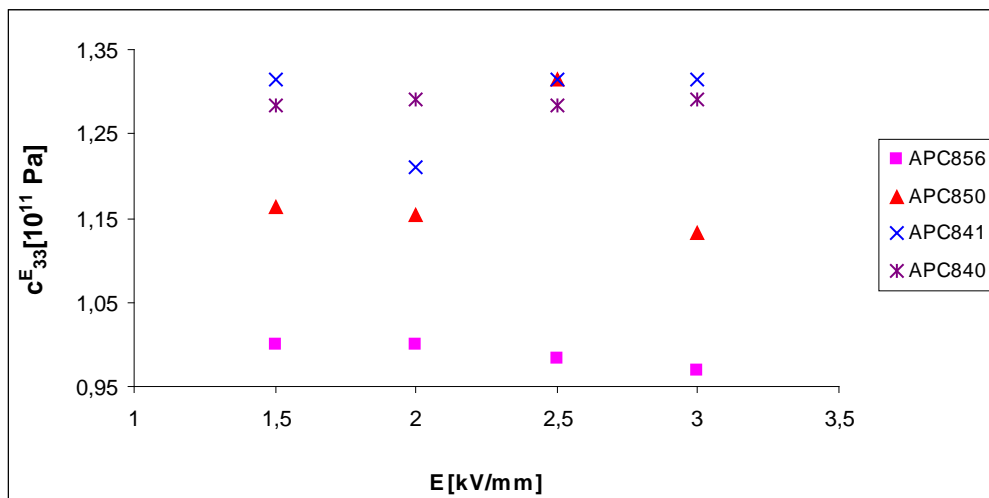





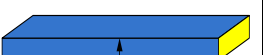
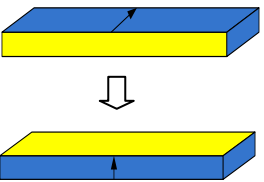

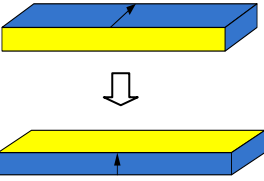

Fig. 4.5.12. Electric field dependence of elastic stiffness c_{33}^E (disc sample).

4.6. Cross-poling method.

Cross-poling was the third experiment which was performed to observe influence of electric field application on material properties of PZT ceramics. The direction of electric field application was described before in Fig.4.1.2. The bar-shaped samples (15mm×4mm×1mm) were chosen for this experiment due to the resonant method applied for the property measurement. Experiment procedure and electrode pattern is described in Tab.4.6.1. Material property measurement (see Appendixes II, III, V) has been done by resonant method [86].

Virgin PZT samples were poled at 130°C by D.C. electric field 2kV/mm for 5min in silicon oil bath. Such poling temperature has been selected to ensure the saturated material properties with moderate aging after the poling. Samples of soft (APC 856, 850) and hard (APC 840,841) PZT ceramics were used. First poling was done in the width direction. Samples were aged for ten days similarly to the previous experiments. Electrodes were replaced as shown in Tab.4.6.1 after ten days of aging. Then samples were poled in the thickness direction. Cross-poling conditions were the same as in width direction poling.

The measured material properties after cross-poling were compared with material properties of reference samples. Reference samples (length-extensional (LE), thickness-extensional (TE) and thickness-shear (TS) modes) were poled under the same electric field and temperature as tested samples. Material properties of reference samples were measured in ten days after poling to have the same aging period as in test samples case.

| | Sample poling | Poling conditions | Measured sample | Measured properties |
|------------------------|---|---|--|---|
| Control sample (LE,TE) |  | $E=2\text{kV/mm}$, $T=130^\circ\text{C}$, 5 min |  | $\epsilon_{33}^T, k_{31},$ d_{31}, s_{11}^E k_t, c_{33}^E |
| Control sample (TS) |  | $E=2\text{kV/mm}$, $T=130^\circ\text{C}$, 5 min |  | $\epsilon_{11}^T, k_{15},$ d_{15}, c_{55}^E |
| Virgin sample (LE,TE) |  | $E=2\text{kV/mm}$, $T=130^\circ\text{C}$, 5 min |  | $\epsilon_{33}^T, k_{31},$ d_{31}, s_{11}^E k_t, c_{33}^E |
| Virgin sample (TS) |  | $E=2\text{kV/mm}$, $T=130^\circ\text{C}$, 5 min |  | $\epsilon_{11}^T, k_{15},$ d_{15}, c_{55}^E |

Tab. 4.6.1. Cross-poling experiment structure.

Resulted values of material properties are shown in Tab.4.6.2–4.6.5. Permittivity ε_{33}^T decreases in all PZT types after cross-poling. For example, permittivity value in APC856 is 30% less after cross-poling than in control sample. Its value is 6% less in hard PZT APC841. Such behavior may be explained in terms of domain walls pinning. Decreasing behavior was observed in transverse piezoelectric coefficient d_{31} . Its value lost 33% in APC856 in comparison with control sample value. Piezoelectric coefficient d_{31} in APC841 decreases only by 16% from the value measured before cross-poling. Transversal tensor components are more dependent on the dipole moment alignment due to the anisotropy of tensor components in the rhombohedral PZT. Piezoelectrically created mechanical stresses may influence material anisotropy in the plane perpendicular to the poling direction, but it will not be further changed by electrical field.

Opposite effect was observed in properties of thickness-extensional mode. Values of k_t and c_{33}^E demonstrate slight increase. Thickness-extensional electromechanical factor shows the increase by 23% in comparison with control sample value for APC856 after cross-poling and by 15% in APC841. Elastic stiffness increases by 7% from control sample value for APC856 and by 5% for APC841 after cross-poling.

| PZT type | $\varepsilon_{33}^T[\varepsilon_0]$ | $k_{31}[-]$ | $s_{11}^E[10^{-11}\text{Pa}^{-1}]$ | $d_{31}[\text{pC/N}]$ | $k_t[-]$ | $c_{33}^E[10^{11}\text{Pa}]$ |
|----------|-------------------------------------|-------------|------------------------------------|-----------------------|----------|------------------------------|
| APC840 | 1149 | 0,24 | 1,21 | 83 | 0,32 | 1,30 |
| APC841 | 1089 | 0,29 | 1,20 | 98 | 0,33 | 1,33 |
| APC850 | 2129 | 0,37 | 1,67 | 206 | 0,36 | 1,33 |
| APC856 | 4490 | 0,37 | 1,76 | 306 | 0,30 | 1,35 |

Tab. 4.6.2. Material properties of control samples (LE and TE mode).

| PZT type | $\varepsilon_{33}^T[\varepsilon_0]$ | $k_{31}[-]$ | $s_{11}^E[10^{-11}\text{Pa}^{-1}]$ | $d_{31}[\text{pC/N}]$ | $k_t[-]$ | $c_{33}^E[10^{11}\text{Pa}]$ |
|----------|-------------------------------------|-------------|------------------------------------|-----------------------|----------|------------------------------|
| APC840 | 1167 | 0,24 | 1,19 | 82 | 0,27 | 1,46 |
| APC841 | 1165 | 0,23 | 1,21 | 83 | 0,45 | 1,40 |
| APC850 | 1808 | 0,28 | 1,63 | 147 | 0,39 | 1,36 |
| APC856 | 3369 | 0,29 | 1,67 | 203 | 0,39 | 1,32 |

Tab. 4.6.3. Material properties after cross-poling (LE and TE mode).

Material properties were studied for soft PZT materials in thickness-shear mode of bar samples. Unfortunately, the impedance spectrum observed in case of hard PZT ceramics gave the third overtone mode frequency in the region with high noise. As a result, the measurement of frequency value was rather complicated (high discrepancies between data) and values of material properties were unreliable. This was the main reason why hard PZT ceramics results were excluded from the discussion of TS mode results. Only soft PZT ceramics APC850 and APC856 will be analyzed. It is not possible to see substantial influence on material properties of soft ceramics after cross-poling (Tab.4.6.4–4.6.5). Such results gave opportunity to resume that cross-poling method had low benefit for material properties change in actual setup. Higher temperature was implemented in cross-poling method as lesson learned from re-poling experiment, but its influence on results was not obvious.

| PZT type | $\epsilon_{11}^T [\epsilon_0]$ | $k_{15} [-]$ | $d_{15} [\text{pC/N}]$ | $c_{55}^E [10^{10} \text{Pa}]$ |
|----------|--------------------------------|--------------|------------------------|--------------------------------|
| APC850 | 1990 | 0,65 | 551 | 2,47 |
| APC856 | 3176 | 0,47 | 438 | 3,22 |

Tab. 4.6.4. Material properties of control samples (TS mode).

| PZT type | $\epsilon_{11}^T [\epsilon_0]$ | $k_{15} [-]$ | $d_{15} [\text{pC/N}]$ | $c_{55}^E [10^{10} \text{Pa}]$ |
|----------|--------------------------------|--------------|------------------------|--------------------------------|
| APC850 | 2032 | 0,67 | 595 | 2,28 |
| APC856 | 3218 | 0,43 | 393 | 3,55 |

Tab. 4.6.5. Material properties after cross-poling (TS mode).

The domain structure of soft PZT ceramics was studied by electron microscopy in [106]. It was observed that some ferroelastic domains existed prior to polarization and they were rearranged in DC field. The stripe structure of ferroelastic domains was formed and became prevalent with the domain-wall orientation almost normal to the poling field. It was established that walls are of 90° type. There are grains containing only 90° type domains, but in other grains domain configuration consists of coexisting 90° and 180° domain types [107]. Part of 90° and 180° domains is switched favorably towards the field direction by the poling. Small number of 90° domain relaxes and gradually changes their polarization direction in the direction of initial state after poling [108]. When PZT is poled under an electric field stronger than the coercive one, the equilibrium state of 90° domain alignments after relaxation is determined by the tetragonality of crystal lattice. It is not determined by the force of domain-wall clamping. Such behavior is valid in soft PZT due to weak force of domain-wall clamping and the internal stress induced by the tetragonality of PZT [109]. Generally, domain wall contributions are dependent on grain size for fine grains, where the spontaneous deformation decreases. Domain wall contribution depends on electric and elastic fields which occurred after domain walls displacement [110]. Poling field provides higher impact on material tensor components at low temperatures, where domain walls have low mobility. The poling field effect is smaller than temperature one at higher poling temperatures [111].

So, it is possible to summarize low contribution of cross-poling method to material properties. First reason may be the cross-poling temperature choice. The poling in the width direction was done under 130°C , so the domain wall movement was easier. As a result poling procedure was easier too. Cross-poling was realized again under the same temperature. If its results are in the consequence of this procedure, the cross-poling method will not be useful for further investigation. Its influence on material properties of bar samples will be finally confirmed as minimal.

4.7. Pulse poling method.

Measurement of switching current is popular method in study of polarization reversal [112, 113]. This method consists of a set of symmetric voltage pulses applied to the sample with the implemented zero field gaps between the pulses of opposite polarity.

The disc-shaped samples of soft (APC 856, 850) and hard (APC 840, 841) ceramics were presented in the experiment. Merz circuit was used in pulse poling measurement to observe the current and voltage on the samples. In such circuit, PZT

sample behaved as capacitor and the resistor was integrated in HV amplifier. Voltage signal was generated by Diametral P230R51D source (output voltage 1-30V; output current 0.1-4A) and amplified by high voltage amplifier (Matsusada Precision Inc., type AMT-5B20, fixed amplification rate 500). Maximum output voltage of amplifier is ± 5 kV and maximum current is 20mA. Such amplified voltage is possible to apply on the samples with thickness below 1mm. Output signals from HV amplifier were detected by AD/DA convertor (Tedia, PCA7428AS; frequency range 0-20kHz). Insulating amplifier (Tedia OPT1020; insulating voltage 3.5kV; frequency range 0-20kHz; amplification 1x/10x selectable) was used in the experiment circuit. Experiment connection is shown in Fig.4.7.1. The program software application Agilent VEE Pro was used.

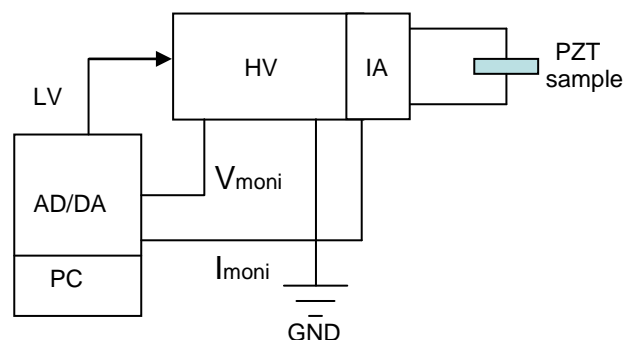


Fig. 4.7.1. Scheme of pulse poling measurement.

Disc samples were pulse poled in silicon oil bath by electric field of bipolar pulse shape. Fig.4.7.2 shows the applied electric field pulse shape and measured current curve behavior during the experiment. First of all, the pulse design must be explained. The electric field bipolar pulse time was totally 28 sec. Pulse structure was 5sec – zero electric field applied, 2sec – time of electric field increase to amplitude value (positive), 5sec – time of amplitude electric field application, 2sec – time of electric field decrease to zero value, 5sec - zero electric field applied, 2sec – time of electric field achieve the amplitude value (negative), 5sec – time of amplitude electric field application, 2sec – time of electric field achieve zero value. There were two regions with zero intensity of electric field applied between pulses of opposite polarity. Mainly they were implemented for better stability of polarization in the sample after poling. The delay in data reading by AD/DA card was the second point, which influenced the installation of such gaps. Amplitudes of electric field applied to the samples were 2kV/mm, 2.5kV/mm, 3kV/mm, 3.5kV/mm and 4kV/mm. Electric field amplitudes less than 2kV/mm (500 V/mm and 1 kV/mm) gave the current value too small for the detection by AD/DA card due to its resolution ($\pm 10\mu\text{A}$). The resulted current curve was in the noise range and such data were unreliable. The Fourier low-pass filter (limiting frequency 50 Hz) was applied to the measured current data. Such filter eliminated the influence of network frequency additional noise on measured data. The 2sec time of electric field increase to amplitude value was chosen to observe switching current peak due to restriction of amplifier. Temperature dependences were studied in the range 20-150°C.

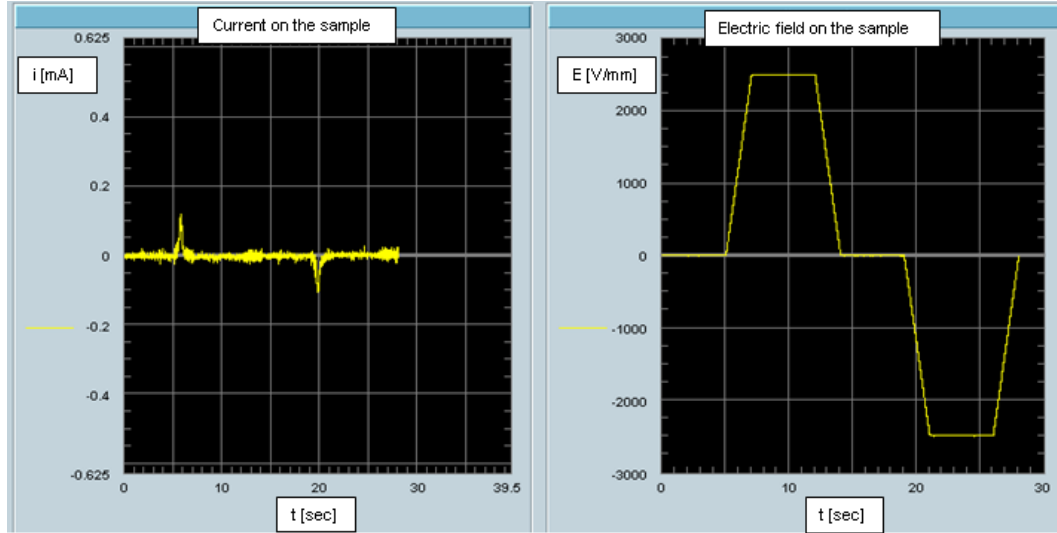


Fig. 4.7.2. Current and applied electric field curves observed for APC856 at 50°C.

The polarization change [114] (if occurred in the whole sample volume) is:

$$\int_0^{\infty} i(t) dt = 2P_s A \quad (6)$$

where A is an electrode area. Experimentally measured value of spontaneous polarization P_s is lower due to the influence of backswitching from previous polarization reversal. The switching process is characterized by the values of applied field E , maximum current value i_{\max} and time t_{\max} (Fig. 1.2.2) [17].

Prior to integration of current data to obtain charge, the data were fitted by Gaussian function (Fig. 4.7.3 – 4.7.4). Gaussian fitting parameters are shown in Appendix VII. The surface under the current curve will be equal to charge on the sample electrodes:

$$j = \frac{I}{A} = \frac{\Delta Q}{A \Delta t} = \frac{\Delta S}{A \Delta t} \quad (7)$$

where A is an electrode area, ΔS is the surface under Gaussian fitting curve. Spontaneous polarization P_s for different ceramics types may be calculated. Change in $\ln(i_{\max})$ versus reciprocal amplitude of applied electric field is shown in Fig. 4.7.5 for all ceramics types.

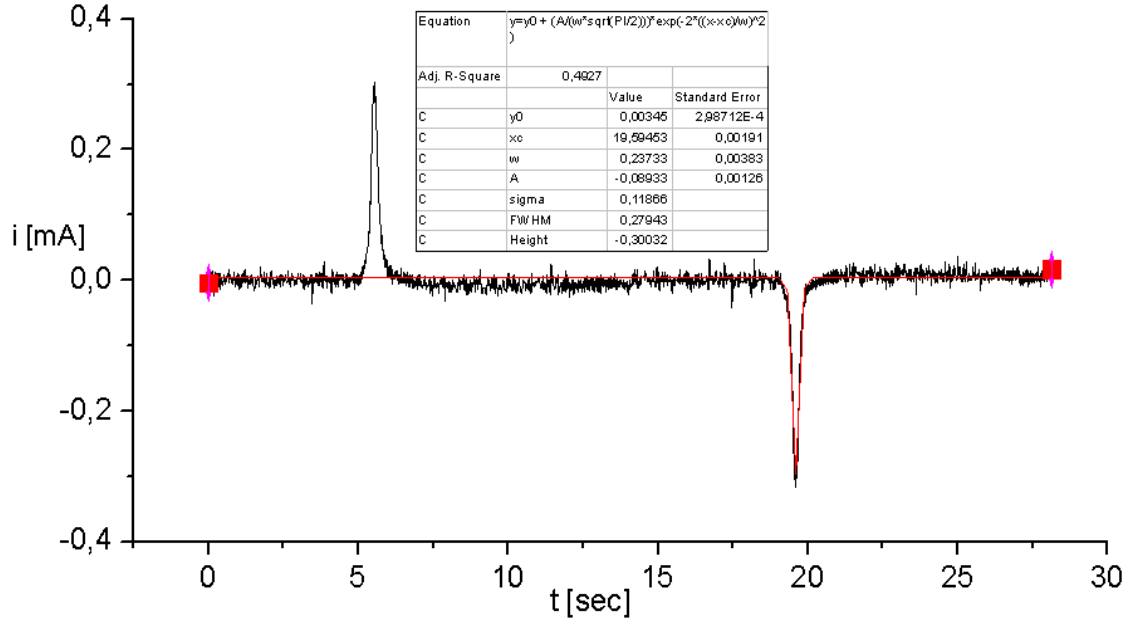


Fig. 4.7.3. Gaussian fitting of current spectrum for APC856 at RT. Applied pulse field amplitude was $\pm 4\text{kV/mm}$).

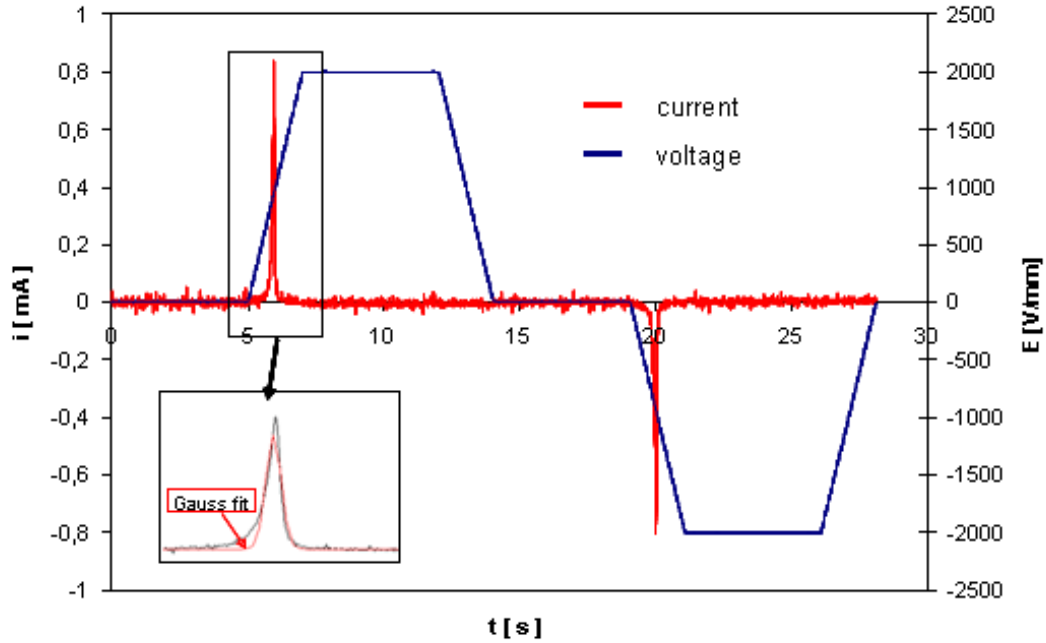


Fig. 4.7.4. Switching current curve of APC850 ceramics at 2kV/mm applied field and $100\text{ }^\circ\text{C}$.

The applied electric fields were chosen higher than E_c . Such value was chosen due to hysteresis loop measurement. Resulted current peak values were increased with the enhanced electric field applied in all studied PZT ceramics. Such behavior is the result of higher switching rate of domains or their amount, which leads to current

increase. Measured data trend is in agreement with values studied by Lee et al. in case of PZN-PT crystals [115]. The current value will increase due to the increased formation of domain nuclei. Switching is achieved by the sideways expansion of nuclei. Nuclei formed at the domain boundaries are in the form of low amplitude and long wavelength fluctuations of the domain walls [116].

The behavior of switching time is shown in Fig. 4.7.6. Measured switching time values (\sim s) for PZT ceramics are higher than in barium titanate single crystals studied by Merz ($\sim\mu$ s). The reciprocal switching time increases when amplitude of applied field is higher in barium titanate crystals [25]. Experimental data show differences in the behavior of soft and hard PZT ceramics. When applied electric field increases, the reciprocal switching time in soft PZT increases, but decreases in hard PZT. Such discrepancy may be caused by several aspects. Microstructure of ceramics is one of them. As a result differences between single samples or material lots are possible. Different kinds of doping elements may create the influence on material properties.

On another side, hard PZT is more conductive than soft one at higher temperatures. There might be free charges in border areas of neighbor's grains, which may contribute to the current inside ceramics during application of electric field. Such charges do not participate in switching process and may contribute to switching time increase. Experimental procedure is one more aspect which must be discussed. Measurement on the samples was done continuously. It means that 2kV/mm amplitude of electric field was applied on the virgin sample at first. Other measurement followed one by one. Repeating polarization by electrical fields of opposite polarity may affect samples. Clamping of domain walls occurred and caused the delay in switching process. Samples have to be transferred to unpoled state by hysteresis loops measurement from the maximum electric field amplitude applied to zero one to eliminate domain clamping influence.

Temperature dependences of $\ln(i_{max})$ are shown in Figs. 4.7.7-4.7.10 in APC850, APC856, APC841 and APC840 ceramics respectively. It is visible, that temperature has greater influence on the current value in comparison with electric field. Generally, the contribution from the thermal fluctuation to the formation of switching nuclei is rather large. Such experimental results are similar to current curves described in [117]. The differences in influence of temperature and electric field on domain switching may be explained from energy point of view. Higher temperature increases the domains mobility. The isotropic temperature field will influence all domains in the same way. So, more active domains imply that more backswitching will occur when applied electric field is removed. Situation is different in case of electric field. The electric field aligns domains in optimal direction [118]. Increased electric field activates the rate of nucleation and amount of domain switching.

Experimental values of spontaneous polarization were calculated by nonlinear fitting of measured current curve with the Gaussian function (Appendix VI). Temperature dependences of P_s in different applied fields for soft PZT ceramics are shown in Fig.4.7.11 and Fig.4.7.12 respectively. Temperature dependences of P_s in different applied fields for hard PZT ceramics APC841 and APC840 are shown in Fig.4.7.13 and Fig.4.7.14. Spontaneous polarization decreases with higher temperature in all types of PZT ceramics. Higher distribution of spontaneous polarization values may be explained by bigger electric field influence in hard PZT ceramics.

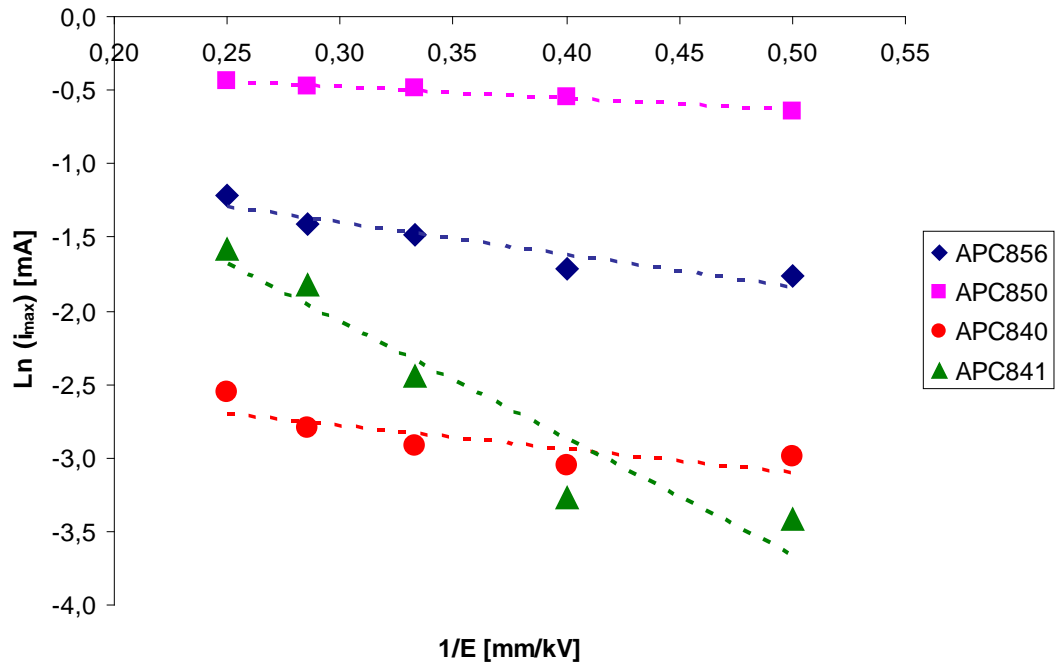


Fig. 4.7.5. Change in $\ln(i_{max})$ vs. $1/E$ in PZT ceramics. Dashed curves are linear fit.

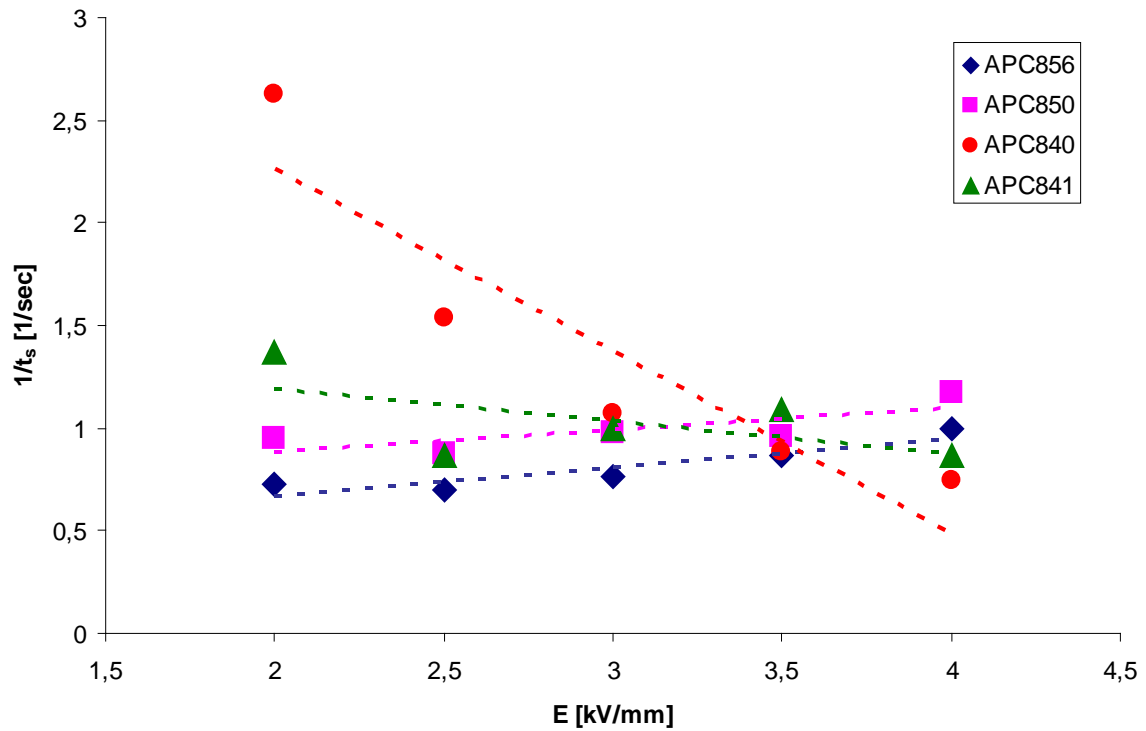


Fig. 4.7.6. Reciprocal switching time t_s vs. electric field for different PZT ceramics. Dashed curves are linear fit.

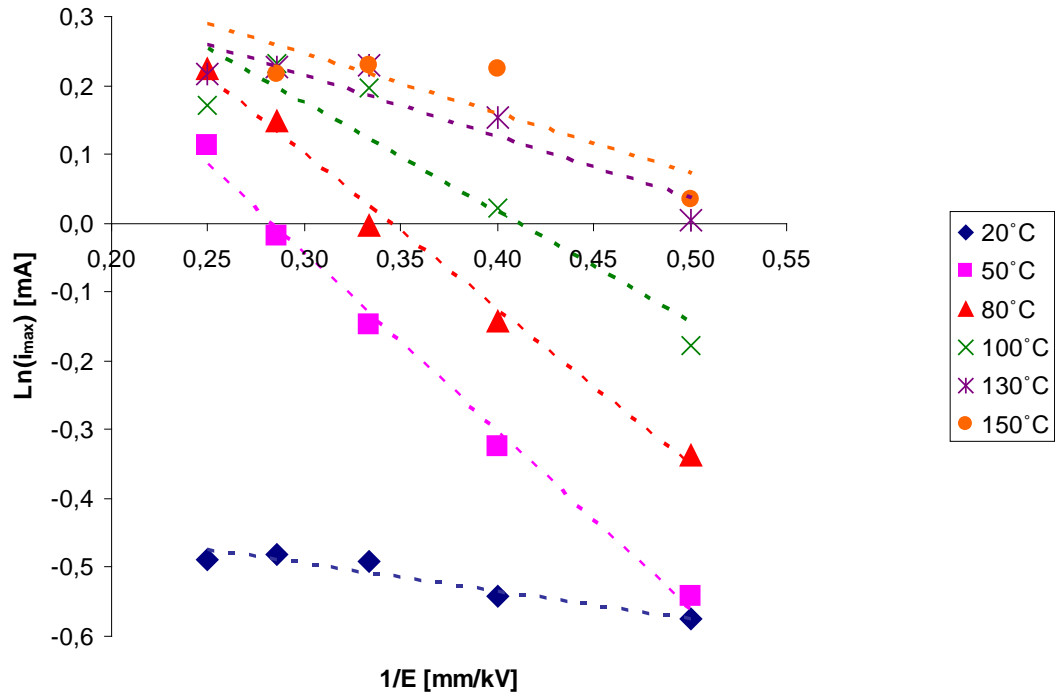


Fig. 4.7.7. Change in $\ln(i_{max})$ vs. $1/E$ as a function of temperature - soft PZT, APC850. Dashed curves are linear fit.

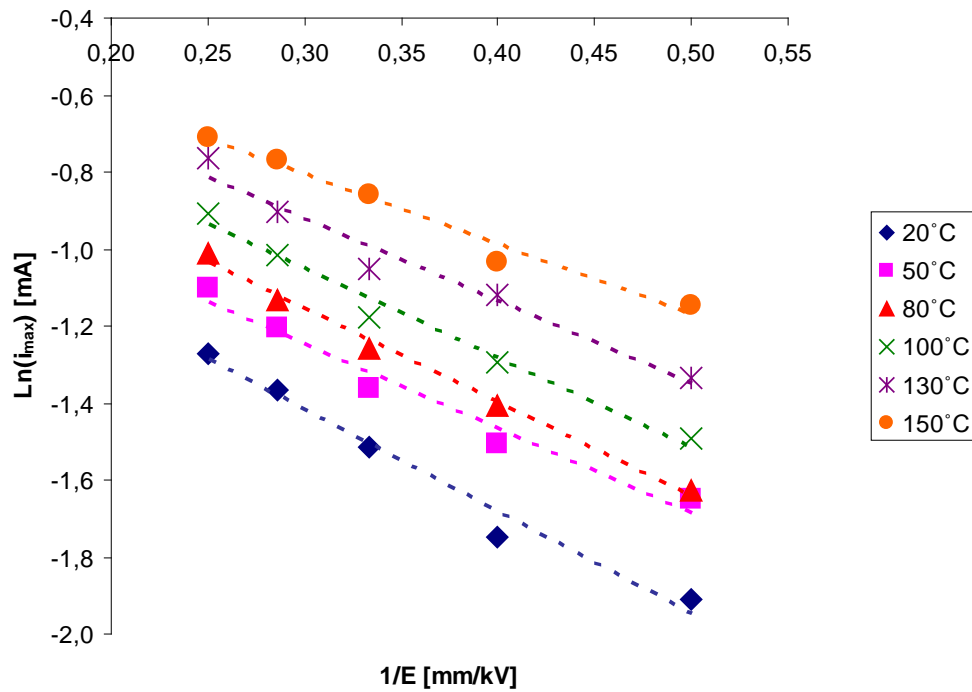


Fig. 4.7.8. Change in $\ln(i_{max})$ vs. $1/E$ as a function of temperature - soft PZT, APC856. Dashed curves are linear fit.

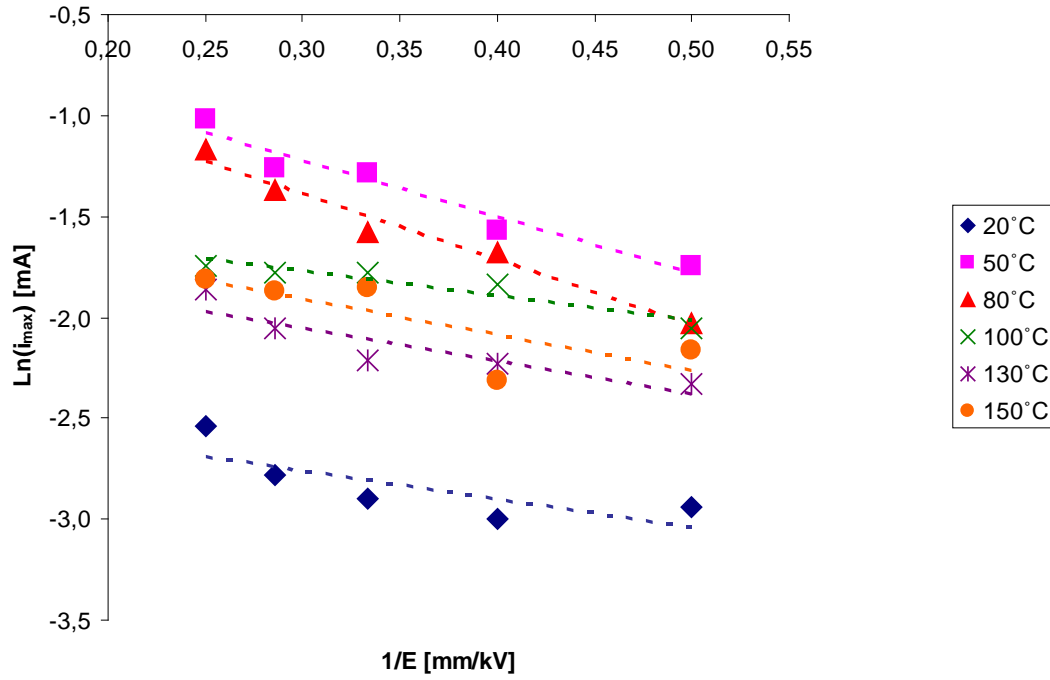


Fig. 4.7.9. Change in $\ln(i_{max})$ vs. $1/E$ as a function of temperature - hard PZT, APC840. Dashed curves are linear fit.

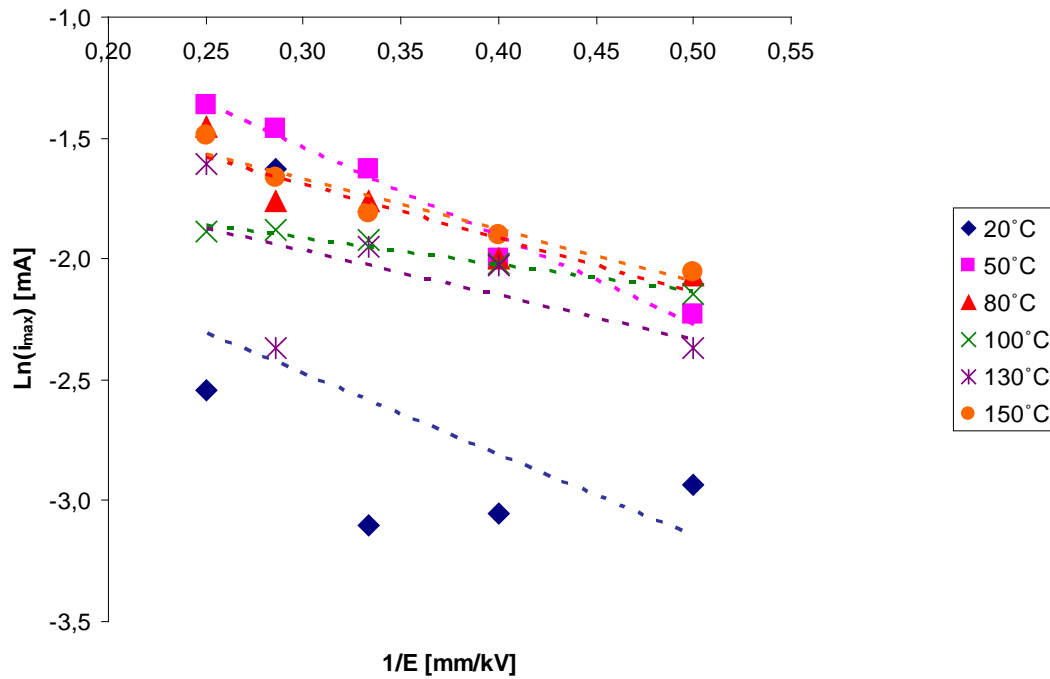


Fig. 4.7.10. Change in $\ln(i_{max})$ vs. $1/E$ as a function of temperature - hard PZT, APC841. Dashed curves are linear fit.

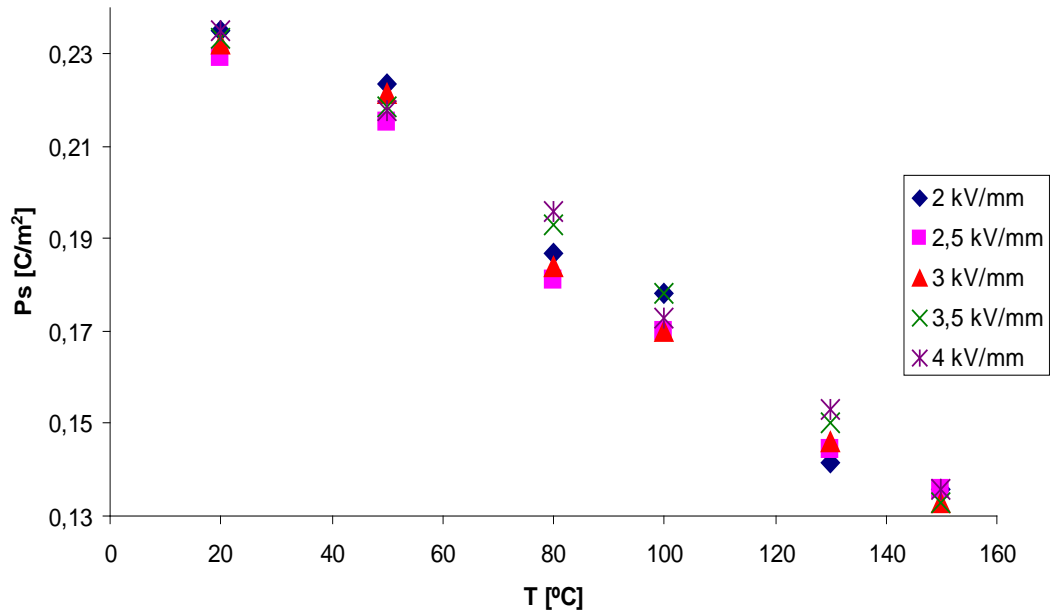


Fig. 4.7.11. Temperature dependence of P_s for APC856 ceramics measured from i_{max} pulse poling.

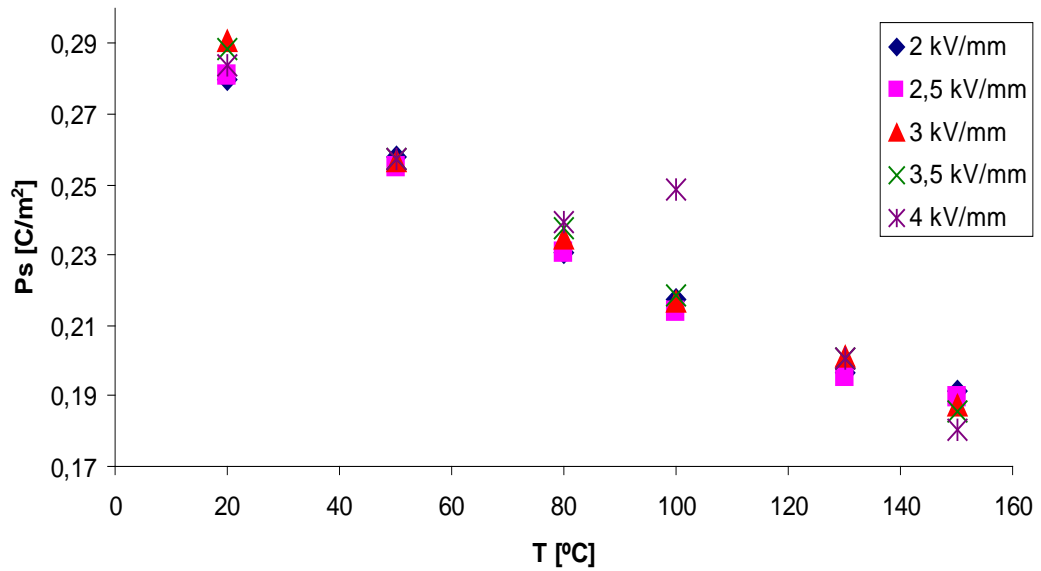


Fig. 4.7.12. Temperature dependence of P_s for APC850 ceramics measured from i_{max} pulse poling.

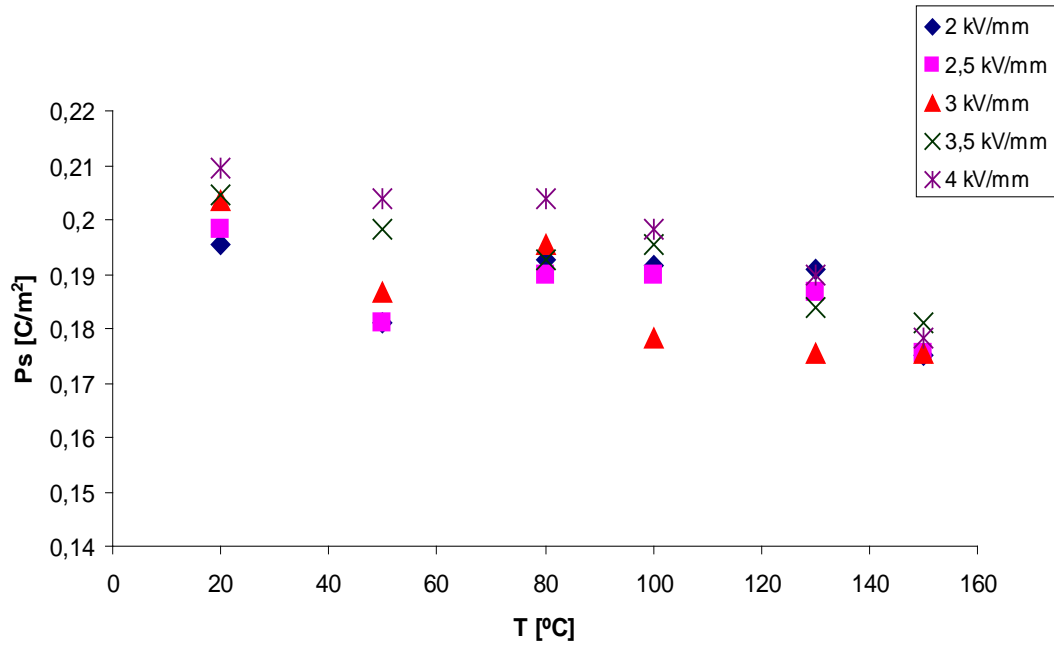


Fig. 4.7.13. Temperature dependence of P_S for APC841 ceramics measured from i_{max} pulse poling.

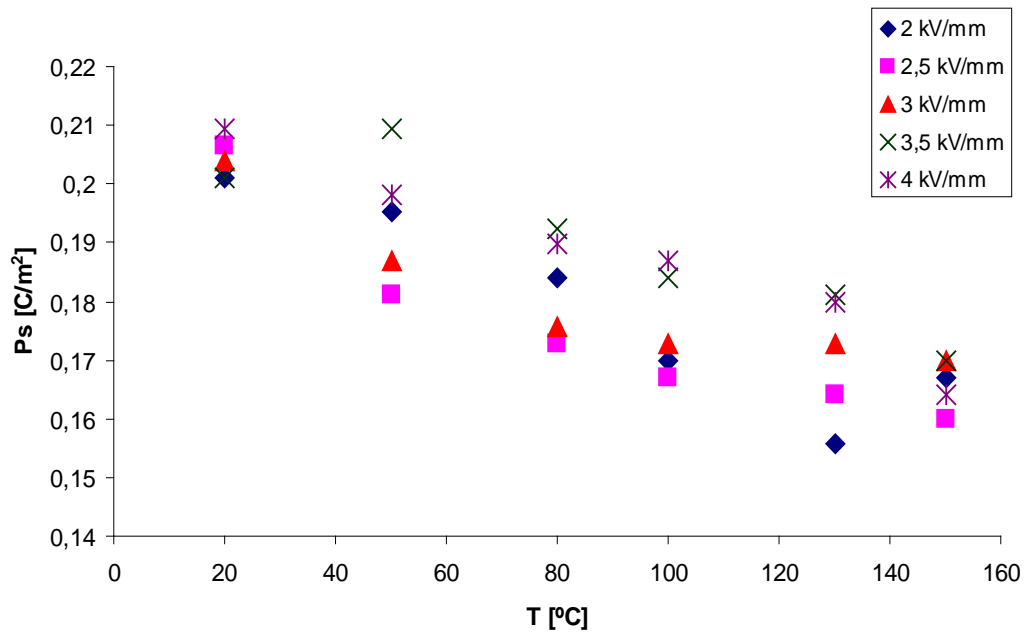


Fig. 4.7.14. Temperature dependence of P_S for APC840 ceramics measured from i_{max} pulse poling.

Fig. 4.7.15 shows the temperature dependence of activation field (α) in PZT ceramics (Eq.1). Activation field was found as coefficient in liner approximation applied to $\ln(I_{max})$. This dependence does not agree with the same one in BaTiO_3 single crystal. Activation field was decreased with higher temperature. The activation field value for BaTiO_3 was 1.6kV/mm at room temperature [114]. The experimental activation field α was located within the range from 0.5kV/mm to 3.7kV/mm for PZT ceramics.

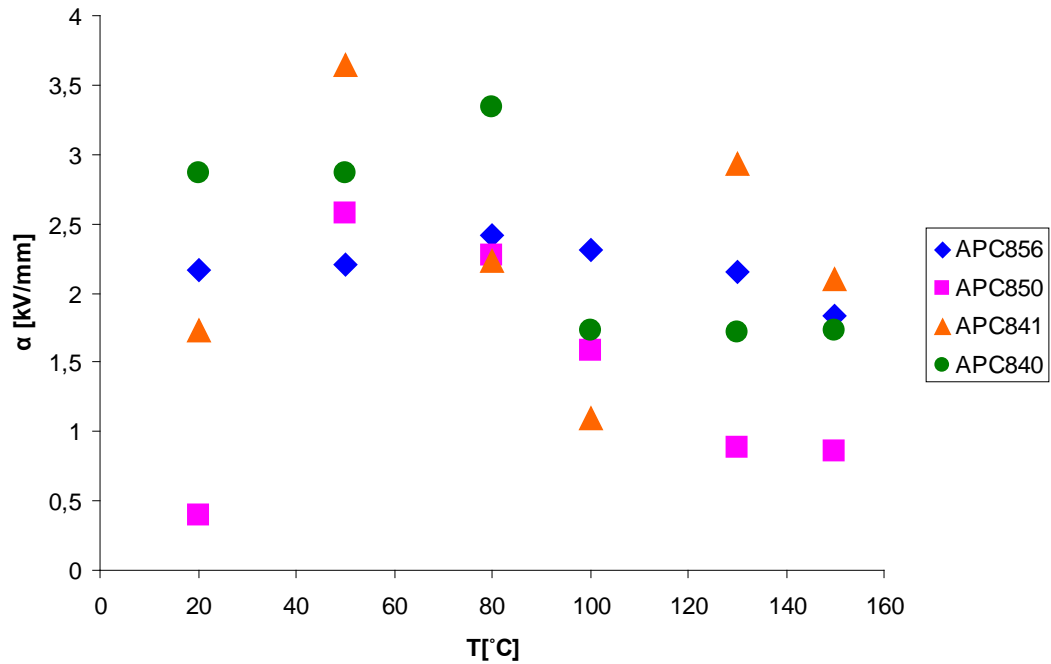


Fig. 4.7.15. Temperature dependence of activation field in PZT ceramics. Data from i_{max} pulse poling.

Measured values of spontaneous polarization, maximum transient current and related electric field are described in Table 4.7.1-4.7.2. Differences between measured values of spontaneous polarization are influenced also by fitting procedure. The reliability of approximations was located in the range 0.8-0.97. Such situation influences the values of activation field too.

| Ceramics type | $P_s, \text{C/m}^2$ |
|---------------|---------------------|
| APC850 | 0,280 |
| APC856 | 0,235 |
| APC840 | 0,201 |
| APC841 | 0,195 |

Tab. 4.7.1. Spontaneous polarization values calculated for different PZT ceramics. Data from i_{max} pulse poling at RT.

| Ceramics type | i_{max} , mA | E, kV/mm |
|---------------|----------------|----------|
| APC 850 | 0,528 | 1,190 |
| APC 856 | 0,171 | 1,050 |
| APC 840 | 0,050 | 1,980 |
| APC 841 | 0,147 | 1,687 |

Tab. 4.7.2. Electric field related to i_{max} for different PZT ceramics. Data from pulse poling.

4.8. Hysteresis loop measurement.

Hysteresis loop method of measurement was chosen to verify the results of pulse poling method on the same disc samples of PZT ceramics. The Sawyer-Tower circuit was used for hysteresis loop measurement (Fig.4.8.1). Amplitude and frequency (1Hz, 10Hz, 100Hz) of harmonic signal were set on function generator (Hameg HM8150). Generator voltage output was amplified by high voltage amplifier (Matsusada Precision Inc., type AMT-5B20) and later detected by AD convertor (Tedia, PCA7428AS). As a result it was possible to calculate the value of dielectric displacement D from measured charge on sample (Fig.4.8.2). The shape of hysteresis loop changed with temperature. Hysteresis loop becomes slimmer and more elongated (less rectangular) with temperature increase. The decrease of coercive field and remnant polarization caused hysteresis loop area decrease at higher temperature.

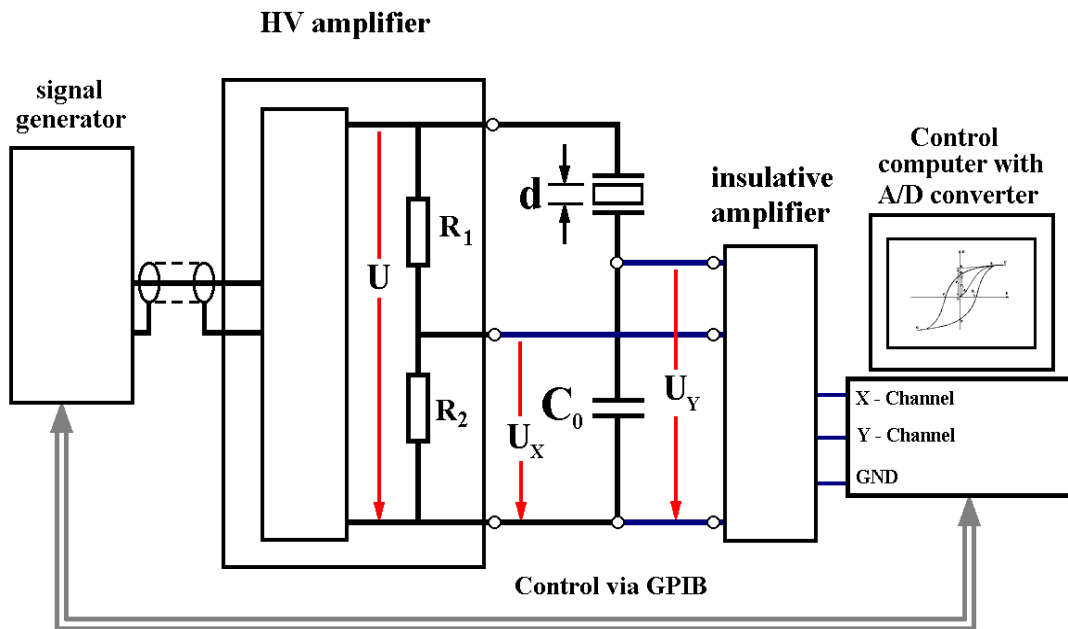


Fig. 4.8.1. Experimental scheme of hysteresis loops measurement.

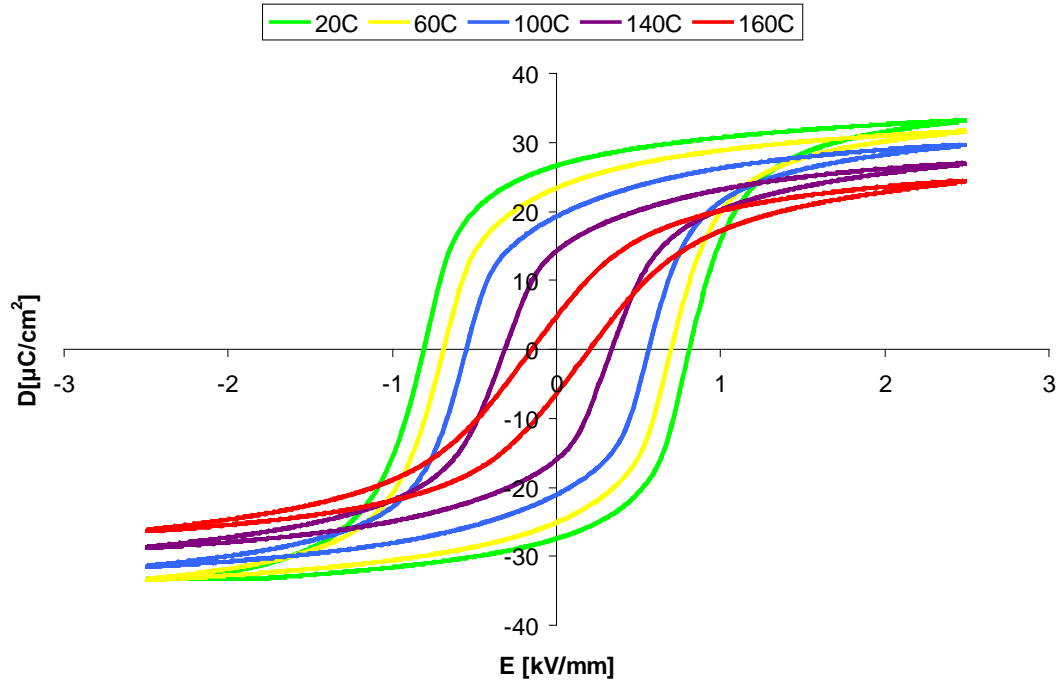


Fig. 4.8.2. Hysteresis loops of APC856 ceramics measured at different temperatures and 10Hz.

Values of spontaneous polarization (P_s) and coercive field (E_c) were calculated from hysteresis loops (Fig.4.8.3 and Fig.4.8.4). Spontaneous polarization and coercive field data for all studied PZT ceramics are given in Table 4.8.1. Measured temperature dependence of coercive field is similar to the result observed in [119] for soft and hard PZT ceramics.

| PZT ceramics | P_s , C/m ² | E_c , kV/mm |
|--------------|--------------------------|---------------|
| APC850 | 0,320 | 1,400 |
| APC856 | 0,270 | 0,800 |
| APC840 | 0,280 | 1,450 |
| APC841 | 0,284 | 1,510 |

Tab. 4.8.1. Spontaneous polarization and coercive field for PZT ceramics at RT. Data from hysteresis loops (frequency 10Hz).

Hysteresis loop measurement was not dealing with P_s or P_r dependences on electric field. Amplitude value of applied electric field was 2.5kV/mm. Increase of P_r with E in PZT ceramics was described for example in [120] for soft and hard PZT ceramics. Such dependence may be explained in terms of 90 (71° or 109°) domain rotation. Remnant polarization will increase when the electric field is enhanced. This dependence was demonstrated by Ogawa in [121].

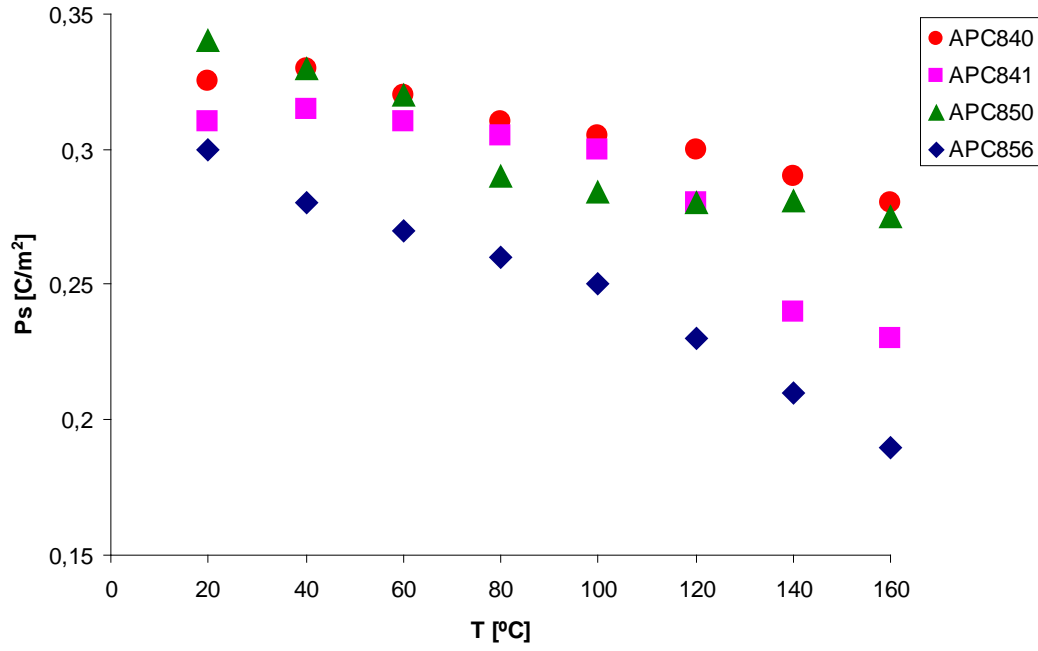


Fig. 4.8.3. Temperature dependence of spontaneous polarization P_s for PZT ceramics. Data from hysteresis loops.

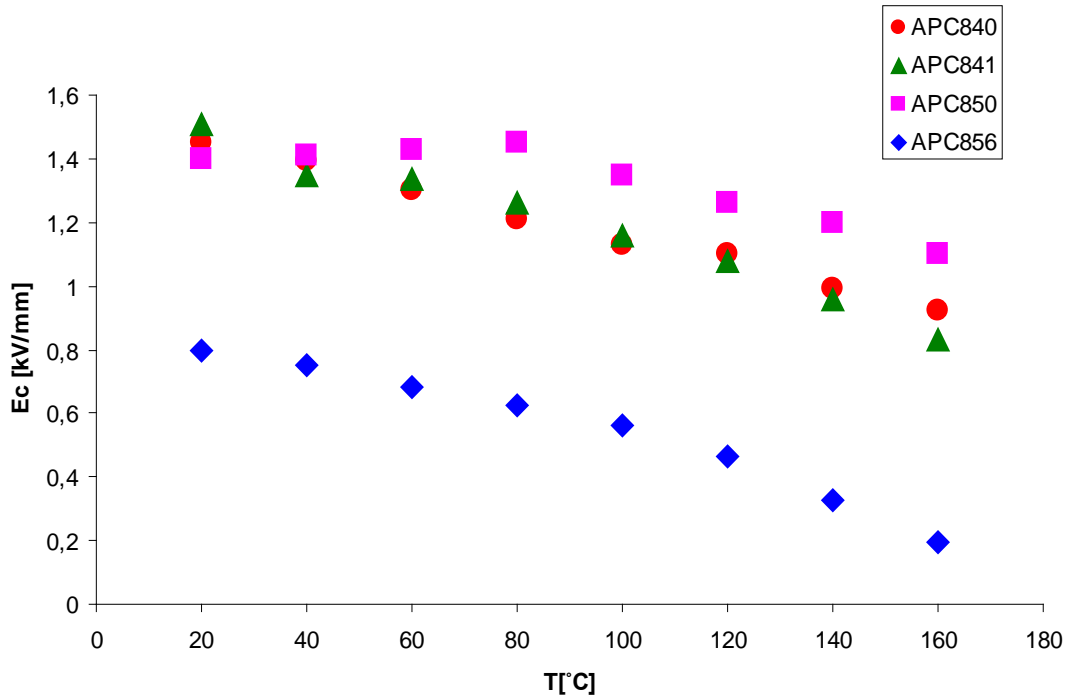


Fig. 4.8.4. Temperature dependence of coercive field E_c for PZT ceramics. Data from hysteresis loops.

Main goal of hysteresis loop measurement was temperature dependence observation of P_s in different PZT types. Normally, the values of spontaneous polarization P_s are higher than remnant polarization P_r in ferroelectric materials. Comparison of measured values P_s from dynamic poling (hysteresis loops) and pulse poling gave the differences in values for PZT ceramics. Spontaneous polarization is smaller in switching current measurement than in hysteresis loop measurement for all PZT ceramics types. Such issue may be explained in terms of domain walls clamping during single bipolar pulse application. This situation does not occur during hysteresis loop measurement. The domain walls may be released by continuously reversed electric field direction. The dramatic decrease of P_s was observed in APC856 near the Curie temperature ($T_c=160^\circ\text{C}$ by manufacturer) during hysteresis loop measurement.

Measured values of E_c are located within the range from 0.8kV/mm to 1.6kV/mm for our studied PZT ceramics during temperature increase. Only APC856 has E_c value in the range from 0.2kV/mm to 0.8kV/mm.

Hysteresis loop behavior of different PZT ceramics at room temperature is shown in Fig.4.8.5. Hysteresis loops were measured at frequency 10Hz. It is possible to see characteristic shape differences between soft and hard PZT ceramics. Hysteresis loops for hard PZT are more rectangular than for soft PZT's.

Fig.4.8.6. shows the hysteresis loops of APC850 ceramics measured at different frequencies and room temperature. Coercive field E_c and remnant polarization P_r increases when the frequency increases from 1Hz to 10Hz as generally expected.

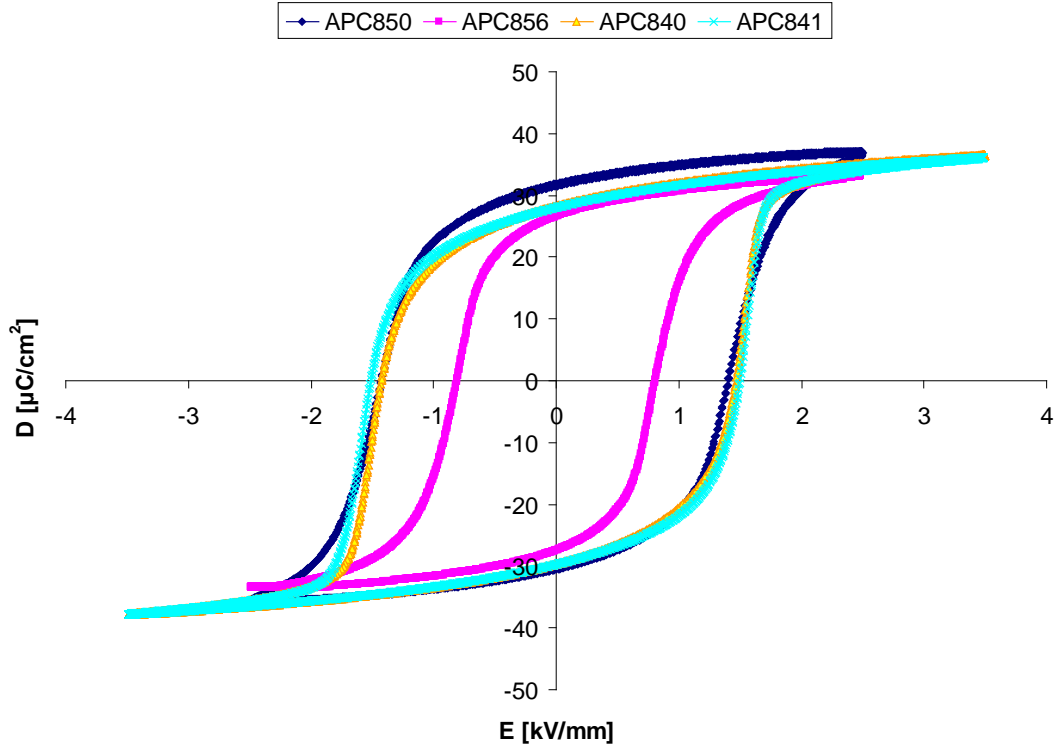


Fig. 4.8.5. Hysteresis loops of different PZT ceramics measured at RT and 10Hz.

However, for the higher frequencies displayed in Fig.4.8.6 (100Hz or 1000Hz) we can observe shrinked loop. This behaviour is due to the higher rate of generated heat in the sample because of dielectric losses. Dissipated loss power is proportional to the hysteresis loop frequency. While the heat is generated locally inside the sample it increases its temperature and the material properties are changed. Heat conductivity from PZT to the surrounding silicon oil bath is not fast enough to compensate temperature rise at higher frequencies. This problem cannot be fully solved. Therefore hysteresis loops at higher frequencies (more than 10Hz in our case) do not follow expected trend of E_c increase with frequency.

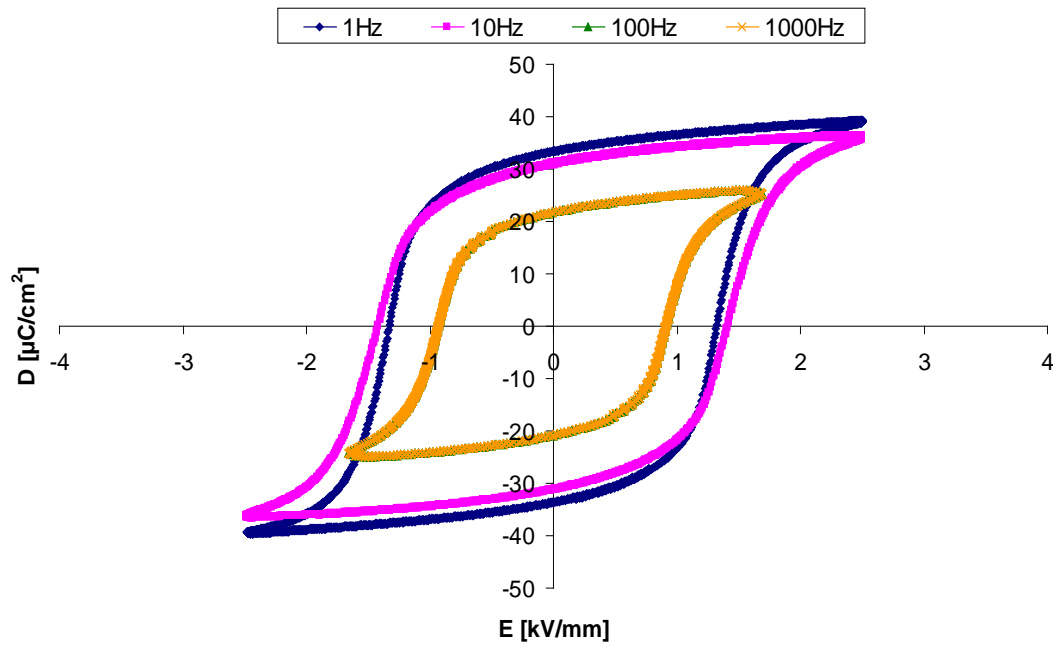


Fig. 4.8.6. Hysteresis loops of APC850 ceramics measured at different frequencies and RT.

Table 4.8.2 shows the values of spontaneous polarization and coercive field for APC850 ceramics measured at different frequencies and room temperature. It is possible to compare these values with Tab.4.7.1. Time of constant voltage application was 8 seconds in pulse poling experiment (frequency 0.125 Hz). The spontaneous polarization equals 0.28 C/m² at such frequency.

| Frequency, Hz | P_s , C/m ² | E_c , kV/mm |
|---------------|--------------------------|---------------|
| 1 | 0,320 | 1,34 |
| 10 | 0,270 | 1,40 |
| 100 | 0,280 | 0,92 |
| 1000 | 0,284 | 0,91 |

Tab. 4.8.2. Spontaneous polarization of APC850 ceramics at RT. Data from hysteresis loops.

4.9. Results discussion.

De-poling method applied to different PZT ceramics types brings the biggest impact on material properties. D.C. and pulse electric field applicability limits were measured for the set of hard as well as soft PZT ceramics up to 1000V/mm electric field strength. Soft PZT ceramics has applicability limits 200-700V/mm for D.C. field and 200-500V/mm for pulses. Ceramics is more sensitive to the pulse electric field than to D.C. signal. The observed limit value of applied electric field in soft PZT ceramics is equal approximately to one half of coercive field value for APC850 and APC856 ceramics in D.C. depoling. Pulse depoling values of applied electric field are equal approximately to one third of coercive field value in both soft PZT types. Changes in the material properties are realized by the domain wall movement, which is more complex phenomenon in pulsed electric fields. Hard PZT's have their electric field applicability limits higher than 1000V/mm at room temperature and therefore out of the tested electric field range. Hard PZT ceramics acquired relative changes in the materials coefficients measured in the range from 3% to 18%. Piezoelectric coefficients are the most sensitive material properties studied with respect to the depoling field.

The impact of re-poling method at room temperature with introduced parameters on plate and disc samples of PZT ceramics was found as ineffective for the electromechanical properties change. The clamping of domain walls was the main reason of re-poling low influence on material properties in ceramics. Even increase of re-poling electric field from 2kV/mm to 3kV/mm was detected as ineffective to achieve bigger changes in material properties. Such method is not useful for the future investigation due to its small contribution for production purpose and low effectiveness. There is only one alternative to achieve higher changes in material properties in such poling method in future investigation. This is the combination of electric field influence with temperature. Such combination helps to release clamped domain walls and gives chance for the material properties increase. Such suggestion is in consequence with temperature effect on material properties during poling, which was studied in [122]. Higher amplitude of the re-poling field must be another aspect for the experiment improvement. There is only limitation in electrical breakdown strength. It is typically 5kV/mm in used PZT material.

Cross-poling method provides the minimum impact to the material properties in the case of bar samples. It is possible to change poling condition during this experiment (for example, higher temperature or time of electric field application) to achieve higher impact on material properties. These actions may improve the final material properties but total impact is not large. This poling method has to be tested on samples with different geometry (for example, ring shaped samples).

Transient current and hysteresis loop measurement shows the similar experimental results. The calculated P_s values from transient current measurement are in good agreement with P_s values from hysteresis loops. Such situation gives opportunity to confirm the good efficiency of transient current method setup and applied pulse design in case of PZT ceramics. Comparison of transient current and hysteresis loop measurement results are similar to results obtained by Lente et. al. [75, 123]. The transient current measurement was described in this work. It was explained as a result of two ferroelectric mechanisms: 90° domain wall rotation immediately followed by 90° domain walls rearrangement. As a result higher reorientation of 90° domains occurred. The 90° domain wall rearrangement has an

important participation in the sample polarization. On the other side, it also participates in the stabilization of the polarization after poling. Spontaneous polarization and coercive field decrease when temperature increases. Such dependence was confirmed in pulse poling experiment and hysteresis loop measurement. Increased value of electric field amplitude generates the higher values of spontaneous polarization. This dependence was described in pulse poling measurement. Hysteresis loop measurement gave opportunity to observe that spontaneous polarization and coercive field decrease when the measurement frequency increases. The values of coercive field calculated from hysteresis loops are in good agreement with values of electric field observed at maximum transient current. Values of coercive field were slightly higher than calculated from pulse poling in soft PZT ceramics. Opposite result was observed in hard PZT.

Chapter 5. Conclusions.

Different poling methods and their influence on material properties of soft and hard PZT ceramics were investigated. Experiment involves de-poling, re-poling, cross-poling and bipolar pulse application techniques for poling procedure. The most important results were observed in the case of de-poling method and bipolar pulse application. In case of re-poling and cross-poling method the influence of poling conditions on material properties of PZT ceramics (soft and hard) did not have a big impact on their changes.

De-poling method application on PZT ceramics gave the opportunity to define the applicability limits of inspected ceramics at room temperature. Electric field applicability limits were measured by the resonant methods for D.C. and pulse electric field de-poled PZT ceramics. It is found that the limiting fields for soft PZT are in the range of 500-700V/mm for D.C. depoling and in the range of 200-500V/mm for pulses. Hard PZT ceramics is resistant to the depoling fields up to 1000V/mm either for D.C., or pulse depoling fields at room temperature. Relative changes in the magnitude of the electromechanical properties are from 3 to 20% for the electric fields up to 1000V/mm. Such results were presented at ECAPD7 conference and later published in *Ferroelectrics* [124].

Temperature dependences of remnant polarization and coercive field were observed for PZT ceramics during hysteresis loop measurement. Both values will decrease with higher temperature. Dramatic reduction of P_r was observed in soft APC856 ceramics near the Curie temperature. Such measurement was important for further confirmation of pulse poling results.

Transient current measurement was the effective tool for switching dynamics observation in ceramics. The special pulse design was created in the experimental part of the thesis. The pulse design was chosen to get the highest influence on poling dynamics for observed samples.

For all types of PZT ceramics maximum switching current value increased with the higher applied electric field. Switching current increased mainly due to higher switching rate of domains. Temperature influence of i_{max} was more essential than electric field amplitude one. Comparison of P_s (hysteresis loop measurement method) and P_s (pulse poling) values showed the differences between these values. The smaller value of P_s for pulse poling may be explained by the clamping of domain walls during pulse application. Switching current behaviour helps to describe the poling dynamics in studied PZT ceramics types. Results of this experiment were presented at the ECMS2011 conference [125].

The direction of future investigation may include investigation of pulse poling application with other pulse waveform in order to get optimum material properties. Final users in device fabrication will be interested in further reduction of manufacturing costs. So there is a possibility to match poling procedure to their

needs. The most interesting item will be connected with various combinations of electric field application and temperature conditions.

References

- [1] S.A. Wise: Displacement properties of RAINBOW and THUNDER piezoelectric actuators, *Sensors and Actuators A*, 69 (1998) 33-38
- [2] I. Chilibon: Ultrasound transducer for medical therapy, *Sensors and Actuators A*, 142 (2008) 124-129
- [3] I.M. Reaney: Microwave dielectric ceramics for resonators and filters in mobile phone networks, *Journal of the American Ceramic Society*, 89, 7 (2006) 2063-2072
- [4] J. Valasek: Piezoelectric and allied phenomena in Rochelle salt, *Physical Review*, 17, 4 (1921) 475-481
- [5] N. Setter, R. Waser: Electroceramic materials, *Acta Mater.* 48 (2000) 151-178
- [6] V. Petržílka, J.B. Slavík, I. Šolc, O. Taraba, J. Tichý, J. Zelenka: Piezoelektrina a její technické použití, Nakladatelství Československé akademie věd, Praha 1960 (in Czech)
- [7] G.H. Hartling: Ferroelectric Ceramics: History and Technology, *Journal of the American Ceramic Society*, 82, 4 (1999) 797-818
- [8] M.B. Smith, K. Page, T. Siegrist, P. Redmond, E. Walter, R. Seshadri, L. Brus, M. Steigerwald: Crystal Structure and the Paraelectric-to-Ferroelectric Phase Transition of Nanoscale BaTiO₃, *Journal of the American Chemical Society*, 130, 22 (2008) 6955-6963
- [9] J. Fousek, L.E. Cross, J. Nosek: Domain phenomena in single crystalline and ceramic ferroics: unresolved and attractive problems, *Microelectronic Engineering*, 66 (2003) 574-583
- [10] J.Fousek, V. Janovec: The Orientation of Domain Walls in Twinned Ferroelectric Crystals, *Journal of Applied Physics*, 40, 1 (1969) 135-142
- [11] R.D. Redin, G.W. Marks, C.E. Antoniak: Symmetry Limitations to Polycrystalline Ferroelectrics, *Journal of Applied Physics*, 34, 3 (1963) 600-610
- [12] A.S. Bhalla, R. Guo, R. Roy: The perovskite structure – a review of its role in ceramic science and technology, *Materials Research Innovations*, 4, 1 (2000) 3-26
- [13] G. Arlt, P. Sasko: Domain configuration and equilibrium size of domains in BaTiO₃ ceramics, *Journal of Applied Physics*, 51, 9 (1980) 4956-4960
- [14] H. Krueger: Stress Sensitivity of Piezoelectric Ceramics: Part I. Sensitivity to Compressive Stress Parallel to the Polar Axis, *Journal of the Acoustical Society of America*, 42, 3 (1967) 636-645
- [15] H. Krueger: Stress Sensitivity of Piezoelectric Ceramics: Part II. Heat Treatment, *Journal of the Acoustical Society of America*, 43, 3 (1968) 576-582
- [16] H. Krueger: Stress Sensitivity of Piezoelectric Ceramics: Part III. Sensitivity to Compressive Stress Perpendicular to the Polar Axis, *Journal of the Acoustical Society of America*, 43, 3 (1968) 583-591

- [17] A.H. Meitzler, S. Troler-McKinstry, J. Ballato, J. Fousek, A. Bhalla, R. Guo, P. Bloomfield, R. E. Newnham W. Cao, S. M. Pilgrim, L. Eric Cross, C. A. Randall, J. P. Dougherty, Q. Zhang: Draft 16 of A Working Document for a Proposed Standard to be entitled: IEEE Standard Definitions of Terms Associated with Ferroelectric and Related Materials, IEEE Transactions on Ultrasonics, Ferroelectrics and Frequency Control, 50 (2003) 1613-1614 (1-32)
- [18] R.C. Miller, A. Savage: Velocity of sidewise 180° domain -wall motion in BaTiO_3 as a function of the applied electric field, Physical Review 112, 3 (1958) 755–762
- [19] C.B. Sawyer, C.H. Tower: Rochelle salt as a dielectric, Physical Review, 35 (1930) 269-273
- [20] N. Wongdamnern, N. Triamnak, A. Ngamjarurojana, Y. Laosiritaworn, S. Ananta, R. Yimnirun: Comparative studies of dynamic hysteresis responses in hard and soft PZT ceramics, Ceramics International, 34 (2008) 731-734
- [21] J. Janta: Sideways Domain-Wall Motion and the Hysteresis Loops of Ferroelectrics, Journal of the Physical Society of Japan, 28 (1970) 340-342
- [22] B. Tadić: Switching current noise and relaxation of ferroelectric domains, The European Physical Journal B, 28 (2002) 81-89
- [23] R.C. Miller, A. Savage: Further Experiments on the Sidewise Motion of 180° Domain Walls in BaTiO_3 , Physical Review, 115, 5 (1959) 1176-1180
- [24] F. Jona, G. Shirane: Ferroelectric crystals, Dover publications, Inc. 1993
- [25] W.J. Merz: Domain formation and domain wall motions in ferroelectric BaTiO_3 single crystals, Physical Review, 95 (1954) 690-698
- [26] D. Berlincourt, H. Jaffe: Elastic and Piezoelectric Coefficients of Single-Crystal Barium Titanate, Physical Review, 111, 1 (1958) 143-148
- [27] W. Merz: The electric and optical behavior of BaTiO_3 single-domain crystals, Physical Review, 76, 8 (1949) 1221-1224
- [28] O. Nakao, K. Tomomatsu, S. Ajimura, A. Kurosaka, H. Tominaga: Influence of Poling Conditions on properties of BaTiO_3 Single Crystal, Japanese Journal of Applied Physics, 31 (1992) 3117-3119
- [29] O. Nakao, K. Tomomatsu, S. Ajimura, A. Kurosaka, H. Tominaga: Influence of 180° Domains on Ferroelectric Properties of BaTiO_3 Single Crystal, Applied Physics Letters, 61, 14 (1992) 1730-1732
- [30] R.C. Miller, G. Weinreich: Mechanism for the Sidewise Motion of 180° domain Walls in Barium Titanate, Physical Review, 117, 6 (1960) 1460-1466
- [31] G.A. Magel, M.M. Fejer, R.L. Byer: Quasi-phase-matched second-harmonic generation of blue light in periodically poled LiNbO_3 , Applied Physics Letters, 56, 2 (1990) 108-110
- [32] E.J Lim, M.M. Fejer, R.L. Byer, W.J. Kozlovsky: Blue light generation by frequency doubling in periodically poled lithium niobate channel waveguide, Electronic Letters, 25 (1989) 731-732

- [33] I.A. Ghambaryan, R. Guo, R.K. Hovsepyan, A.R. Poghosyan, E. S. Vardanyan, V.G. Lazaryan: Creation of Periodical Antiparallel Domain Structure in Lithium Niobate Crystals During Growth Process, *Ferroelectric Letters*, 30 (2003) 59-67
- [34] M.C. Wengler, M. Miller, E. Soerger, K. Buse: Poling dynamics of lithium niobate crystals, *Applied Physics B*, 76 (2003) 393-396
- [35] A.C. Busacca, C.L. Sones, R.W. Eason, S. Mailis: Surface domain inversion in ferroelectric lithium niobate, *Ferroelectrics*, 296 (2003) 91-97
- [36] M. Mohagen, D.V. Strekalov, A. A. Savchenkov, A. B. Matsko, V. S. Ilchenko, L. Maleki: Calligraphic poling of Lithium Niobate, *Optics Express*, 13, 9 (2005) 3408-3419
- [37] S. Kim, V. Gopalan, A. Gruverman: Coercive fields in ferroelectrics: A case study in lithium niobate and lithium tantalate, *Applied Physics Letters*, 80, 15 (2002) 2740-2742
- [38] L. Arizmendi: Photonic applications of lithium niobate crystals, *physica status solidi (a)*, 201, 2 (2004) 253-283
- [39] V. Gopalan, T. Mitchell, K.E. Sicakfus: Switching kinetics of 180° domains in congruent LiNbO_3 and LiTaO_3 crystals, *Solid State Communication*, 109 (1999) 111-117
- [40] V.Y. Shur: Kinetics of ferroelectric domains: Application of general approach to LiNbO_3 and LiTaO_3 , *Journal of Materials Science*, 41 (2006) 199-210
- [41] P.T. Brown, G.W. Ross, R.W. Eason, A.R. Poghosyan: Control of domain structures in lithium tantalate using interferometric optical patterning, *Optics Communication*, 163 (1999) 310-316
- [42] V.Y. Shur, A.L. Gruverman, V.V. Letuchev, E.L. Rumyantsev, A.L. Subbotin: Domain structure of lead germanate, *Ferroelectrics* 98 (1989) 29-49
- [43] J.P. Meyn, M.E. Klein, D. Woll, R. Wallenstein: Periodically poled potassium niobate for second-harmonic generation at 463 nm, *Optics Letters*, 24 (1999) 1154-1156
- [44] J. Hirohashi, K. Yamada, H. Kamio, S. Shichijyo: Differential vector poling for artificial domain control of KNbO_3 single crystals, *Transactions of the Materials Research Society of Japan*, 28, 1 (2003) 185-188
- [45] J. Hirohashi, K. Yamada, H. Kamio, S. Shichijyo: Artificial fabrication of 60° domain structures in KNbO_3 single crystals, *Journal of the Korean Physical Society*, 42 (2003) S1248-S1251
- [46] J. Hirohashi, K. Yamada, H. Kamio, S. Shichijyo: Fabrication of 90° domain structures in KNbO_3 single crystals, *Ferroelectrics*, 282 (2003) 29-36
- [47] M. Řepka: PZT ceramics material properties dependence on the mechanical stress, Diploma thesis, FM TUL, Liberec 2005
- [48] Q.M. Zhang: Electromechanical properties of lead zirconate titanate piezoceramics under the influence of mechanical stresses, *IEEE Transactions on Ultrasonics, Ferroelectrics and Frequency Control*, 46 (1999) 1518-1526
- [49] Piezoelectric ceramics: Data Handbook, Philips Components, 1997

-
- [50] R.Y. Nishi, R.F. Brown: Behaviour of piezoceramic projector materials under hydrostatic pressure, *Journal of the Acoustical Society of America*, 36 (1964) 1292-1296
- [51] A.J. Masys, W. Ren, G. Yang, B.K. Mukherjee: Piezoelectric strain in lead zirconate titanate ceramics as a function of electric field, frequency, and dc bias, *Journal of Applied Physics*, 94 (2003) 1155-1162
- [52] Z.Q. Zhuang, M. Haun, S. J. Jang, L. E. Cross: Composition and temperature dependence of the dielectric, piezoelectric and elastic properties of pure PZT ceramics, *IEEE Transactions on ultrasonics, ferroelectrics and frequency control*, 36 (1989) 413-416
- [53] V. Bobnar, Z. Kutnjak, A. Levstik: Temperature Dependence of Material Constants of PLZT Ceramics, *Journal of the European Ceramic Society*, 19 (1999) 1281-1284
- [54] G.L. Messing, S. Trolier-McKinstry, E. M. Sabolsky, C. Duran, S. Kwon, B. Brahmaroutu, P. Park, H. Yilmaz, P.W. Rehrig, K. B. Eitel, E. Suvaci, M. Seabaugh, K. S. Oh: Templated grain growth of textured piezoelectric ceramics, *Critical Reviews in Solid State and Materials Science*, 29 (2004) 45-96
- [55] M. Granahan, M. Holme, W.A. Schulze, R.E. Newnham: Grain-Oriented PbNb_2O_6 ceramics, *Journal of the American Ceramic Society*, 64 (1981) C68-69
- [56] N. Setter: Piezoelectric materials in Devices, *Ceramics Laboratory, EPFL Lausanne*, 2002
- [57] H.S. Lee, T. Kimura: Effects of microstructure on the dielectric and piezoelectric properties of lead metaniobate, *Journal of the American Ceramic Society*, 81 (1998) 3228-3236
- [58] E. M. Sabolsky: Dielectric and piezoelectric properties of $\langle 001 \rangle$ fiber-textured $0.675\text{Pb}(\text{Mg}_{1/3}\text{Nb}_{2/3})\text{O}_3 - 0.325\text{PbTiO}_3$ ceramics, *Journal of Applied Physics*, 93 (2003) 4072-4080
- [59] K. Kinoshita, A. Yamaji: Grain-size effects on dielectric properties in barium titanate ceramics, *Journal of Applied Physics*, 47, 1 (1976) 371-373
- [60] N. Setter, E.L. Colla: *Ferroelectric ceramics*, *ETH Zurich, Birkhauser Verlag*, 1993
- [61] A.V. Polotai, A.V. Ragulya, C.V. Randall: Preparation and size effect in pure nanocrystalline barium titanate ceramics, *Ferroelectrics* 288 (2003) 93-102
- [62] K. Takagi, S. Kikuchi, J.F. Li, H. Okamura, R. Watanabe, A. Kawasaki: Ferroelectric and photostrictive properties of fine-grained PLZT ceramics derived from mechanical alloying, *Journal of the American Ceramic Society*, 87 (2004) 1477-1482
- [63] G. Arlt, P. Sasko: Domain configuration and equilibrium size of domains in BaTiO_3 ceramics, *Journal of Applied Physics*, 51 (1980) 4956-4960
- [64] A.J. Moulson, J. M. Herbert: *Electroceramics*, *J.Wiley & Sons Inc.*, 2003

-
- [65] S. Kim, D. Kim: Stabilization and Memory of the Domain Structures in Barium Titanite Ceramics: Microstructural Observation, *Journal of the American Ceramic Society*, 83 (2000) 1495-1498
 - [66] H. Jaffe, D. Berlincourt, J.M. McKee: Effect of Pressure on the Curie Temperature of Polycrystalline Ceramic Barium Titanate, *Physical Review*, 105, 1 (1957) 57-58
 - [67] M. R. Soares, A. M. R. Senos, P. Q. Mantas: Phase coexistence region and dielectric properties of PZT ceramics, *Journal of the European Ceramic Society*, 20, 3 (2000) 321-334
 - [68] J. Fan, W. A. Stoll, S. C. Lynch: Nonlinear constitutive behaviour of soft and hard PZT: experiments and modelling, *Acta Mater.* 47, 17 (1999) 4415-4425
 - [69] K. Uchino, *Ferroelectric devices*. New-York, Marcel Dekker, 2000
 - [70] Q. M. Zhang, W. Y. Pan, S.J. Jang, L.E. Cross: Domain wall excitations and their contributions to the weak-signal response of doped lead zirconate titanate ceramics, *Journal of Applied Physics*, 64 (1998) 6445 – 6451
 - [71] M.E. Lines, A.M. Glass: *Principles and applications of ferroelectrics and related materials*, Oxford University Press, 2000
 - [72] D. Zhou, M. Kamlah, D. Munz: Effects of uniaxial prestress on the ferroelectric hysteretic response of soft PZT, *Journal of the European Ceramic Society*, 25 (2005) 425-432
 - [73] P.M. Chaplya, G. P. Carman: Dielectric and piezoelectric response of lead zirconate–lead titanate at high electric and mechanical loads in terms of non-180° domain wall motion, *Journal of Applied Physics*, 90, 10 (2001) 5278-5286
 - [74] T. Granzow, A.B. Kouna, E. Aulbach, J. Rodel: Electromechanical poling of piezoelectrics, *Applied Physics Letters*, 88 (2006) 252907
 - [75] M.H. Lente, J.A. Eiras: 90° domain reorientation and domain wall rearrangement in lead zirconate titanate ceramics characterized by transient current and hysteresis loop measurements, *Journal of Applied Physics*, 89 (2001) 5093-5099
 - [76] M.H. Lente, J.A. Eiras: Domain reorientation anisotropy in ferroelectric polycrystals, *Journal of Applied Physics*, 92 (2002) 2112-2117
 - [77] T. Ogawa, K. Nakamura: Bipolar pulse poling and space field in lead zirconate titanate ceramics, *Journal of the European Ceramic Society*, 21 (2001) 1391-1394
 - [78] S. Wan, K.J. Bowman: Thermal depoling effects on anisotropy of lead zirconate titanate materials, *Journal of the American Ceramic Society*, 81 (1998) 2717-2720
 - [79] S. Wan, K.J. Bowman: Cross-poling textures in a lead zirconate titanate piezoelectric material, *Journal of Materials Research*, 15, 6 (2000) 1248-1249
 - [80] S. Wan, K.J. Bowman: Modeling of electric field induced texture in lead zirconate titanate ceramics, *Journal of Materials Research*, 16, 8 (2001) 2306-2313

-
- [81] J. Mendiola, C. Alemany, B. Jimenez, E. Maurer: Poling strategy of PLZT ceramics, *Ferroelectrics*, 54, 1 (1984) 195-198
- [82] T. Ogawa: Domain structure of ferroelectric ceramics, *Ceramics International*, 26 (2000) 383-390
- [83] T. Ogawa, K. Nakamura: Effect of Domain Switching and Rotation on Dielectric and Piezoelectric Properties in Lead Zirconate Titanate Ceramics, *Japanese Journal of Applied Physics*, 38 (1999) 5465-5469
- [84] T. Ogawa: Poling Field Dependence of Crystal Orientation and Ferroelectric Properties in Lead Titanate Ceramics, *Japanese Journal of Applied Physics*, 39 (2000) 5538-5541
- [85] T. Ogawa: Poling field dependence of Ferroelectric properties in Barium Titanate Ceramics, *Japanese Journal of Applied Physics*, 40 (2001) 5630-5633
- [86] IRE Standards on Piezoelectric Crystals: Measurements of piezoelectric ceramics (1961)
- [87] C. Alemany, L. Pardo, B. Jimenez, F. Carmona, J. Mendiola: Automatic iterative evaluation of complex material constants in piezoelectric ceramics, *Journal of Physics D: Applied Physics*, 27 (1994) 148-155
- [88] L. Amarande, C. Miclea, C. Tanasoiu: Iterative evaluation of the complex constants of piezoceramic resonators in the radial mode, *Journal of European Ceramic Society*, 22 (2002) 1873-1881
- [89] X. Du, Q. Wang, K. Uchino: Accurate Determination of the Complex Materials Coefficients of Piezoelectric Resonators, *IEEE Transactions on Ultrasonics, Ferroelectrics and Frequency Control*, 50, 3 (2003) 312-320
- [90] X. Du, J. Zheng, U. Belegundu, K. Uchino: Crystal orientation dependence of piezoelectric properties of lead zirconate titanate near the morphotropic phase boundary, *Applied Physics Letters*, 72, 19 (1998) 2421-2423
- [91] X. Du, U. Belegundu, K. Uchino: Crystal Orientation Dependence of Piezoelectric Properties in Lead Zirconate Titanate: Theoretical Expectation for thin Films, *Japanese Journal of Applied Physics*, 36 (1997) 5580-5587
- [92] A.G. Luchaninov, A.V. Shilnikov, L.A. Shuvalov: Piezoelectric effect in poled and electrically depoled ferroelectrics, *Kristallografiya*, 44, 2 (1999) 289-296 (in Russian)
- [93] J. Zelenka: *Piezoelectric Resonators and their Applications*, Academia, Prague, 1986
- [94] K. Okada, T. Sekino: *Agilent Technologies Impedance Measurement Handbook*, Agilent Technologies Co. Ltd., 2003
- [95] Agilent Technologies: 4192A LF Impedance Analyser Operating and Service Manual, 04192-90011, March 2000
- [96] R. Herbiet, H. Tenbrock, G. Arlt: The Aging Behaviour of the Complex Material Parameters ϵ , d and s in Ferroelectric PZT ceramics, *Ferroelectrics*, 76 (1987) 319-326

-
- [97] J. Erhart, L. Burianova: What is really measured on a d33-meter?, *Journal of the European Ceramic Society*, 21 (2001) 1413-1415
- [98] T. Ogawa, K. Nakamura: Poling Field Dependence of Ferroelectric Properties and Crystal Orientation in Rhombohedral Lead Zirconate Titanate Ceramics, *Japanese Journal of Applied Physics*, 37 (1998) 5241-5245
- [99] A. Yamada, Y.-K. Chung, M. Takahashi, T. Ogawa: Poling Field Dependence of Ferroelectric Domains in Tetragonal Lead Zirconate Titanate Ceramics, *Japanese Journal of Applied Physics*, 35 (1996) 5232-5235
- [100] Piezoelectric ceramics: Principles and Applications, APC International Ltd., 2002
- [101] Data book for designers: Piezoelectric ceramics, Morgan Matroc Ltd.
- [102] B. Jaffe, W. Cook, H. Jaffe: *Piezoelectric Ceramics*, Academic Press, London and New York, 1971
- [103] Q.M. Zhang, H. Wang, N. Kim, L.E. Cross: Direct evaluation of domain-wall and intrinsic contributions to the dielectric and piezoelectric response and their temperature dependence on lead zirconate-titanate ceramics, *Journal of Applied Physics*, 75, 1 (1994) 454-459
- [104] D. Damjanovic: Contributions to the piezoelectric effect in ferroelectric single crystals and ceramics contributions to the piezoelectric single crystals and ceramics, *Journal of the American Ceramic Society*, 88, 10 (2005) 2663-2676
- [105] D. Damjanovic, M. Demartin: Contribution of the irreversible displacement of domain walls to the piezoelectric effect in barium titanate and lead zirconate titanate ceramics, *Journal of Physics: Condensed Matter*, 9 (1997) 4943-4953
- [106] E.I. Eknadosyants, A.N. Pinskaya, V.Z. Borodin: Domain Structure of Lead Zirconate-Titanate-Based Soft Ferroelectric Ceramics, *Crystallography Reports*, 44, 3 (1999) 462-466
- [107] Y.-Y. Lee, L. Wu, J.-S. Chang: Domain Structure in Modified Lead Titanate Ferroelectrics, *Ceramics International*, 20 (1994) 117-124
- [108] R. Herbiet, U. Robbels, H. Dederichs, G. Arlt: Domain Wall and Volume Contributions to Material Properties of PZT Ceramics, *Ferroelectrics*, 98 (1989) 107-121
- [109] T. Tsurumi, Y. Kumano, N. Ohashi, O. Fukunaga: Contribution of 90° Domains in Electric-Field-Induced Strain of PZT ceramics, *Journal of the Korean Physical Society*, 32 (1998) S1241-S1244
- [110] G. Arlt, N. Pertsev: Force constant and effective mass of 90° domain walls in ferroelectric ceramics, *Journal of Applied Physics*, 70, 4 (1991) 2283-2289
- [111] P. Púlpán, L. Rusin, J. Erhart: Influence of Poling conditions on Material Properties of Lead Zirconate-Lead Titanate Ceramics, *Japanese Journal of Applied Physics*, 47, 10 (2008) 7953-7958
- [112] U. Belegundu, K. Uchino: Switching current measurement in $\text{Pb}(\text{Zn}_{1/3}\text{Nb}_{2/3})\text{O}_3\text{-PbTiO}_3$ Relaxor Ferroelectric Single Crystals, *Journal of Electroceramics*, 6:2 (2001) 109-114

-
- [113] H.W. Gundel, P. Limousin, R. Seveno, D. Averty: Pulse polarization inversion and phase transition in ferroelectric and antiferroelectric thick films, *Journal of European Ceramic Society*, 21 (2001)1619-1623
 - [114] A. K. Tagantsev, L. E. Cross, J. Fousek: Domains in ferroic crystals and thin films, Springer New York Dordrecht Heidelberg London, 2010
 - [115] J. K. Lee, J. Y. Yi, K. S. Hong, S. E. Park: Polarization switching in $\text{Pb}(\text{Zn}_{1/3}\text{Nb}_{2/3})\text{O}_3$ -5% PbTiO_3 crystals, *Japanese Journal of Applied Physics*, 40 (2001) 6506-6509
 - [116] K. B. Chong, F. Guiu, M. J. Reece: Thermal activation of ferroelectric switching, *Journal of Applied Physics*, 103, 1 (2008) 014101
 - [117] H.C. Nie, X.F. Chen and N.B. Feng, G.S. Wang, X.L. Dong, Y. Gu, H.L. He, Y.S. Liu: Effect of external fields on the switching current in PZT ferroelectric ceramics, *Solid State Communication*, 150 (2010) 101-103
 - [118] E. Little: Dynamic behavior of domain walls in barium titanate, *Physical Review*, 98, 4 (1954) 978-984
 - [119] L. Burianova, P. Hana, M. Suchankova, S. Panos: Non-linear hysteresis properties of PZT ceramics, *Ferroelectrics*, 351 (2007) 153-162
 - [120] T. Ogawa, K. Nakamura: Pulse response measurement of transient phenomena on ferroelectric domains in PZT Ceramics, *Ferroelectrics*, 231 (1999) 19-24
 - [121] T.Ogawa: Poling field dependence of ferroelectric properties in piezoelectric ceramics and single crystals, *Ferroelectrics*, 237 (2002) 371-376
 - [122] C. Miclea, T. Tanasoiu, C.F. Miclea, L. Amarande, M. Cioangher, L. Trupina, A. Iuga, I. Spanulescu, C.T. Miclea, C. David, M. Susu: Behavior of the main properties of hard and soft type piezoceramics with temperature from 2 to 600K, *Proceedings of the International Semiconductor conference, CAS2*, 978-1-4244-5781-6/10 (2010) 301-304
 - [123] M. H. Lente, A. Picinin, J.P. Rono, J.A. Eiras: 90° domain wall relaxation and frequency dependence of the coercive field in the ferroelectric switching process, *Journal of Applied Physics*, 95, 5 (2004) 2646-2653
 - [124] T. Malysh, J. Erhart: Electric field applicability limits for PZT Ceramics, *Ferroelectrics*, 319 (2005) 45-56
 - [125] T. Malysh, J. Erhart: Pulse poling of PZT ceramics, *IEEE Information Proceedings of ECMS2011*, June 2011 Liberec

Appendixes

I. Parameters of impedance measurement.

| Equivalent series circuit | | Equivalent parallel circuit | |
|---------------------------|----------------------|-----------------------------|----------------------|
| $ Z $ impedance | Θ phase angle | $ Y $ admittance | Θ phase angle |
| R resistance | X reactance | G conductance | B susceptance |
| L inductance, C | Q quality factor | L, C capacitance | Q quality factor |
| L inductance, C | D dissipation factor | L, C capacitance | D dissipation factor |
| L inductance, C | R resistance | L, C capacitance | G conductance |

Table 1. Display A/B functions for impedance measurement.

| Measured parameter | Equivalent series circuit | Equivalent parallel circuit |
|--------------------|---------------------------|-----------------------------|
| $ Z $ | $\sqrt{R^2 + X^2}$ | - |
| $ Y $ | - | $\sqrt{G^2 + B^2}$ |
| Θ | $\tan^{-1}(X/R)$ | $\tan^{-1}(B/G)$ |
| L | X/ω | $-1/(\omega B)$ |
| C | $-1/(\omega X)$ | B/ω |
| Q | $ X /R$ | $ B /G$ |
| D | $R/ X $ | $G/ B $ |

Table 2. Measurement parameter formulae for complex impedance measurement.

II. Length-extensional vibration of thin bar (LE).

$$(l/t)^2 > 10; (l/w)^2 > 10$$

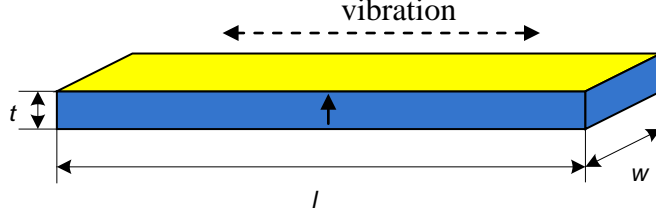


Fig. 1. LE vibration of thin bar.

The transverse electromechanical coupling factor for the length-extensional mode is given by:

$$\frac{k_{31}^2}{1 - k_{31}^2} = \frac{\pi}{2} \frac{f_a}{f_r} \tan\left(\frac{\pi}{2} \frac{f_a - f_r}{f_r}\right), \quad (1)$$

where f_a, f_r are the antiresonant and resonant frequencies.

It is possible to define:

$$k_{31}^2 = \frac{\pi}{2} \frac{f_a}{f_r} \tan\left(\frac{\pi}{2} \frac{f_a - f_r}{f_r}\right) \left[1 + \frac{\pi}{2} \frac{f_a}{f_r} \tan\left(\frac{\pi}{2} \frac{f_a - f_r}{f_r}\right) \right]^{-1}. \quad (2)$$

Resonant frequency is given by

$$f_r = \frac{1}{2l} \sqrt{\frac{1}{\rho s_{11}^E}}. \quad (3)$$

Elastic compliance will be defined from equation (3)

$$s_{11}^E = \frac{1}{4\rho l^2 f_r^2} \quad (4)$$

The transverse electromechanical coupling factor is defined

$$k_{31}^2 = \frac{d_{31}^2}{\epsilon_{33}^T s_{11}^E}, \quad (5)$$

and d_{31} may be determined:

$$d_{31} = \sqrt{\epsilon_{33}^T s_{11}^E k_{31}^2}. \quad (6)$$

III. Thickness-extensional vibration of thin plate (TE).

$l/t > 10$ and $w/t > 10$

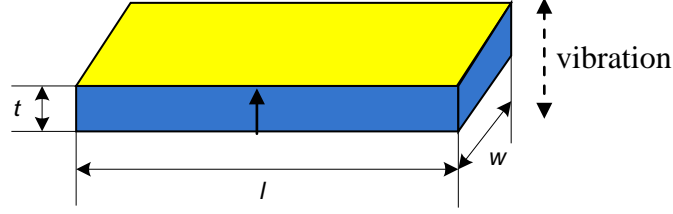


Fig. 2. TE vibration of plate.

Thickness-extensional vibrations of thin plate result in the transcendental equation with dimensionless wave number x .

$$\tan x = \frac{1}{k_t^2} x \quad (7)$$

where k_t is thickness electromechanical coupling factor.

It holds for the first (f_1) and third (f_3) resonant frequencies and corresponding wave numbers x_1 and x_3

$$\frac{x_1}{x_3} = \frac{f_1}{f_3} \Rightarrow x_3 = x_1 \frac{f_3}{f_1} \quad (8)$$

If equation (8) is implemented into (7) we can get

$$\tan\left(\frac{f_3}{f_1} x_1\right) = \frac{1}{k_t^2} \frac{f_3}{f_1} x_1 \quad (9)$$

Comparing equations (9) and (7) we can eliminate the unknown k_t value

$$\tan\left(\frac{f_3}{f_1} x_1\right) = \frac{f_3}{f_1} \tan x_1. \quad (10)$$

Equation (10) can be solved numerically. k_t^2 can be calculated when $x = x_1$ is implemented into (7)

$$k_t^2 = \frac{x_1}{\tan x_1}. \quad (11)$$

Thickness electromechanical coupling factor is defined by

$$k_t^2 = \frac{e_{33}^2}{c_{33}^E \epsilon_{33}^S \left(1 + \frac{e_{33}^2}{c_{33}^E \epsilon_{33}^S}\right)}. \quad (12)$$

Resonant frequency is defined

$$f_r^2 = \frac{x_1^2}{\pi^2 t^2} \frac{c_{33}^E + \frac{e_{33}^2}{\epsilon_{33}^S}}{\rho}. \quad (13)$$

Combination of (12) and (13) give opportunity to express

$$c_{33}^E = \left(\frac{\pi t}{x_1} \right)^2 (1 - k_t^2) \rho f_r^2, \quad (14)$$

where $f_r = f_{1r}$ and ρ is the sample's density.

IV. Radial (planar) vibrations of thin disc (RE).

$$d/t > 20$$

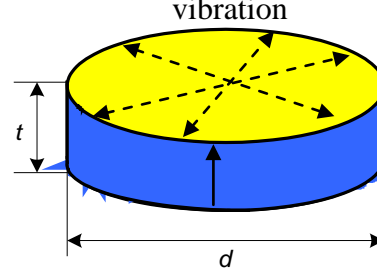


Fig. 3. Radial vibration of disc.

Radial vibrations of thin disc (RE) are used for the measurement of planar electromechanical coupling factor k_p .

$$\frac{k_p^2}{1 - k_p^2} = \frac{(1 - \sigma^E) J_1 \left(\eta_1 \frac{f_a}{f_r} \right) - \eta_1 \frac{f_a}{f_r} J_0 \left(\eta_1 \frac{f_a}{f_r} \right)}{(1 + \sigma^E) J_1 \left(\eta_1 \frac{f_a}{f_r} \right)}, \quad (15)$$

where σ^E is the Poisson's ratio, J_0 and J_1 are the first kind Bessel's functions of zero and first order, η_1 is the least positive root of equation $(1 - \sigma^E) J_1(\eta) = \eta J_0(\eta)$.

Then k_{31} can be found

$$k_p^2 = \frac{2}{1 - \sigma^E} k_{31}^2 \quad (16)$$

V. Thickness-shear vibration of thin plate (TS).

$l/t > 10$ and $w/t > 10$

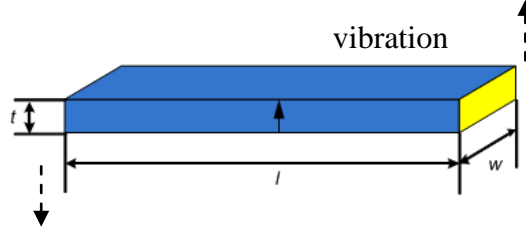


Fig. 4. Thickness-shear vibrations of thin plate (TS).

The antiresonance condition is

$$\tan x = \frac{k_{15}^2 - 1}{k_{15}^2} x \quad (17)$$

$$k_{15}^2 = \frac{x}{x - \tan x} \quad (18)$$

Elastic constant s_{55}^E can be calculated

$$s_{55}^E = \frac{1}{4\rho t^2 f_a^2} \quad (19)$$

where f_a is antiresonance frequency.

Now it is possible to define

$$s_{55}^E = \frac{s_{55}^D}{1 - k_{15}^2} \quad (20)$$

From the next equation

$$k_{15}^2 = \frac{d_{15}^2}{\epsilon_{11}^T s_{55}^E}, \quad (21)$$

it is possible to calculate

$$d_{15} = \sqrt{\epsilon_{11}^T s_{55}^E k_{15}^2}. \quad (22)$$

VI. Other calculations.

Elastic modulus c_{55}^E in case of ∞mm symmetry is

$$c_{55}^E = \frac{1}{s_{55}^E} \quad (23)$$

From the next equation

$$e_{i\alpha} = d_{i\beta} c_{\alpha\beta}^E \quad (24)$$

it is possible to define

$$e_{15} = d_{15} c_{55}^E \quad (25)$$

$$e_{33} = 2d_{31} c_{13}^E + d_{33} c_{33}^E \quad (26)$$

The elastic modulus will be calculated from Eq. (26)

$$c_{13}^E = \frac{e_{33} - d_{33} c_{33}^E}{2d_{31}} \quad (27)$$

The permittivity difference is

$$\varepsilon_{33}^T - \varepsilon_{33}^S = e_{33} d_{33} + 2d_{31} e_{31} \quad (28)$$

Equation (28) gives piezoelectric modulus

$$e_{31} = \frac{\varepsilon_{33}^T - \varepsilon_{33}^S - e_{33} d_{33}}{2d_{31}} \quad (29)$$

The next equation

$$d_{i\alpha} = e_{i\beta} s_{\alpha\beta}^E \quad (30)$$

will describe the piezoelectric coefficient

$$d_{31} = e_{31} (s_{11}^E + s_{12}^E) + e_{33} s_{13}^E \quad (31)$$

From equation (31) elastic compliance s_{13}^E will be calculated

$$s_{13}^E = \frac{1}{e_{33}} [d_{31} - e_{31} (s_{11}^E + s_{12}^E)] \quad (32)$$

It is possible to calculate planar electromechanical factor k_p according to the formula

$$k_p^2 = 1 - \frac{\varepsilon_{33}^S}{\varepsilon_{33}^T} \frac{1}{1 - k_t^2} \quad (33)$$

For planar electromechanical factor it is also given

$$k_p^2 = \frac{2d_{31}^2}{\varepsilon_{33}^T (s_{11}^E + s_{12}^E)} \quad (34)$$

so from (34) it will follow

$$(s_{11}^E + s_{12}^E) = \frac{2d_{31}^2}{\varepsilon_{33}^T k_p^2} \quad (35)$$

Equation (35) combined with Eq. (32) can get

$$s_{13}^E = \frac{1}{e_{33}} \left[d_{31} - \frac{2e_{31}d_{31}^2}{\varepsilon_{33}^T k_p^2} \right]. \quad (36)$$

From (16) let's find σ^E and compare it with relation

$$\sigma^E = -\frac{s_{12}^E}{s_{11}^E}. \quad (37)$$

As a result we will get

$$1 - 2 \frac{k_{31}^2}{k_p^2} = -\frac{s_{12}^E}{s_{11}^E} \quad (38)$$

From (38) we will define

$$s_{12}^E = \left(2 \frac{k_{31}^2}{k_p^2} - 1 \right) s_{11}^E. \quad (39)$$

To input the equation (39) into (35) we will find

$$s_{11}^E = \frac{2 \frac{d_{31}^2}{\varepsilon_{33}^T k_p^2}}{2 \frac{k_{31}^2}{k_p^2} - 1} = \frac{d_{31}^2}{\varepsilon_{33}^T k_{31}^2}. \quad (40)$$

The elastic compliance s_{12}^E is

$$s_{12}^E = \left(2 \frac{k_{31}^2}{k_p^2} - 1 \right) \frac{d_{31}^2}{\varepsilon_{33}^T k_{31}^2}. \quad (41)$$

From the next relation

$$1 = s_{33}^E c_{33}^E + 2s_{13}^E c_{13}^E \quad (42)$$

it is possible to calculate

$$s_{33}^E = \frac{1 - 2s_{13}^E c_{13}^E}{c_{33}^E}. \quad (43)$$

VII. Gauss fit method (OriginPro 8)

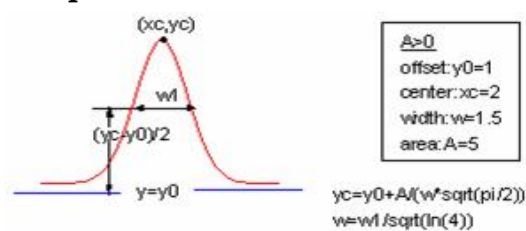
Function

$$y = y_0 + \frac{A}{w\sqrt{\pi/2}} e^{-\frac{2(x-x_c)^2}{w^2}}$$

Brief Description

Area version of Gaussian function.

Sample Curve



Parameters

Number: 4

Names: y_0 , x_c , w , A

Meanings: y_0 = offset, x_c = center, w = width, A = area

Lower Bounds: $w > 0.0$

Upper Bounds: none

Script Access

`gauss(x,y0,xc,w,A)`

Function File

FITFUNC\GAUSS.FDF

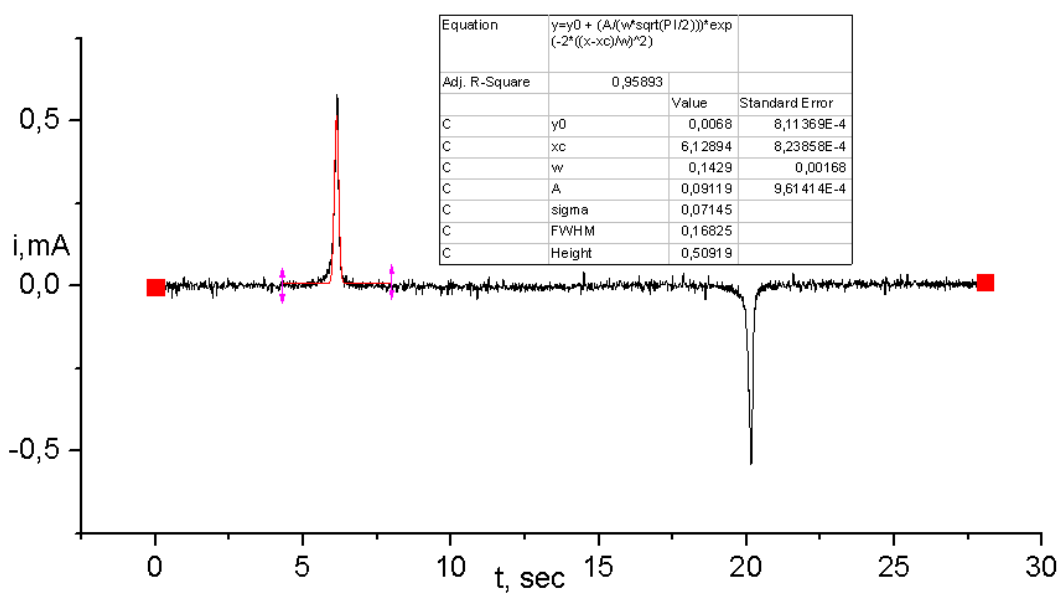


Fig. 5. Switching current fitting curve of disc sample APC850 at 2kV/mm and 50°C.

Publications and presentations

Publications:

- T. Malysh, J. Erhart: The influence of the re-poling in the weak electrical field on the electromechanical properties of PZT ceramics, ECAPD7, 7th European Conference on Applications of Polar Dielectrics, Technical University of Liberec, Czech Republic (2004), abstract
- T. Malysh, J. Erhart: Electric field applicability limits for PZT Ceramics, Ferroelectrics, 319 (2005) 45-56
- T. Malysh, J. Erhart: Pulse poling of PZT ceramics, IEEE Information Proceedings of 10th Workshop on Electronics, Control, Measurement and signals 2011, (2011) Liberec

Presentations:

- T. Malysh, J. Erhart: The influence of the re-poling in the weak electrical field on the electromechanical properties of PZT ceramics, ECAPD7, 7th European Conference on Applications of Polar Dielectrics, Technical University of Liberec, Czech Republic (2004), poster
- T. Malysh, J. Erhart: Pulse poling of PZT ceramics, ECMS2011, 10th Workshop on Electronics, Control, Measurement and signals 2011, Technical University of Liberec, Czech Republic (2011), oral speech

Curriculum Vitae

Name: Tetyana Malysh
Address: Kominická 600/5
460 01 Liberec 4
Česká Republika
E-mail: tamal@centrum.cz
Date of birth: 9.2.1979
Place of birth: Nizhyn, Ukraine

Education

from 10/2003 Ph.D. study
Study program: Applied sciences in engineering
Specialization area: Physical engineering
Department of Physics, Faculty of Sciences, Humanities and
Education, Technical University of Liberec, Czech Republic

06/2002 Master's study
Study program: Pedagogics and methods of secondary school
Specialization area: Mathematics and Physics
Department of Physics, Faculty of Mathematics and Physics,
Nizhyn Mykola Gogol Teachers' Training University, Ukraine

Skills

Software: MS Office, Wolfram Mathematica, OriginPro, Adobe -
Acrobat, Photoshop

Languages: English (intermediate), Czech (intermediate), Russian (native
speaker), Ukrainian (native speaker)

118 pages
4 prints
(Digital version on CD is included)
© 2012 Technical university of Liberec